

SEISMIC RETROFIT OF CURVED BRIDGES
ON SOFT SOILS USING BUCKLING
RESTRAINED BRACES

by

Anurag Upadhyay

A thesis submitted to the faculty of
The University of Utah
in partial fulfillment of the requirements for the degree of

Master of Science

Department of Civil and Environmental Engineering

The University of Utah

May 2016

Copyright © Anurag Upadhyay 2016

All Rights Reserved

The University of Utah Graduate School

STATEMENT OF THESIS APPROVAL

The thesis of _____ **Anurag Upadhyay** _____

has been approved by the following supervisory committee members:

_____ **Chris P. Pantelides** _____ , Chair _____ **12/16/2015** _____
Date Approved

_____ **Luis F. Ibarra** _____ , Member _____ **02/10/2016** _____
Date Approved

_____ **Evert Lawton** _____ , Member _____ **02/10/2016** _____
Date Approved

and by _____ **Michael E. Barber** _____ , Chair/Dean of

the Department/College/School of _____ **Civil and Environmental Engineering** _____

and by David B. Kieda, Dean of The Graduate School.

ABSTRACT

Damage to bridges has been evident during many earthquakes, even when the structure was designed according to model codes. Abutments act like a retaining wall during a seismic event. Past studies show that there have been several incidents of damage to abutments and shear keys due to pounding. This research attempts to study the performance of an existing multispan curved bridge supported on rigidly capped vertical pile groups which pass through a deep layer of soft clay. The soil-structure interaction (SSI) between the pile group and soil is idealized as linear springs in two perpendicular horizontal directions. At the expansion joints and abutments, steel shear walls are provided to improve the performance and concrete shear keys are utilized to restrain the lateral movement of the girders and deck during seismic events. A seismic retrofit scheme using Buckling Restrained Braces (BRB) is implemented at the abutments to prevent pounding damage.

It is observed that the soft soil surrounding the piles has a significant effect on the dynamic response of the bridge; in addition, the bearing displacements are underestimated if SSI is ignored. Damage to the abutments and the deck due to pounding can be prevented by using a combination of BRBs. Similarly, pounding between steel girders at the expansion joints can be prevented by using BRBs instead of seismic restrainer rods. BRBs are idealized using bilinear plastic link elements with a backbone curve adopted from actual experiments. A sensitivity analysis is carried out for modeling the BRBs using two different software packages.

Dedicated to my parents.

TABLE OF CONTENTS

ABSTRACT.....	iii
LIST OF TABLES.....	vii
ACKNOWLEDGEMENTS.....	viii
1. INTRODUCTION.....	1
1.1 Bridge Retrofit.....	3
1.2 Soil-Structure Interaction.....	5
2. MODELING OF CURVED BRIDGE INCLUDING SOIL-STRUCTURE INTERACTION.....	7
2.1. Soil-Structure Interaction.....	8
2.2. Ground Motion Data.....	19
3. BRB MODEL VALIDATION.....	30
3.1. Comparison of Several Models for Each Step.....	33
3.2. Comparison of Hysteresis Loops of Each Model with BRB Test Data.....	38
4. RESULTS AND DISCUSSION.....	41
4.1. Modal Analysis.....	41
4.2. Time History Analysis.....	41
4.2.1. Neglecting Soil-Structure Interaction.....	41
4.2.2. Effect of Soil Structure Interaction.....	48
4.2.3. Application of Buckling Restrained Braces.....	59
5. CONCLUSIONS.....	70
Appendices	
A. CURVED BRIDGE DRAWINGS AND SITE PHOTOGRAPHS.....	73
B. SOIL SPRING CONSTANTS.....	83

C. COMPARISON OF BRB PERFORMANCE IN SAP 2000, PERFORM 3D, AND OPENSEES	92
REFERENCES	109

LIST OF TABLES

Tables

2.1	Sectional and reinforcement details for the columns	8
2.2	Ground motions used for time-history analysis	20
3.1	Test model back-bone curves subjected to cyclic test in SAP 2000®	31
3.2	Comparison of hysteretic energy for various SAP 2000® models	37
4.1	Periods and mass participation ratios of first 30 modes of the bridge	42
4.2	Effect of soil-structure interaction on first three modes of vibration.....	48
A.1	Details of pile groups and pile caps at various bents.	78
A.2	Steel girder sections used in the curved bridge.....	80
B.1	Calculation of Y_s , Y_c , and P at various depth	89
B.2	Calculation of P-y curve at depth $Z = 2$ m.	90
B.3	Tri-linear curve points for P-y curve at $Z=2$ m	91
C.1	Period of vibration for the first 3 modes	102

ACKNOWLEDGEMENTS

I am thankful to Dr. Pantelides for his trust in my capabilities to accomplish this research work. This research was not possible without constant support and suggestions by Dr. Ibarra and Dr. Lawton. I would like to thank Wenjing Xu for providing the experimental data for this research, and MJ Ameli and Matt Wang for helping me with the modeling and providing suggestions. I would also like to thank my friend Vishal Bholra and my beautiful fiancé Shima Yoshida for their help in writing this thesis and for emotional support.

1. INTRODUCTION

Structural pounding related to earthquakes is a well-documented phenomenon in buildings and bridges. Evidence of damage to bridge abutments and decks from structural pounding is abundant. Performance of steel bridges in the 1995 Hyogo-ke Nanbu (Kobe) earthquake was investigated by Bruneau et al. (1996) and in the 2011 Great East Japan earthquake, Buckle et al. (2011) investigated several types of failures that occurred during these earthquakes. A large number of bridges experienced damage in the seismic restrainers, or in the concrete and steel shear keys, resulting in unseating or total collapse of spans at expansion joints and abutments (Itani et al. 2004; Hao and Chouw 2008). A number of studies have been carried out to predict the seismic response of existing bridges and specifically the pounding damage at the abutments and expansion joints. Most of these studies did not include soil-structure interaction which has a significant effect on the response of bridge structures, particularly for soft soils.

A number of studies have analytically evaluated the seismic response of typical Multi Span Simply Supported (MSSS) and Multi Span Continuous (MSC) steel girder bridges in order to better understand the seismic behavior and impact of modeling fidelity on the performance of these bridges. Dicleli and Bruneau (1995) found that bearing stiffness significantly affects the response of MSSS steel girder bridges, and indicated that if pounding were considered in the longitudinal direction, there could be a large potential for shearing of bearings and span unseating; for MSC bridges, damage to steel bearings is

probable, but may serve as an effective way of isolating the superstructure and preventing further column damage.

DesRoches and Muthukumar (2002) investigated the effect that pounding and restrainers have on the global demand of bridge frames in multiframe bridges and showed that the primary factors affecting pounding were the frame stiffness ratio or period ratio of adjacent frames in a bridge and the ground motion effective period ratio. Pounding increases when the two frames are highly out-of-phase and reduces when the frames vibrate near the characteristic time period of the ground motion. Also, the effect of restrainers was evident significantly in highly out-of-phase frames and was marginal in other cases.

Padgett and DesRoches (2008) evaluated the three-dimensional nonlinear seismic performance of retrofit measures for typical steel girder bridges; they showed that use of elastomeric bearings in MSC bridges increased passive deformations from 17.4 to 29.0 mm due to pounding. Pan et al. (2007, 2010) performed parametric studies to evaluate seismic fragility of MSSS highway bridges and showed that pounding of girders at abutments may lead to a change in curvature ductility of the concrete piers.

Li (2013) studied the effect of abutment excitations on seismic pounding in bridges. Bi and Hao (2012) performed a detailed 3D analysis to understand pounding between girders and between bridge girders and the corresponding abutment of a two span simply supported bridge subjected to spatially varying ground motions. The results showed that 1D excitations overestimate the pounding forces as 2D excitations lead to eccentric pounding, which has more pounding events but smaller pounding forces. Permanent girder displacements of up to 100 mm were also observed in the analysis. However, soil structure interaction was not considered in the analysis.

Huo and Zhang (2013) used the fragility function method to study the effects of pounding and skewness on the seismic behavior of typical multispan RC highway bridges. Accelerations in pounding cases were five to ten times more than those without pounding and severity of damage increased with irregularity in the bridge structure.

However, a different modeling methodology may lead to different results, as shown by Kaiming et al. (2012), who studied the pounding response of bridge structures to spatially varying ground motions. A 3D finite element model was used; a lumped mass model and a beam model were suitable only for longitudinal response. The study showed that pounding resulted into smaller mean peak displacements in the longitudinal and transverse direction but larger mean peak torsional responses. Nielson and DesRoches (2006) studied the influence of modeling assumptions on the seismic response of multispan simply supported steel girder bridges in moderate seismic zones. The study showed the importance of the selection of appropriate modeling parameters.

1.1 Bridge Retrofit

EL-Bahey and Bruneau (2011, 2012) performed nonlinear time history analysis using BRBs as structural fuses for the retrofit of bents of concrete bridges and presented a design procedure for BRBs. The design procedure was found satisfactory and was similar to the procedure available in the AISC (2010) manual but with modified values. Capron (2003) retrofitted a bridge using shock transmission type longitudinal restrainers at expansion piers, between concrete blocks and steel bumpers for increased transverse force transfer capacity. Time-history analysis of the retrofitted bridge showed that the restrainers provided significant longitudinal displacement control. Shock transmission devices allow

slow thermal expansion movements but resist relatively fast movements. Kanaji et al. (2003) used BRBs to retrofit the Minato Bridge, one of the longest steel truss bridges.

Andrawes and DesRoches (2007) used shape memory alloy (SMA) seismic restrainers for possible retrofit of a bridge and compared the performance with steel cable restrainers, metallic dampers and visco-elastic dampers using OpenSees 2D analysis. The sensitivity analysis showed that all devices except the steel restrainers performed well. Tension-only behavior of the steel restrainers combined with the yielding behavior of steel results in an accumulation of residual displacement. Tension only SMA devices were 34% more effective in compared to the steel restrainers. Padgett and DesRoches (2008) and Zhou and Meng (2011) showed that use of cable restrainers to mitigate pounding can be effective in multispan continuous steel girder bridges.

Raheem (2009) presented results from a nonlinear analysis on a multispan steel girder bridge by idealizing it as a two-dimensional nonlinear numerical finite element model utilizing three types of restrainer configurations at the expansion joint. Pounding reduced the segment displacement response when vibrating near the characteristic period of the ground motion and increased the adjacent segment response. The restrainers attached through the bent cap to the girders perform better in preventing unseating of the girders and reducing the displacements between superstructure and substructure. The study showed that by using shock absorbers between the bridge segments or the restrainers' ends as potential practical mitigation measures against impact due to pounding, the sudden changes of stiffness can be smoothed. However, the shock absorbers do not work once restrainer rods fail in earthquakes.

Reno and Pohll (2013) presented a possible retrofit of a steel bridge with BRBs at both

the ends to avoid pounding and presented satisfactory results from numerical analysis. However, the study did not state any consideration of soil-structure interaction for the analysis. Sun et al. (2013) used BRBs as possible energy dissipators in dual piers in a cable stayed bridge. However, the study did not find the use of BRBs in dual piers to be effective.

Much of the research used BRBs in the transverse direction as a cross fuse element; Celik and Bruneau (2009, 2012) used BRBs in both the transverse and longitudinal directions. Celik and Bruneau developed closed-form solutions for two retrofit schemes for straight and skewed steel girder bridges using BRBs in ductile end diaphragms. The purpose of the retrofit scheme was to reduce the seismic demand in the superstructure by hysteretic energy dissipation. No time-history analysis was performed to support the closed-form solutions.

1.2 Soil-Structure Interaction

Not many studies have been performed regarding pounding damage to bridges considering soil-structure interaction (SSI) (Ingham et al. 1999; Konagai et al. 2002). However, the literature shows that SSI has a significant role in determining the behavior of a bridge. Makris and Zhang (2002) performed a nonlinear numerical analysis of a freeway overcrossing equipped with elastomeric bearings and fluid dampers. A parametric study of nonlinear seismic response of the bridge accounting for the effects of soil-structure interaction showed that fluid dampers reduced the large displacements and accelerations at the deck ends. Also, soil-structure interaction increased the displacements and forces at the abutments.

Soneji and Jangid (2008) studied the effect of soil-structure interaction on the response

of a seismically isolated cable-stayed bridge. Time-history analyses showed that depending on the ground motion, the displacement response of the bridge varied to a large extent when SSI was taken into account. SSI increased the fundamental period of the structure which changed the spectral acceleration range for response and the displacement controlled behavior dominated. However, as the stiffness of the soil strata increased, the effect of SSI diminished. Konagai et al. (2002) presented a single beam analogy for a pile group which shows that using appropriate values for soil and pile stiffness, a pile group can be considered as a single pile which makes numerical analysis feasible.

Review of the research shows that there have not been enough investigations of pounding damage in curved steel girder bridges taking soil-structure interaction into consideration. Recognizing the complexities involved with the bridge pounding problem, this study is an attempt to examine the retrofit measures with Buckling Restrained Braces for an existing curved bridge on pile foundations in soft soil.

2. MODELING OF CURVED BRIDGE INCLUDING SOIL-STRUCTURE INTERACTION

A nonlinear time history analysis has been performed taking nonlinearity of bearings, restrainer rods and soil springs into account. Two spans of an existing bridge in Salt lake City, span 2 (from bent 5 to bent 10) and span 3 (bent 10 to abutment 15), have been modeled in SAP 2000 Nonlinear. Three-dimensional beam elements, with six degrees of freedom at each node, and section properties of different elements assigned according to the construction drawings available, have been used to model the girders of the superstructure. The bridge consists of a reinforced concrete deck supported on three steel girders which are robustly connected with each other via cross-frames at every 15 feet. This truss assembly helps the superstructure to act as a continuous deck with effective strength much higher than the individual girder thus, minimizing deck displacements. These cross-frames are connected to the main girders through bolted joints, details of which are provided in the fabrication drawings provided by UDOT (1998). For computer analysis, the connection between cross-frames and girders has been considered as rigid and modelled using a rigid link; cross-frames have been assigned moment release at the ends to simulate the pinned connections in the cross-frames.

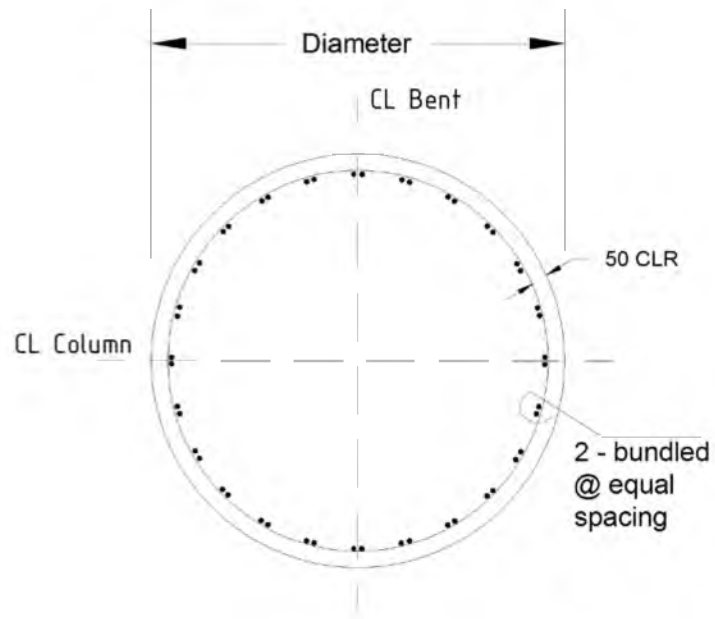
2.1. Soil-Structure Interaction

The beam column elements used to model the columns have concrete section properties as per the design drawings (Appendix A). The diameter of the columns varies from 1.980 m to 2.100 m and the height of the columns from 12.5 m to 18 m. Section properties of the columns and reinforcement details along with confining steel have been given in Table 2.1 and Fig. 2.1. Mander's (1988) confinement model which is available in SAP 2000[®] has been used in the plastic hinge regions. All reinforcing steel complies with ASTM A706 grade 60 and the 28-day compressive strength of concrete is assumed as 25 MPa. Pier cap beams are nonprismatic and therefore, nonprismatic sections have been generated and assigned to the beam elements representing the beams. The connection between the pier cap and the column is considered as rigid; the joint is designed to fail only after the column develops plastic hinges at top and bottom of the column. All bents are single column bent which makes it unlikely to develop a plastic hinge in the beam.

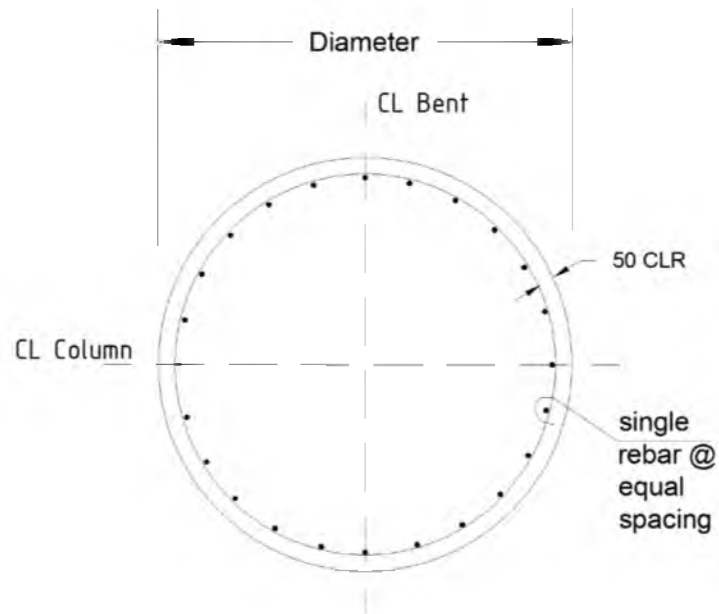
Table 2-1 Sectional and reinforcement details for the columns

Column No.	Diameter (m)	Vertical Rebar # - bar size	Spiral Rebar @ mm
6	2.314	#36 Total 48	#22 @60
7	1.981	#36 Total 52	#22 @76
8	2.134	#36 Total 44	#22 @76
9	1.981	#36 Total 44	#22 @76
10	1.981	#36 Total 32	#22 @76
11	2.134	#36 Total 64	#22 @60
12	1.981	#36 Total 36	#22 @79
13	2.134	#36 Total 36	#22 @76
14	2.134	#36 Total 56	#22 @63

Note- Refer to Appendix B for bar sizes.



(a)

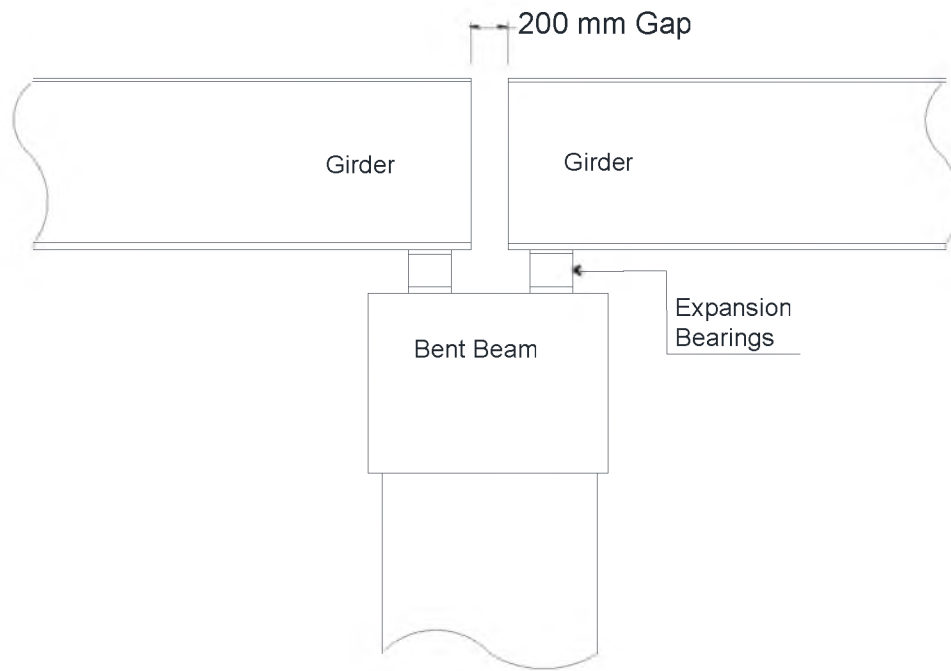


(b)

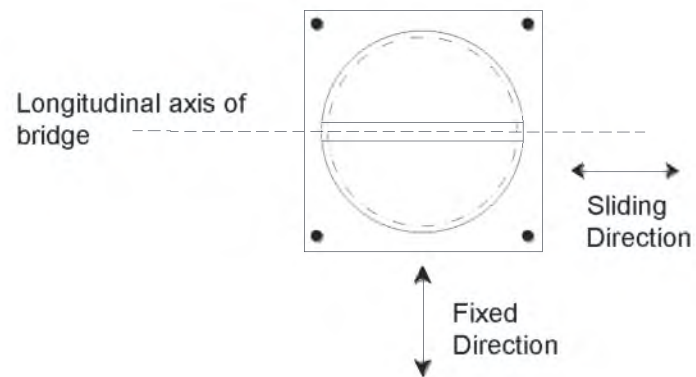
Figure 2.1 Section details for (a) column 6, 7, 8, 9, 11, 14 and, (b) column 10, 12, and 13.

The girders rest on bearings which are connected to the pier cap with grouted bolts. Except at the expansion joint and the abutments, all bearings are of the rocker type, and are restrained in translation but free in rotation about the vertical axis. These bearings have been modeled with linear link elements with free rotation about the vertical axis. The bearings at the abutment and expansion joint are ‘expansion type’ and free to slide in the longitudinal direction of the girders. The expansion pot bearing at bent-10 is shown in Fig. 2.2. Pot bearings consist of two layers of steel plate, with the top layer sliding, longitudinally or rotationally, on the bottom layer. Both layers are coated with PTFE (Polyethylene Tetra Fluoro Ethylene) which has a very low coefficient of friction and helps in sliding. Rotation type pot bearings have the top layer sitting in a pot type bottom layer while unidirectional expansion pot bearings have a bar, attached to the top layer, sliding in a groove in the bottom layer, to direct the translation. Expansion pot bearings are modeled using nonlinear link elements. The force-displacement relationship for the link elements was determined using the allowable load on the expansion bearings in the vertical and lateral direction. For the longitudinal direction, a coefficient of friction between PTFE sheets was assumed as 0.05 to 0.08. The backbone curve used for link element to simulate expansion bearing is shown in Fig. 2.3.

Evaluation of the effects of soil-structure interaction on the behavior of the bridge is a central part of this study; the soil was modeled using nonlinear link elements with a kinematic hysteretic rule. The bridge bent foundations have rigid pile-caps and the pile groups vary from 24 piles to 30 piles. Foundation-soil interaction was simplified by performing separate calculations for spring constants of the soil and piles. The pile diameter is 624 mm and the pile-cap thickness varies from 1.050 m. to 1.200 m.



(a)



(b)

Figure 2.2 Expansion joint (a) side elevation and (b) plan of expansion pot bearing

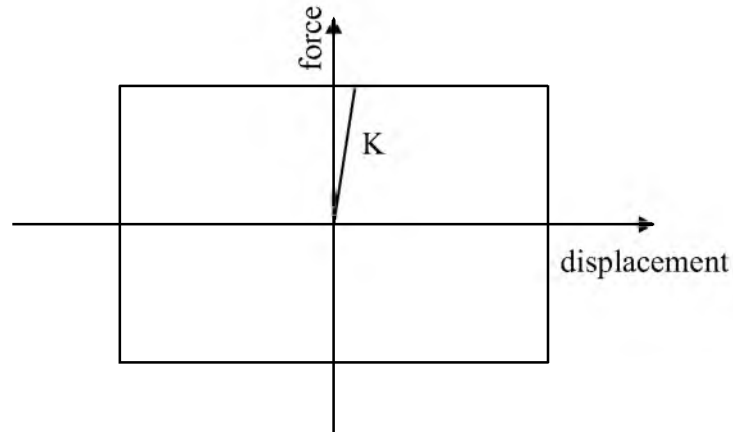


Figure 2.3 Analysis model for friction in expansion bearing

Soil-pile interaction is generally modeled with the help of P-y springs, which vary with the depth along the pile. The P-y curve for a soil spring depends on the diameter of the pile, soil unit weight and the stresses at that particular depth. Using the soil borehole data provided with the drawings, P-y curves at different depths for one pile at each bent have been calculated. Then the group P-y curves have been calculated by multiplying the P-y curves for single pile with the group participation factors for piles in a pile group.

The participation factors recommended by AASHTO LRFD have been used in this study. The soil spring for pile-cap has been calculated following guidelines of the FEMA 356 (4.4.2.1) document. Appendix I of the thesis shows that the spring constant for the pile-cap is much higher than the spring constant for the pile-group for given soil conditions. Assuming the soil to be nonliquefiable, the soil spring for the pile-cap dominates the behavior of the foundation. Therefore, the pile-cap was modeled as a point mass with soil springs in two principal directions (Fig. 2.4).

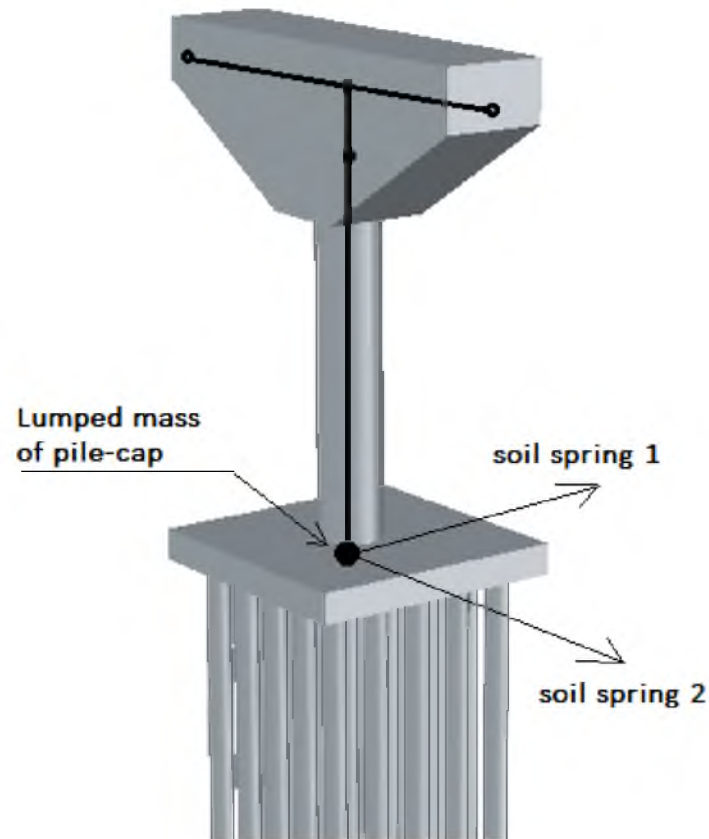


Figure 2.4 Simplified pile-cap model in SAP 2000

The California Department of Transportation (Caltrans SDC 2010) recommends a spring constant for the abutment, which includes the piles and the abutment wall length. The following equation, based on results from large-scale abutment testing at UC Davis (Maroney 1995) is recommended for soil-spring constant at the abutment,

$$k_a = k_s + k_p$$

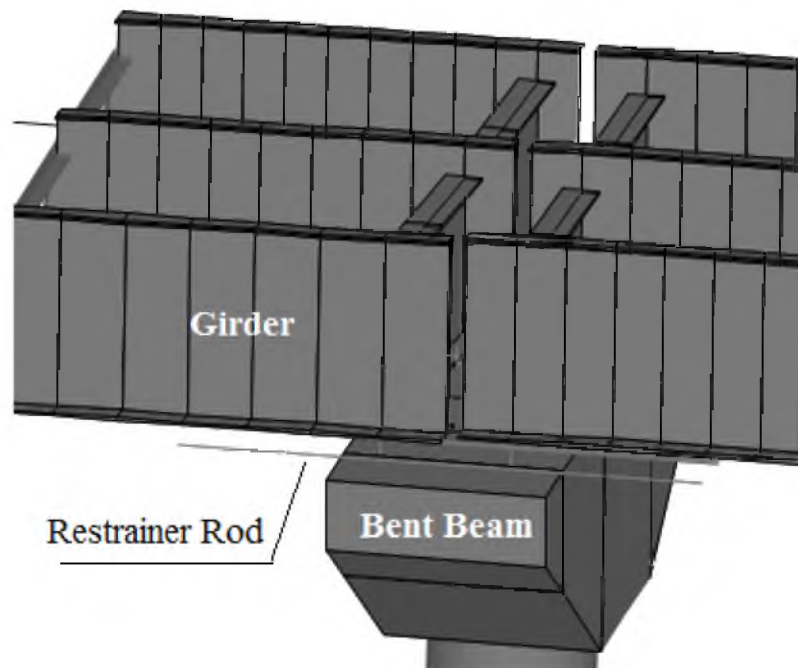
$$k_s = 115 \left(\frac{kN}{m} \right) \cdot B \quad , \text{ and } k_p = 7 \left(\frac{kN}{m} \right) \cdot n_p$$

Here B represents the effective abutment width and n_p is the number of piles. In the transverse direction, the effective width B is taken as the length of the wing walls multiplied by a factor for wall effectiveness ($C_L = 2/3$) and participation coefficient ($C_W = 4/3$) to account for differences in participation of both wing walls.

One of the critical components of a bridge is the expansion joint, which must allow traffic to cross the bridge structure while permitting movement of the bridge deck due to thermal effects, wind, traffic loading and seismic effects. Since the characteristics of the expansion joint have a major influence on the seismic performance of bridge structures, they must be modeled accurately. The existence of a gap introduces nonlinearity into the seismic analysis of the structure. The unidirectional pot bearing at the expansion joints, increases the possibility for the girders to experience large displacements during seismic events. To restrict large displacements, steel restrainer rods with a 40-mm diameter and 3600 mm length are deployed at this bridge; these are connected to both girders at either end with a bolted assembly. The restrainer rods improve the performance of bridges in an earthquake but may fail if the axial load is higher than the maximum allowable load. Fig. 2.5 (a) and (b) show the restrainer rod arrangement for the bridge under investigation. Previous studies have shown that pounding between two structural components depends on the coefficient of restitution, which is used to define damping during the impact (Anagnostopoulos 2004). Experimental studies and mathematical models to obtain load-time history during the pounding between two structures can be found in the literature (Mier et al. 1989; Jankowski 2005, Takabatake et al. 2014). Generally, a linear force-deformation relationship is used to define the pounding force which can estimate elastic forces developed between the two structural components. Nonlinear spring models like the



(a)



(b)

Figure 2.5 Expansion joint with restrainer rod (a) site photograph and (b) SAP 2000 model

Hertz model, a general nonlinear model and Jankowski's model have also been used to simulate the pounding behavior more realistically (Pantelides and Ma 1998; Takabatake et al. 2014).

A linear force-deformation model is used to simulate pounding in this study. The external nodes of adjacent girders are linked using nonlinear gap elements to model the impact forces resulting from pounding between girders, and between girders and abutment. The force-deformation characteristics of such elements are shown in Fig. 2.6. The gap-type link element doesn't provide any stiffness in the tension direction. While closure of the gap, in compression, the stiffness K_i is activated once the gap is closed completely. Spring stiffness, K_i , is fixed and is equal to the axial stiffness of the neighboring structural segments. Through a sensitivity analysis of the impact element stiffness using a nonlinear time history analysis for a wide range of impact element stiffness of this bridge model, K_i is taken equal to 1.39 GN/m. A simplified computer model for bent 10 is shown in Fig. 2.7 which has a single soil spring for each degree of freedom and four impact elements between concrete shear keys and steel shear keys.

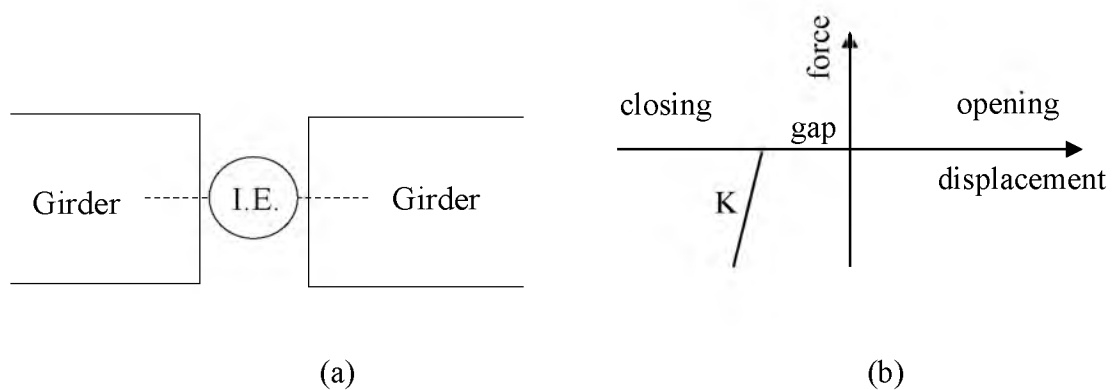


Figure 2.6 Impact element (I.E.) (a) location and (b) analysis model

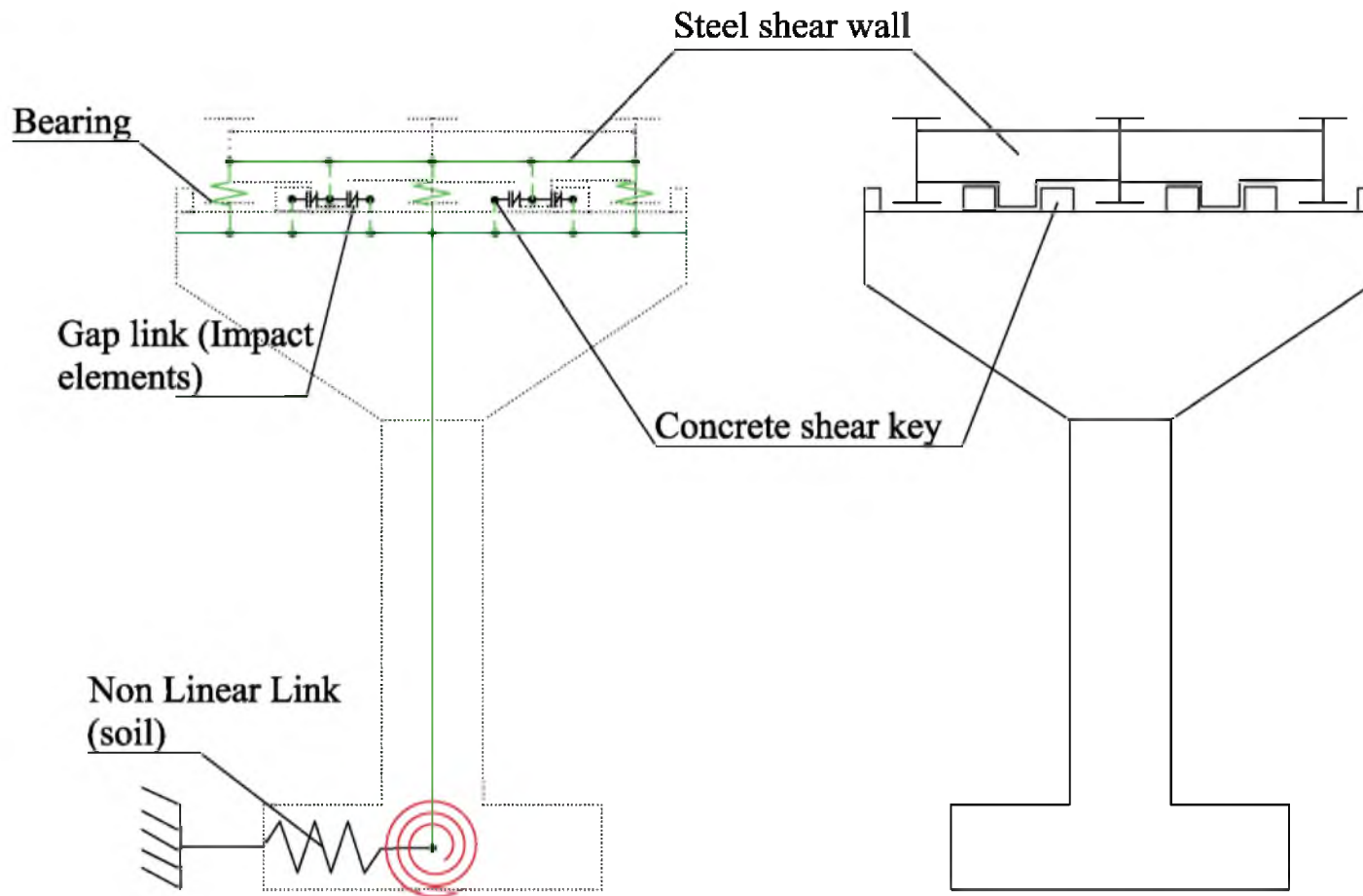


Figure 2.7 SAP 2000 model for the bridge bent

This study recommends use of Buckling Restrained Braces (BRB) to mitigate the pounding forces at the abutment and expansion joints. BRBs are a widely used metallic energy dissipater for the seismic protection of buildings and other structures. They normally provide hysteretic energy dissipation by restraining a steel core against global buckling behavior and hence can achieve stable yielding in both tension and compression. Nonlinear link elements with kinematic hysteretic rule have been used to model BRBs in this model. The force-deformation curve has been adopted from various tests performed on BRBs by Xu (2016), as shown in Fig. 2.8, and parameters for the SAP 2000 model have been adopted through sensitivity analysis by performing cyclic load tests on a single BRB element. A detailed sensitivity analysis is presented in Chapter 3 of this thesis.

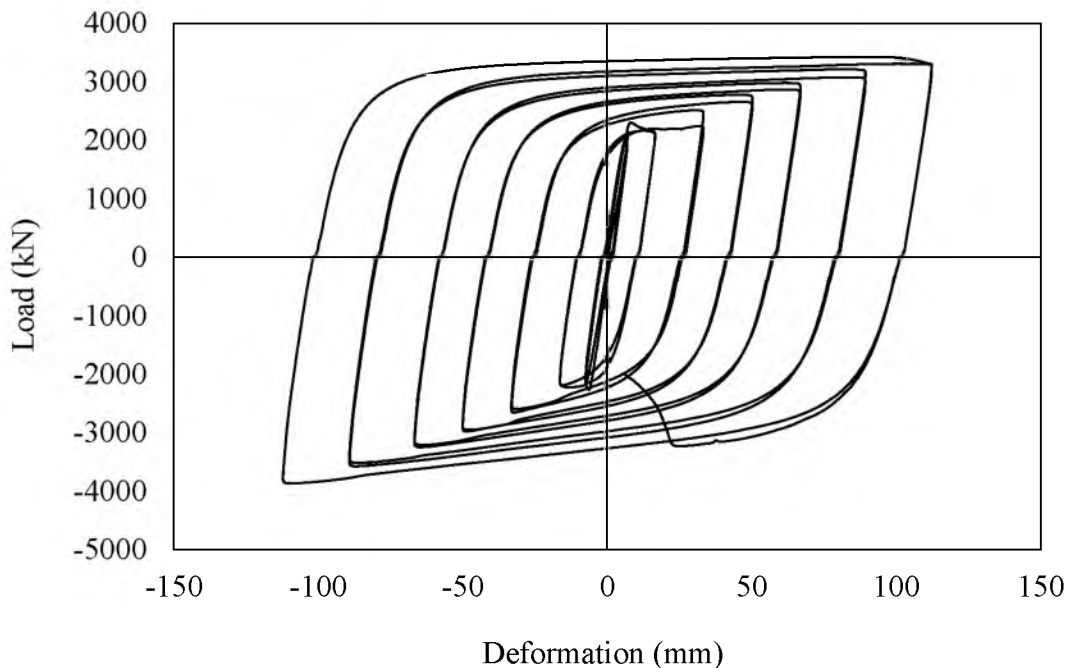


Figure 2.8 BRB hysteresis (Xu, forthcoming dissertation 2016)

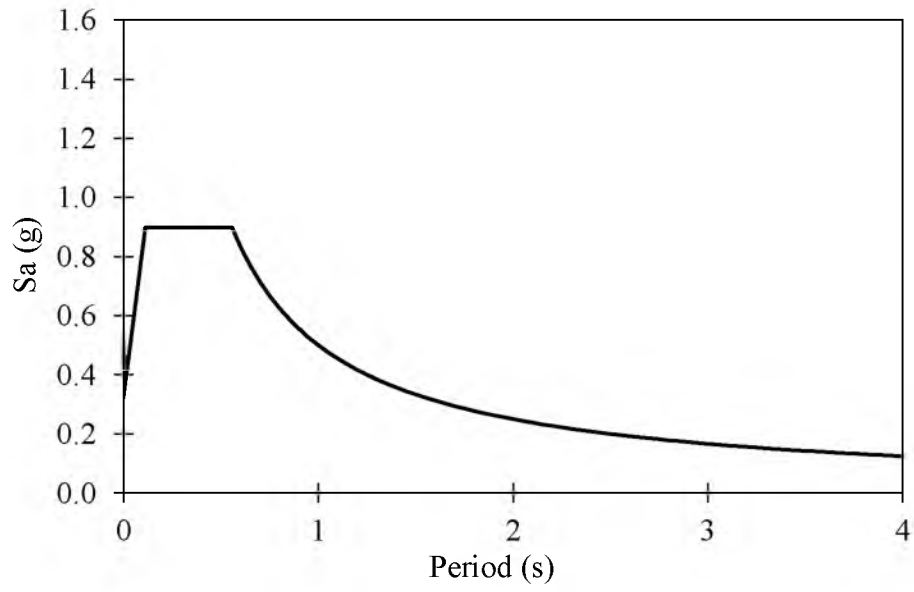
In this study, it is assumed that the connection between the BRB and steel girder or abutment concrete does not fail. Thus, this study investigates the possible use of BRBs to retrofit bridges vulnerable to pounding damage. Material deterioration due to pounding and connection details of BRBs to structural members are not within the scope of this research.

2.2. Ground Motion Data

A combination of pulse type and long period earthquake ground motions is selected for time-history analysis. The Pacific Earthquake Engineering Research Center (PEER) strong motion database was searched by using a target spectrum obtained using ASCE -7 (2010) documentation and 15 ground motions, given in Table 2.2, were selected for the study. FEMA P-752, NEHRP Recommended Provisions, Section 16.1.3 requires the use of at least three ground motions in any response history analysis. When at least seven ground motions are used, Sections 16.1.4 and 16.2.4 permit the use of average response quantities for design. The objective of the response history analysis is not to evaluate the response of the structure for each record, but to determine the expected average response. This procedure helps in reducing the effort and time required to analyze the seismic response of a structure. Horizontal design response spectrum and Risk-Targeted maximum considered earthquake (MCE_R) response spectra for the Salt Lake City site of the existing bridge are developed using the USGS design maps tool (Fig. 2.9). The soil data provided by Utah department of Transportation (UDOT) suggests the soil to be between soft to stiff clay and hence the site to be of class D. The ground-motions are matched to the target spectrum using SeismoMatch (Seismosoft® 2013) software. Fig. 2.10 shows the matched 5% damping elastic spectra of the ground motions (Fig. 2.11 to Fig. 2.24) used in this study.

Table 2-2 Ground motions used for time-history analysis

ID	Earthquake Name	Year	Station Name	Magnitude	Fault
1	Parkfield	1966	Cholame - Shandon Array #12	6.19	strike slip
2	San Fernando	1971	Santa Felita Dam (Outlet)	6.61	Reverse
3	Imperial Valley	1979	Cerro Prieto	6.53	strike slip
4	Irpinia Italy	1980	Rionero In Vulture	6.2	Normal
5	Chalfant Valley	1986	Bishop - Paradise Lodge	5.77	strike slip
6	Duzce Turkey	1999	Lamont 1061	7.14	strike slip
7	Manjil Iran	1990	Abbar	7.37	strike slip
8	Northridge	1994	Newhall	6.7	strike slip
9	Kobe	1995	KJMA	6.9	strike slip
10	Chi-Chi Taiwan-03	1999	TCU074	6.2	Reverse
11	Cape Mendocino	1992	Loleta Fire Station	7.01	Reverse
12	Landers	1992	North Palm Springs Fire Sta #36	7.28	strike slip
13	Chuetsu-oki Japan	2007	Ojiya City	6.8	Reverse
14	Iwate Japan	2008	Tamati Ono	6.9	Reverse
15	Iwate Japan	2008	Semine Kurihara City	6.9	Reverse



(a) Design response spectrum

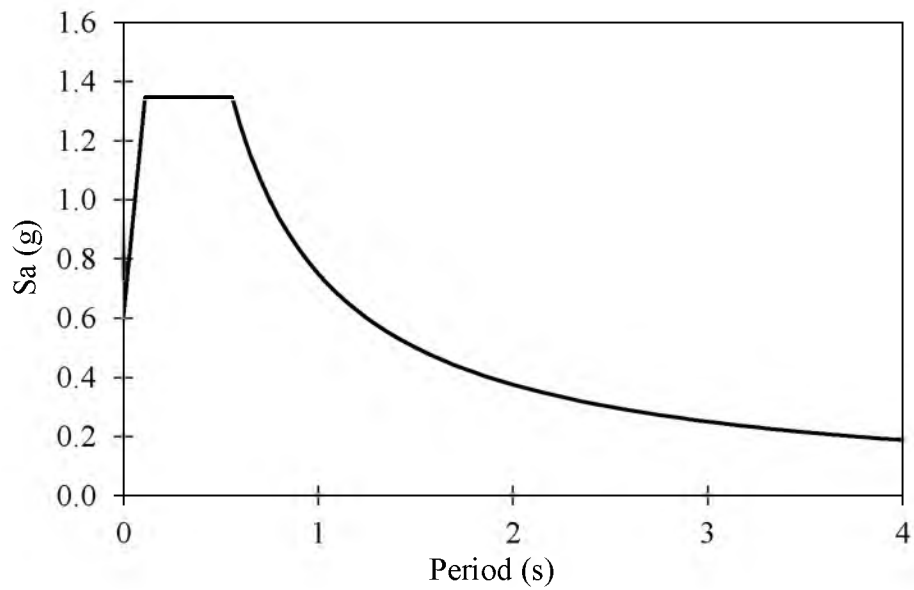
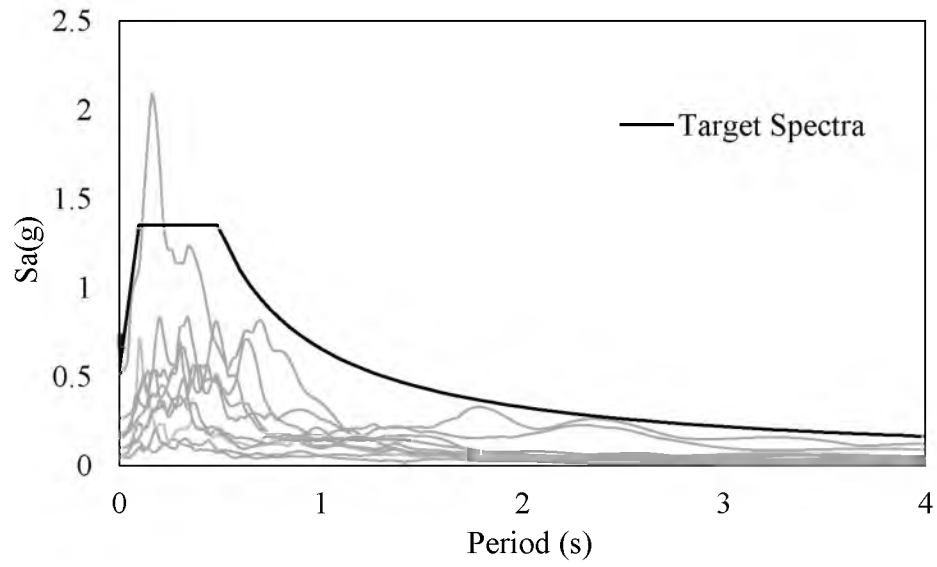
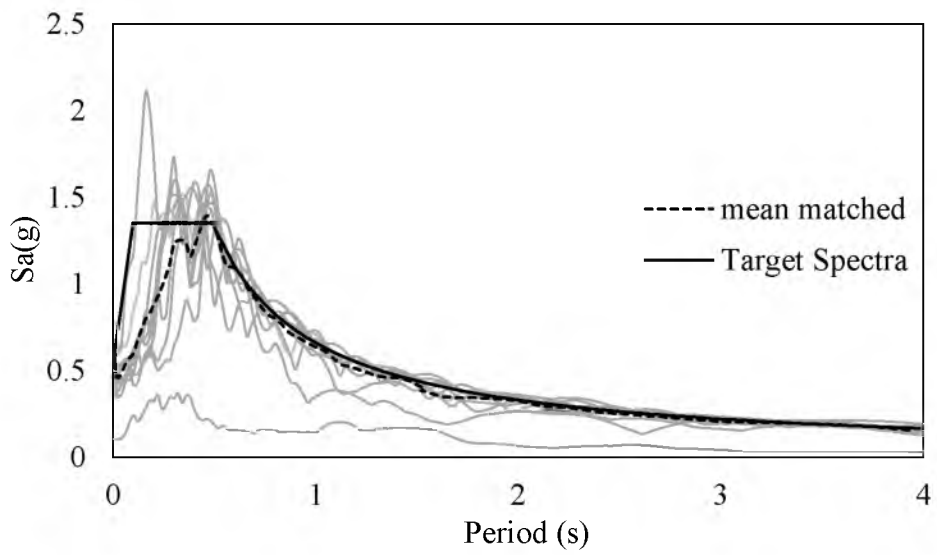
(b) Risk-targeted MCE_R

Figure 2.9 5% damped elastic response spectra for the site



(a)



(b)

Figure 2.10 Acceleration response spectra of selected ground motions. (a) Unmatched and (b) matched

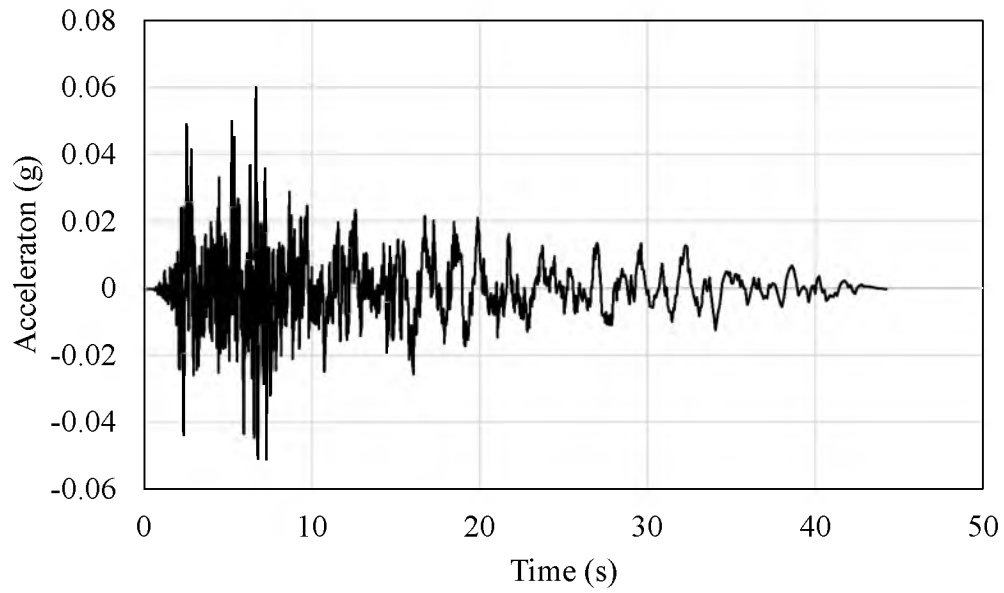


Figure 2.11 Parkfield, 1966, Cholame – Shandon Array

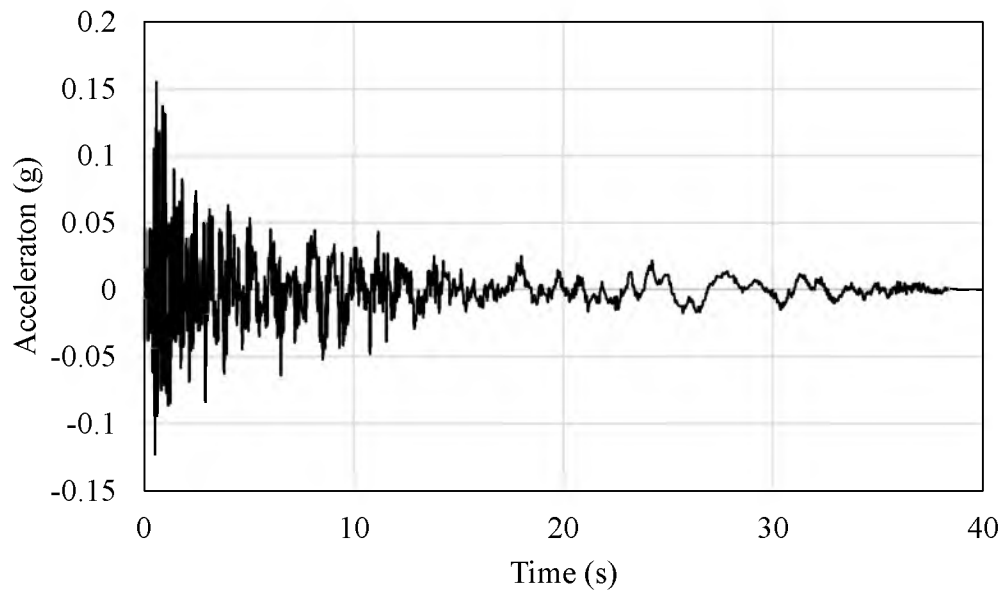


Figure 2.12 San Fernando, 1971, Santa Felita Dam (Outlet) Station

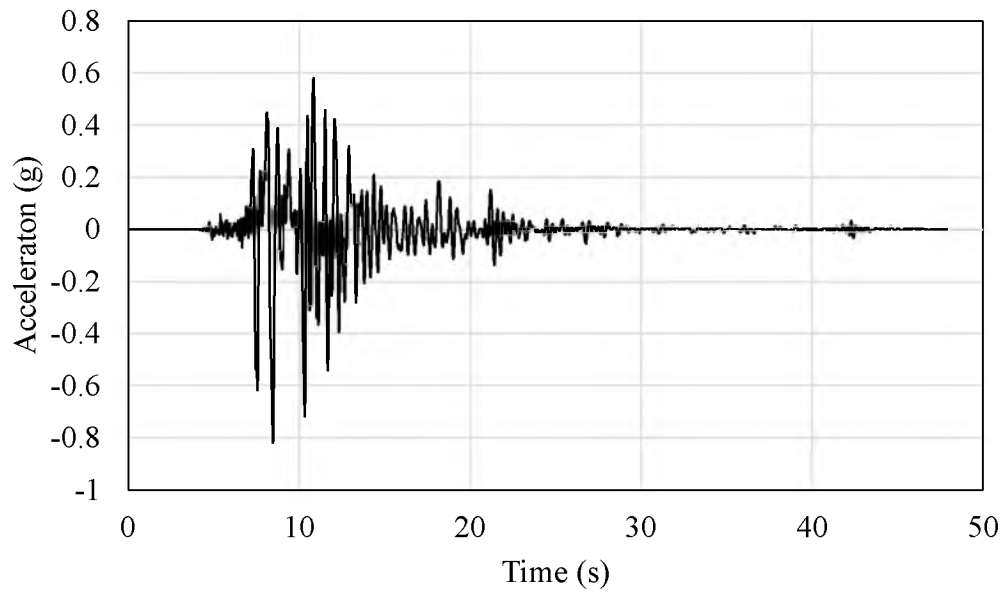


Figure 2.13 Kobe, 1995, Japan

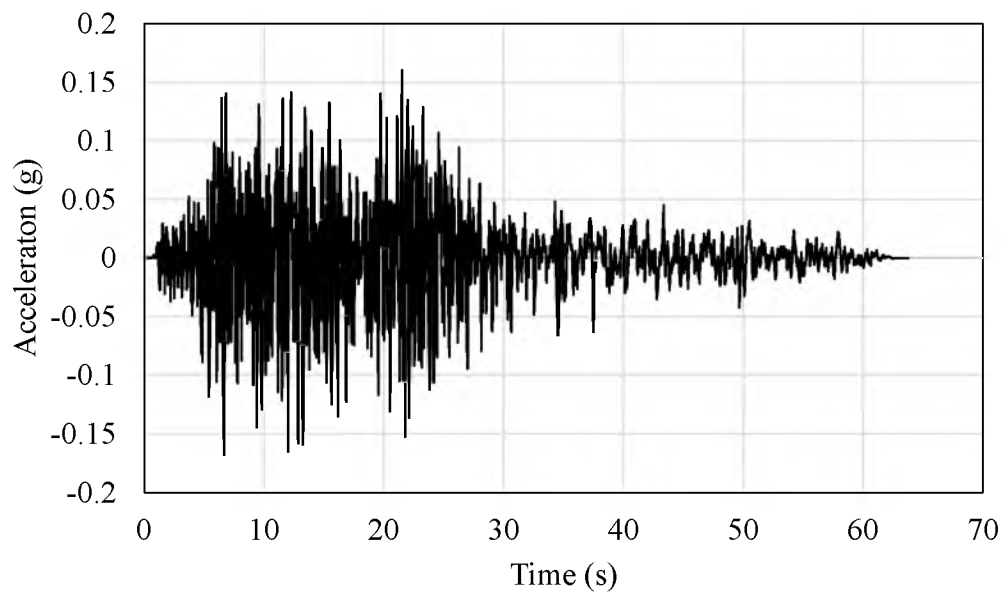


Figure 2.14 Imperial Valley, 1979, Cerro Prieto Station

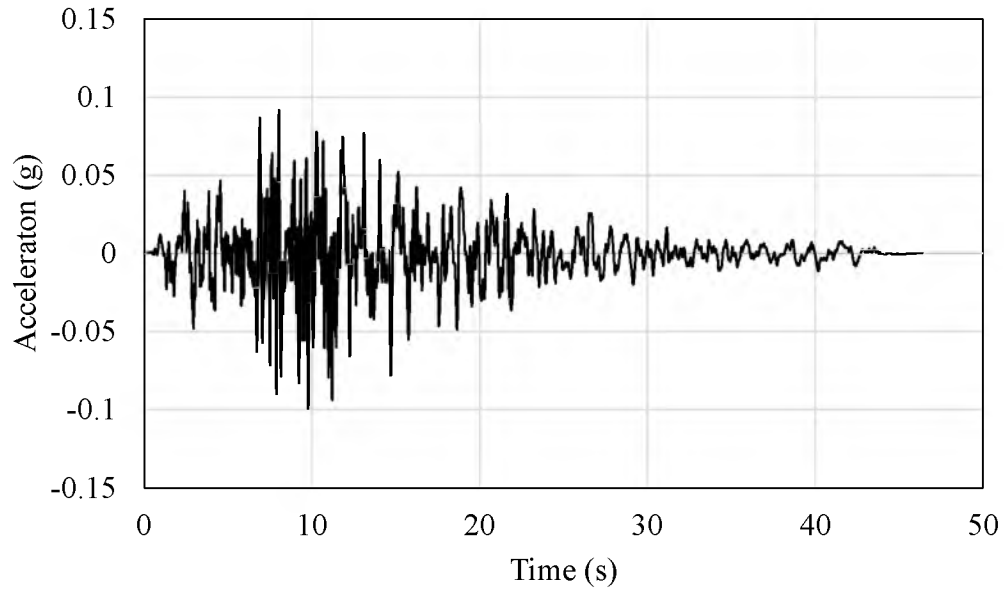


Figure 2.15 Irpenia – Italy, 1980, Rionero In Vulture Station

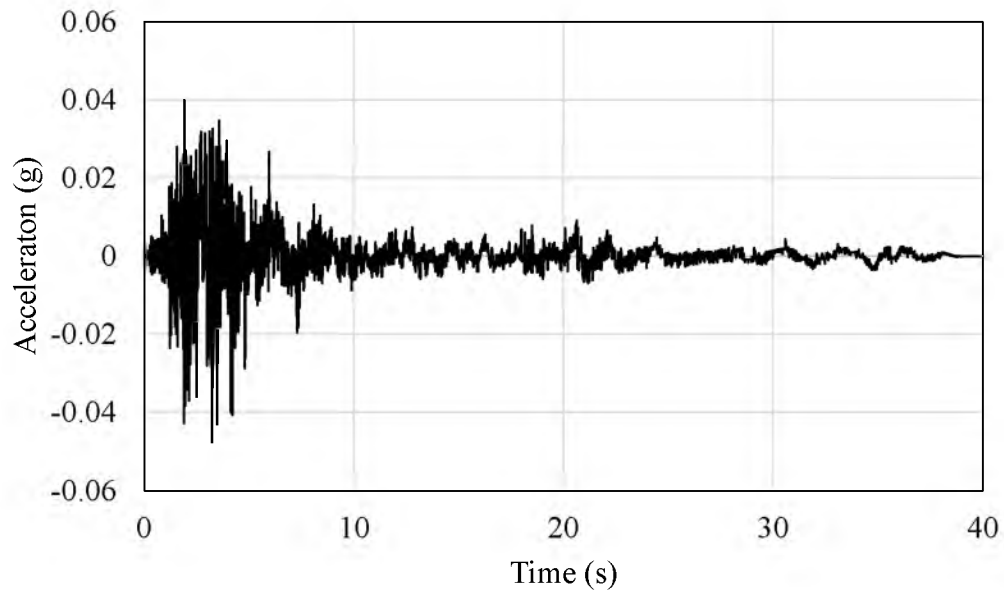


Figure 2.16 Chalfant Valley, 1986, Bishop-Paradise Lodge Station

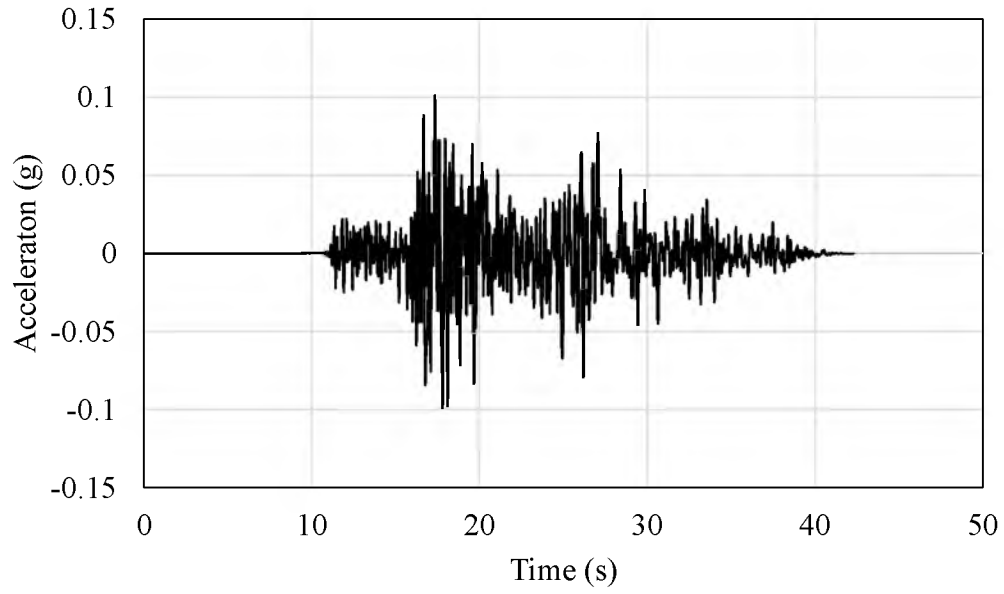


Figure 2.17 Duzce – Turkey, 1999, Lamont 1061 Station

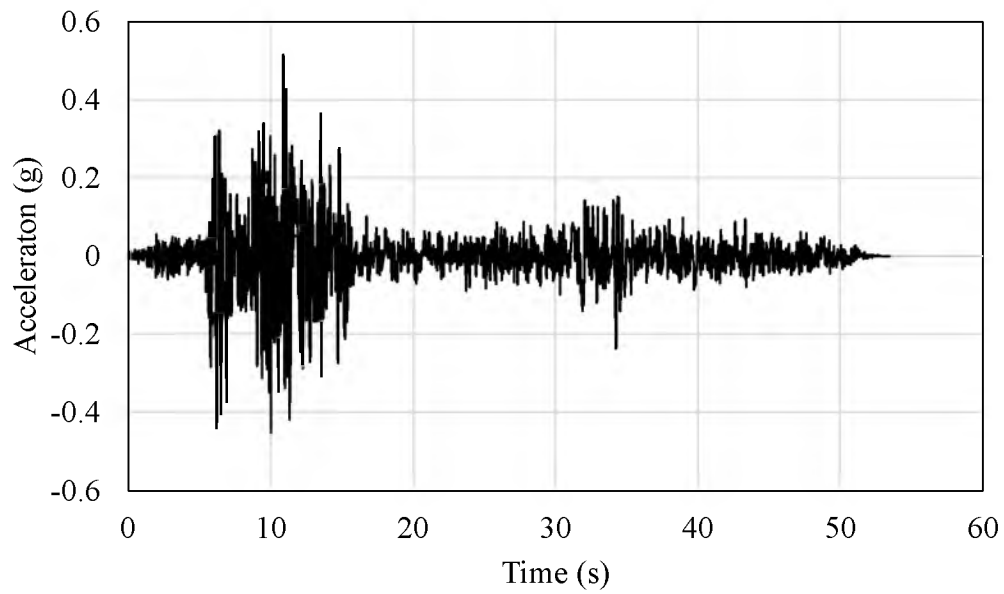


Figure 2.18 Manjil – Iran, 1990, Abbar Station

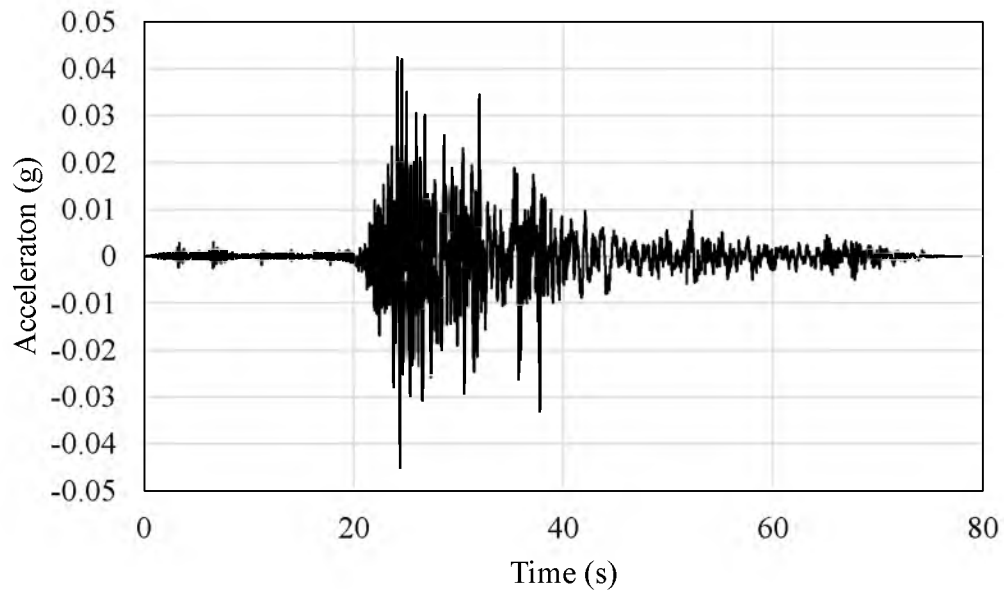


Figure 2.19 ChiChi – Taiwan, 1999, TCU074 Station

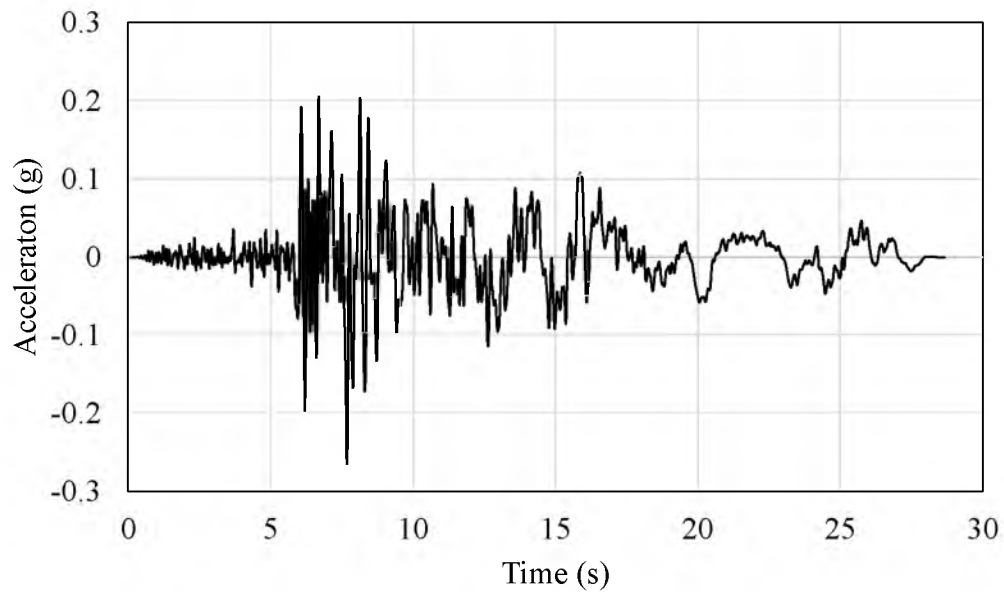


Figure 2.20 Cape Mendocino- USA, 1992, Loleta Fire Station

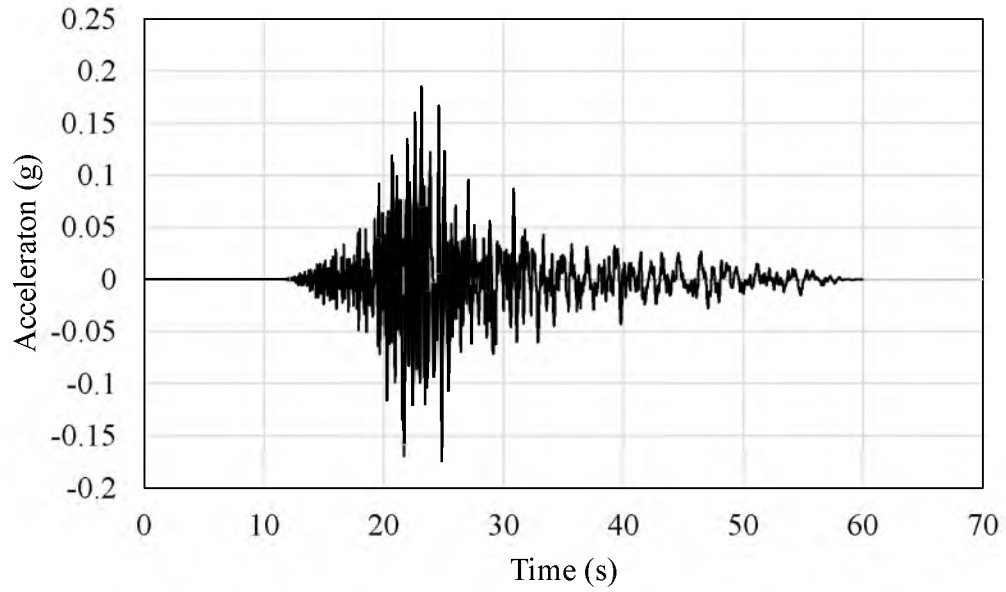


Figure 2.21 Chuetsu-oki, Japan, 2007, Ojiya City Station

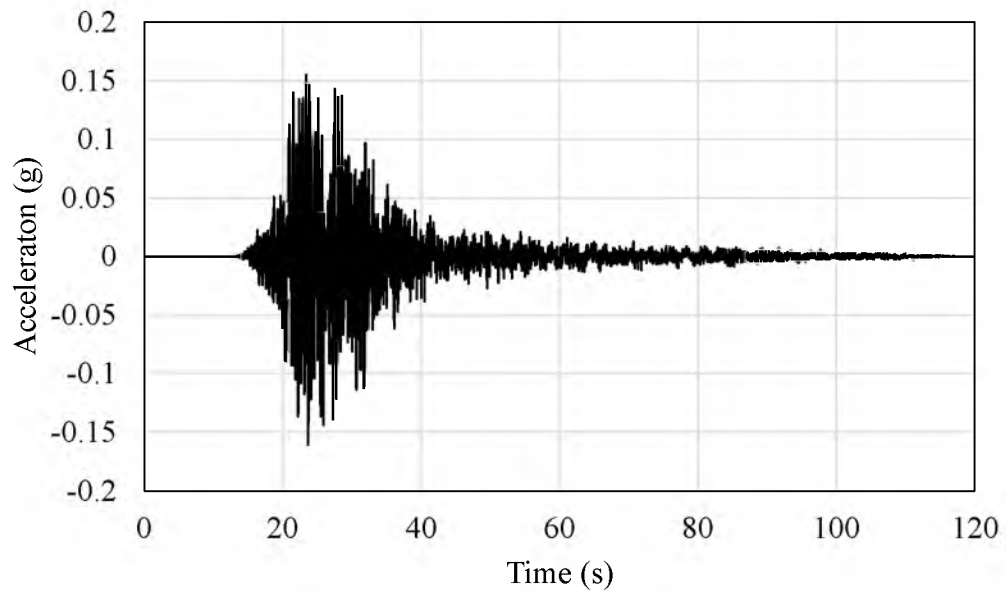


Figure 2.22 Iwate – Japan, 2008, Semine Kurihara City Station

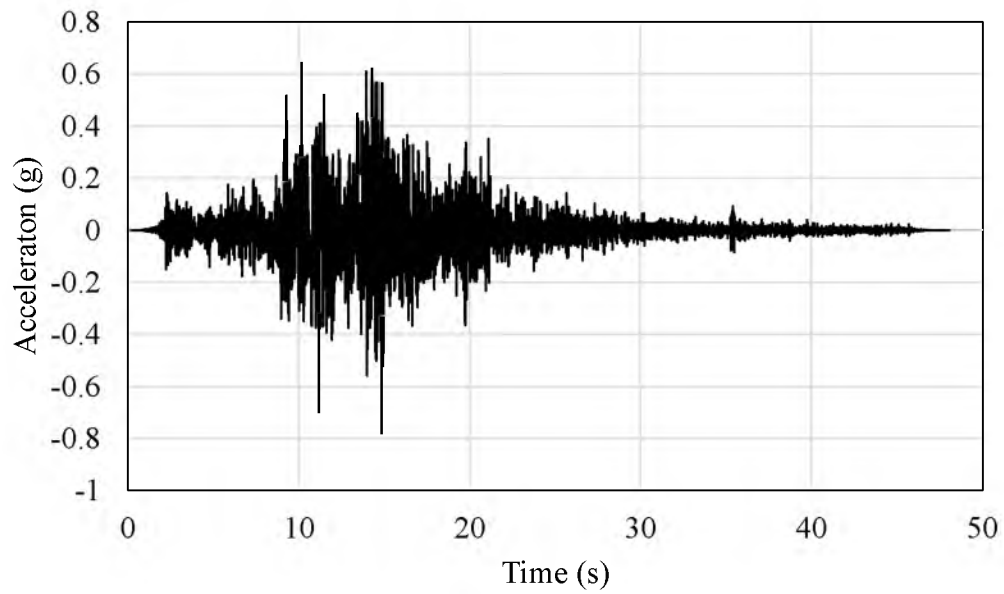


Figure 2.23 Landers, 1992, North Palm Springs Fire Station #36

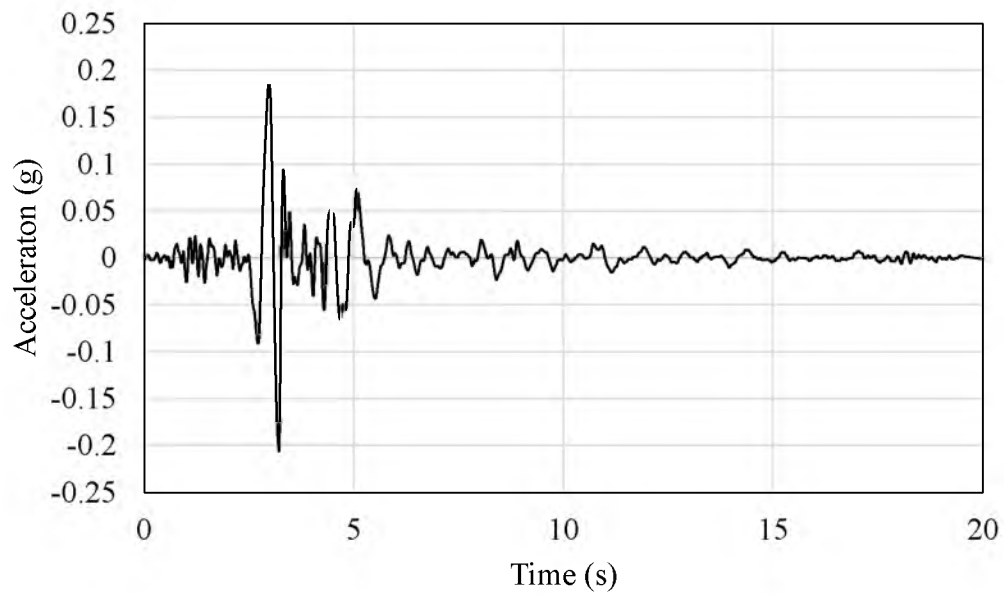


Figure 2.24 Northridge, 1994, Newhall Station

3. BRB MODEL VALIDATION

Kinematic behavior is characterized by the shift of the neutral position, whereas isotropic behavior is characterized by enlargement of hysteresis. BRBs show isotropic behavior when subjected to cyclic loading which is combined with Kinematic hardening towards the end cycles. The postyield stiffness ratio changes with the number of cycles (Black et al., 2004). In order to predict the behavior of the bridge, it is important to validate the BRB element used for the analysis. SAP 2000[®] has nonlinear link elements which can be used with Kinematic, Takeda, and Pivot hysteresis rules to model different types of properties. To select the best-fit back-bone curve as an input for SAP 2000[®] the BRB multi-linear plastic link element with Kinematic hysteresis was used, and five models were analyzed. Hysteretic energy dissipated (both total and in each cycle) in all SAP 2000[®] analyses was compared with the energy dissipation in laboratory tests (Xu 2016). Table 3.1 and Fig. 3.1 show the different backbone curves analyzed in SAP 2000[®].

The test loading protocol used for PB 500 (Xu 2016) was used for the SAP 2000[®] model to keep the loading conditions consistent. The loading protocol, as shown in Fig. 3.2, is a 'sine' displacement based curve which was divided into 6 steps and each step has 2 cycles. The quantities presented in Table 3.1 are D_y (yield deformation), D_U (ultimate deformation), F_y (yield force) and F_U (ultimate force). While presenting deformation in all the tables and figures, positive values show tension and negative values show compression in BRB.

Table 3-1 Test model back-bone curves subjected to cyclic test in SAP 2000®

Test No.	+D_y	+D_U	+F_y	+F_U	-D_y	-D_U	-F_y	-F_U
	mm	mm	kN	kN	mm	mm	kN	kN
BL 1	5.99	119.89	2566.61	3202.70	-5.99	-119.89	-2566.61	-4003.38
BL 2	7.62	119.89	2721.60	3202.70	-7.62	-119.89	-2721.60	-4003.38
BL 3	7.03	119.89	2891.33	3202.70	-7.03	-119.89	-2891.33	-4003.38
BL 4	7.11	119.89	3113.74	3291.67	-7.11	-119.89	-3113.74	-4003.38
BL 5	7.11	119.89	3287.22	3291.67	-7.11	-119.89	-3287.22	-4003.38

BL – Bi-Linear test

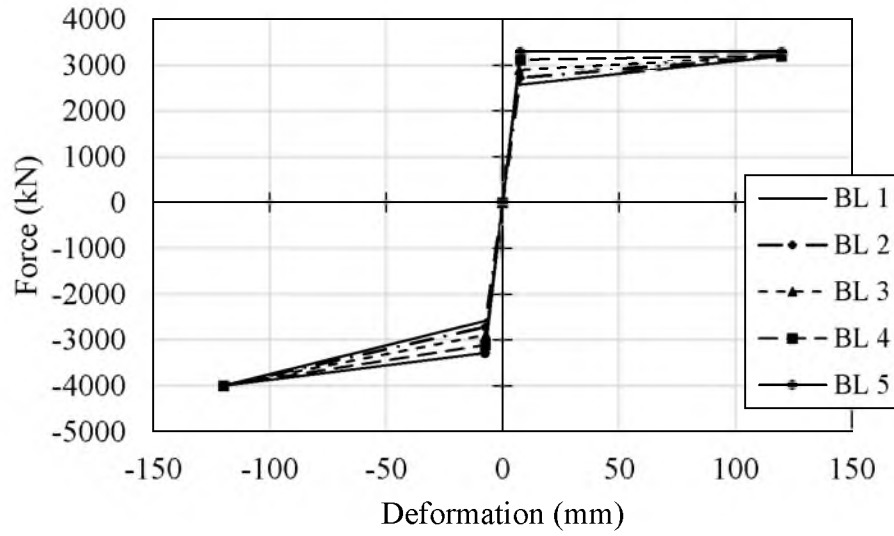


Figure 3.1 Load-deformation curves tested in SAP 2000

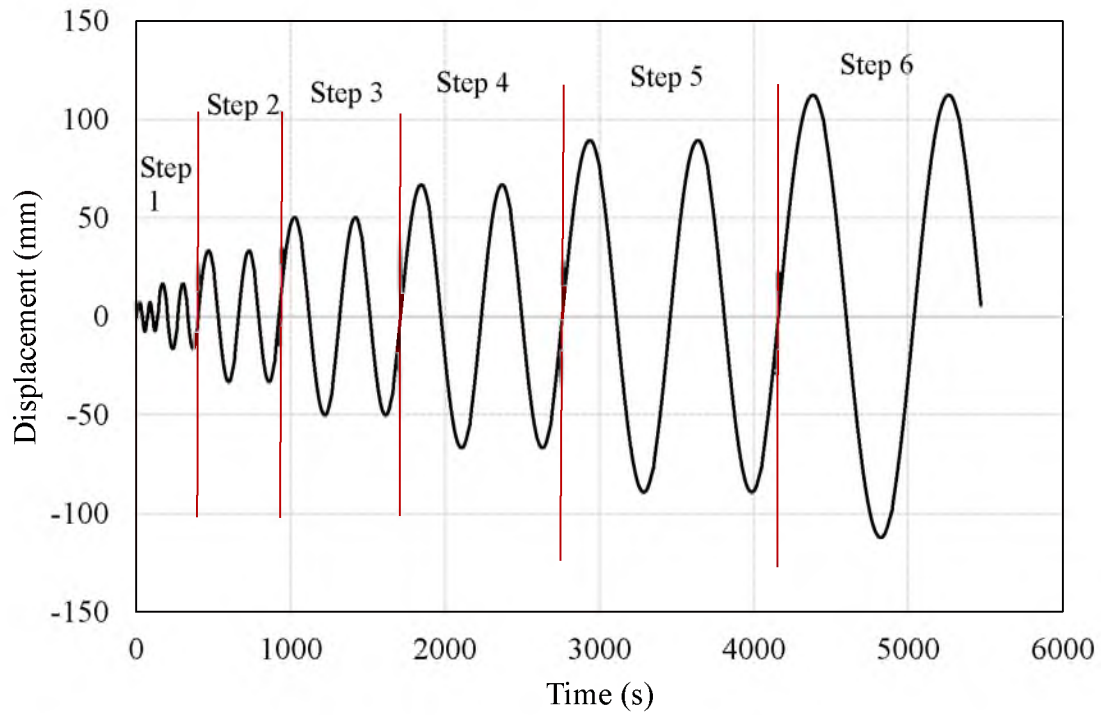


Figure 3.2 Test loading protocol

3.1. Comparison of Several Models for Each Step

A displacement-based cyclic analysis was performed on all SAP 2000[®] bilinear models and hysteresis energy dissipated in each step and total energy was compared to the laboratory experiments of PB500 (Xu 2016). Hysteresis energy is calculated by the area enclosed by the force-displacement curve and it is a measure of energy dissipation by the system. Fig. 3.3 to Fig. 3.8 show the comparison of hysteresis of various models with the actual BRB test in each step. The hysteretic energy dissipated in each step and total energy dissipated by the test BRB (PB 500) and the SAP 2000[®] model are compared in Table 3.2.

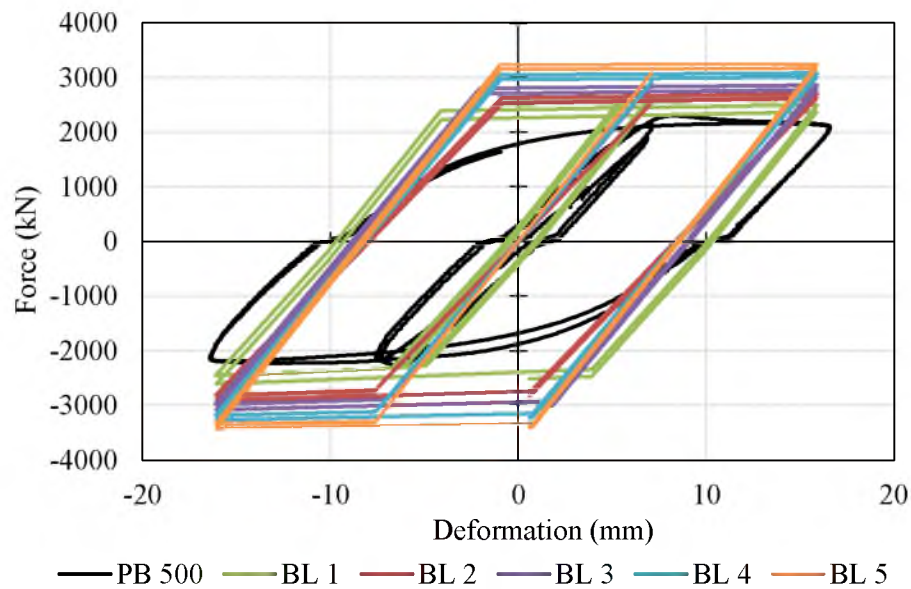


Figure 3.3 Hysteretic energy comparison in 1st step

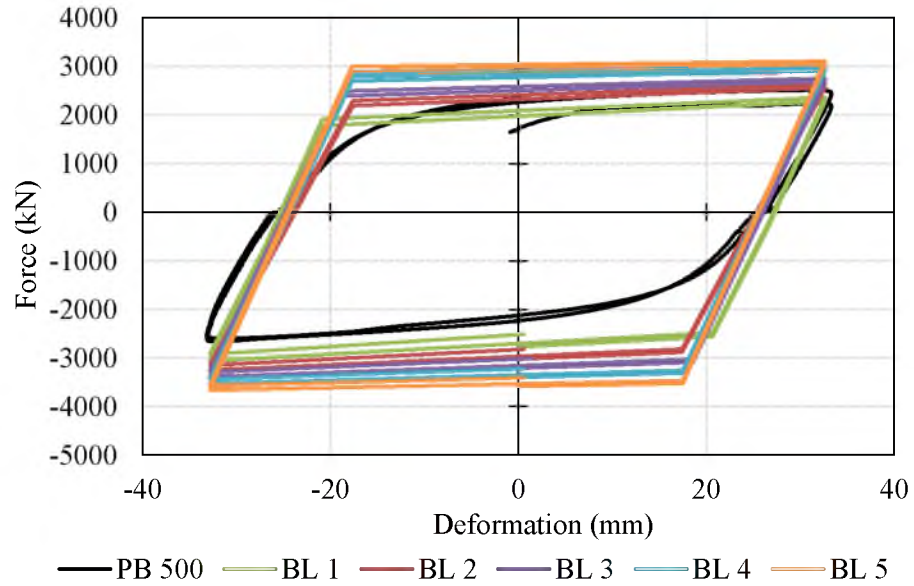


Figure 3.4 Hysteretic energy comparison in 2nd step

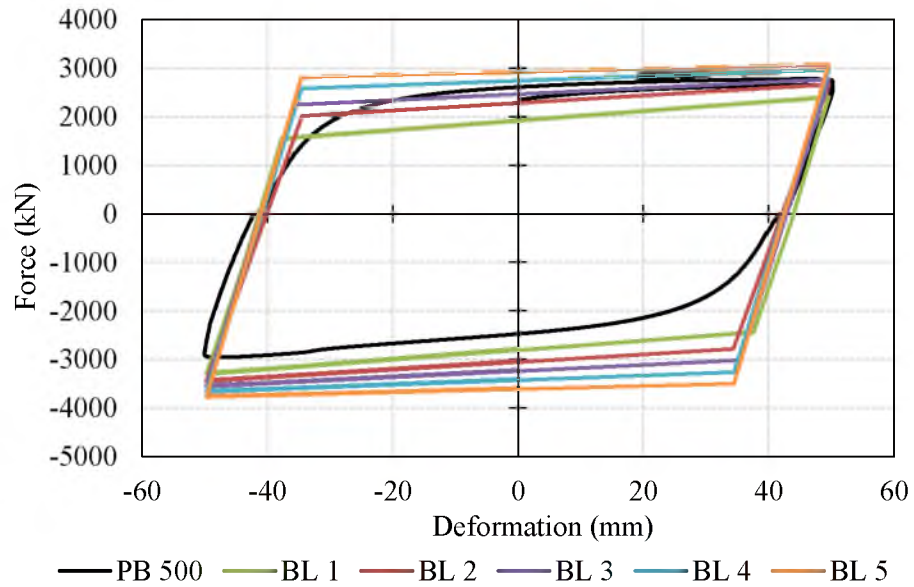


Figure 3.5 Hysteretic energy comparison in 3rd step

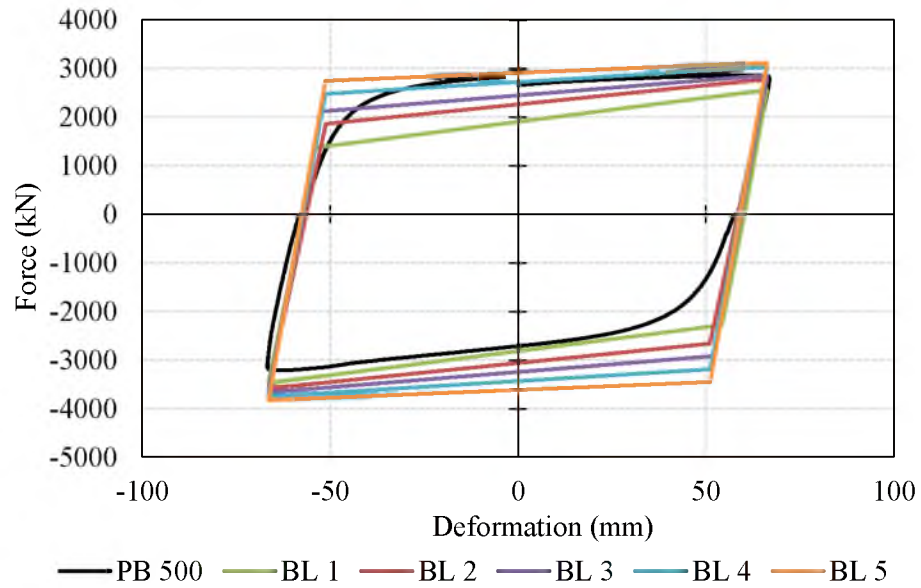


Figure 3.6 Hysteretic energy comparison in 4th step

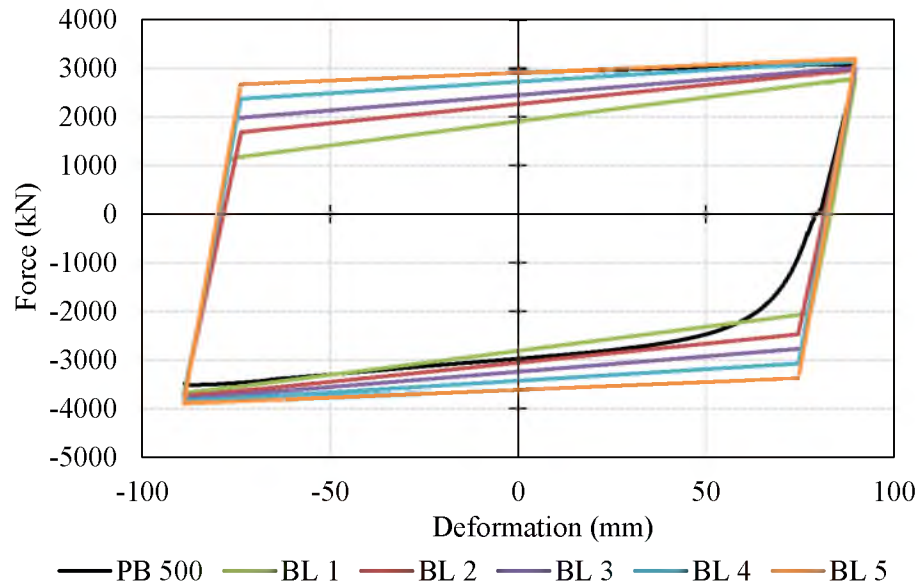


Figure 3.7 Hysteretic energy comparison in 5th step

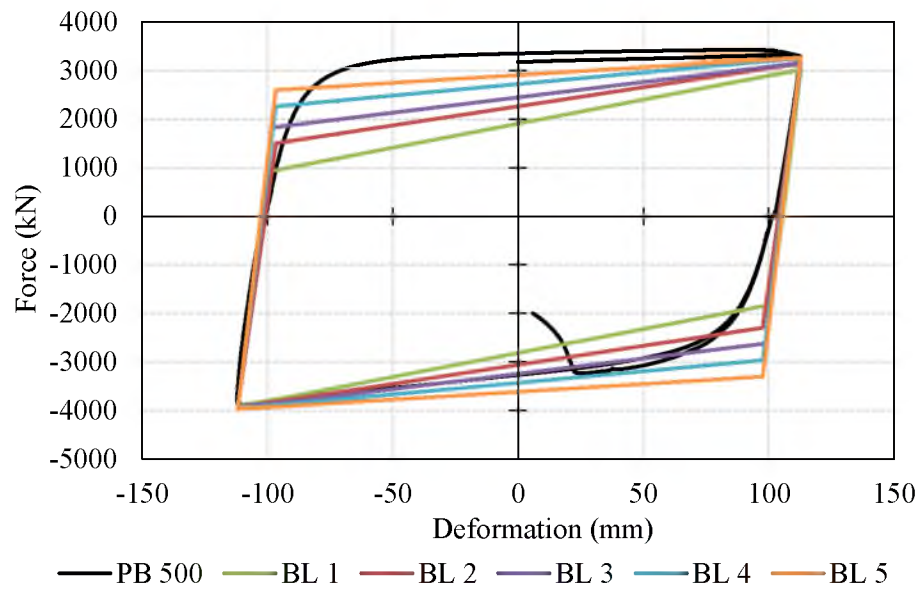


Figure 3.8 Hysteretic energy comparison in 6th step

Table 3-2 Comparison of hysteretic energy for various SAP 2000® models

Test	PB 500	BL 1		BL 2		BL 3		BL 4		BL 5	
	Hysteretic Energy	Hysteretic Energy	% Error	Hysteretic Energy	% Error	Hysteretic Energy	% Error	Hysteretic Energy	% Error	Hysteretic Energy	% Error
	kN-m	kN-m		kN-m		kN-m		kN-m		kN-m	
Total	6499	5735	-11.8	6250	-3.8	6760	4.0	7232	11.3	7667	18.0
Cycle 1	167	195	16.6	167	-0.3	190	13.7	194	16.1	206	23.0
Cycle 2	448	506	12.9	536	19.7	592	32.0	621	38.6	659	47.0
Cycle 3	828	823	-0.6	893	7.9	968	17.0	1034	24.9	1096	32.4
Cycle 4	1253	1140	-9.0	1252	-0.1	1346	7.4	1449	15.6	1534	22.4
Cycle 5	1891	1574	-16.8	1740	-8.0	1880	-0.6	2012	6.4	2133	12.8
Cycle 6	1916	1495	-22.0	1660	-13.4	1785	-6.8	1922	0.3	2034	6.2

3.2. Comparison of Hysteresis Loops of Each Model with BRB Test Data

From Table 3.2, it can be observed that both BL-2 and BL-3 models predict the energy dissipation with almost 4% error. However, BL-2 model has low error in the 1st and 2nd steps as compared to the BL-3 model. Fig. 3.9 shows the comparison of complete hysteresis of PB 500 BRB test and BL-2 model subjected to the same cyclic loading protocol.

A comparison between the hysteretic energy dissipated by the SAP 2000 bilinear models is given in Fig. 3.10, which also shows the actual energy dissipated in the PB 500 BRB test. For the 1st, 2nd and 3rd cycle, models BL-1 and BL-2 predicted values very close to the BRB test. For the 4th cycle, the energy predicted by BL-2 had an error of -0.08%. However, for higher cycles, when the BRB shows Kinematic strain hardening, BL-2 and BL-3 predicted the energy dissipation with an error within 13.37%. Error prediction in overall energy dissipation was the lowest (-3.84%) by the BL-2 model, as shown Fig. 3.11. BL-2 (-3.84% error) was preferred over BL-3 (4.02% error) as BL-2 is conservative in energy prediction and has an initial stiffness close to the theoretical stiffness of the brace. Hence the BL-2 model, with a postyield stiffness ratio of 10%, was adopted to represent a BRB nonlinear link in further study of the bridge.

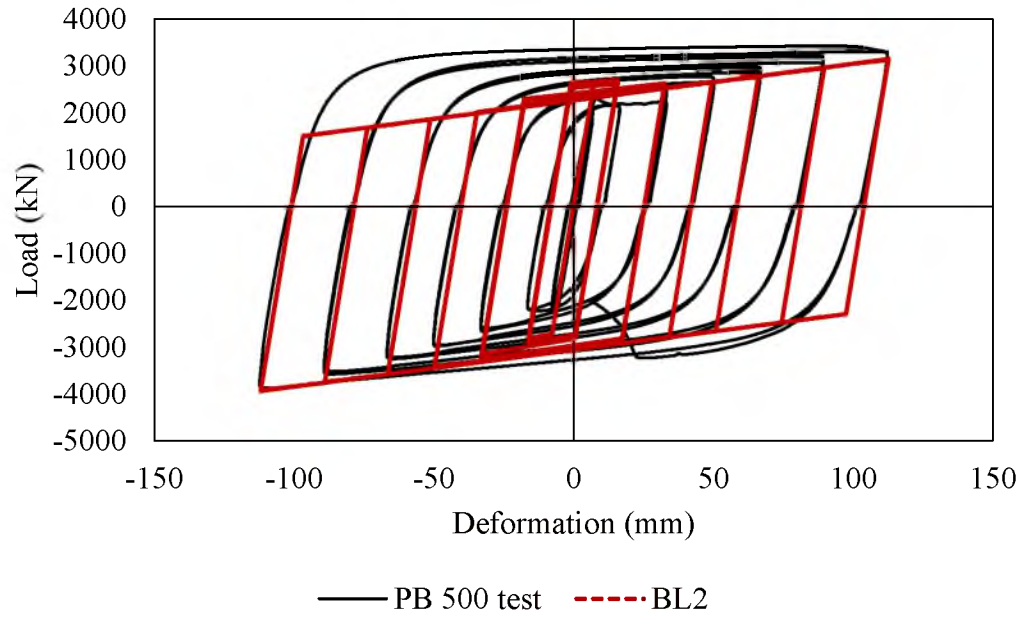


Figure 3.9 Cyclic performance of PB 500 BRB test and BL 2 model in SAP 2000

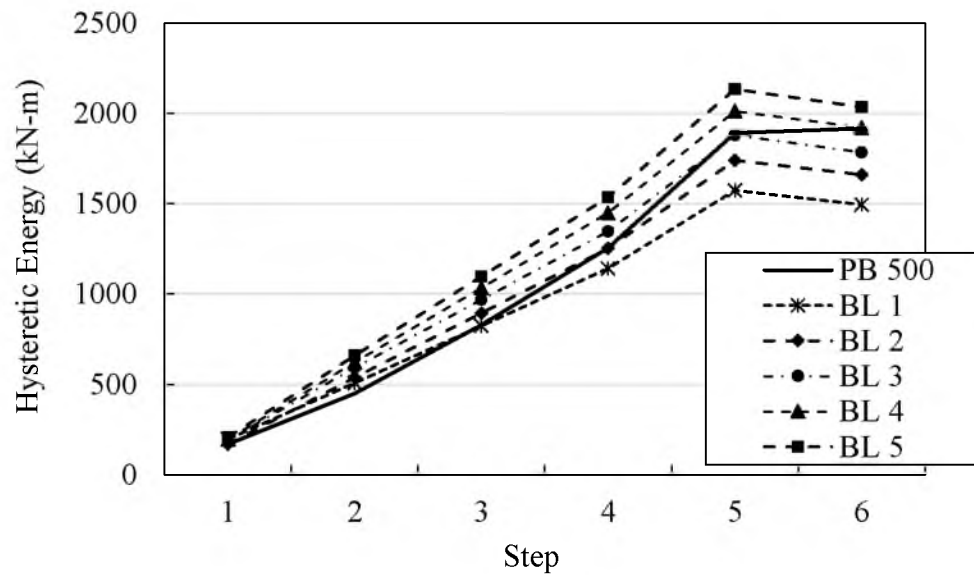


Figure 3.10 Hysteretic energy dissipated per cycle by test BRB and bilinear models in SAP 2000.

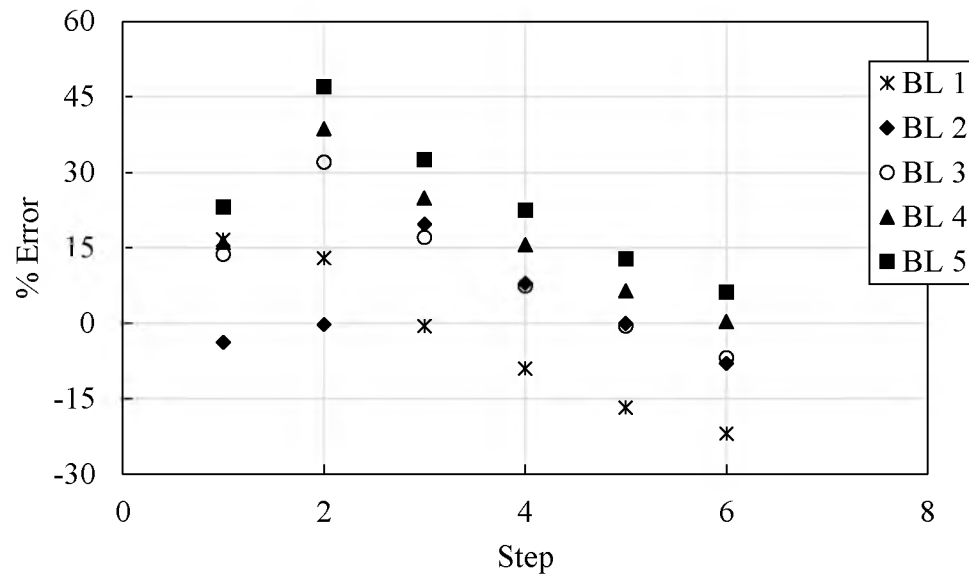


Figure 3.11 Error in calculation of energy dissipation by bilinear models in SAP 2000.

4. RESULTS AND DISCUSSION

4.1. Modal Analysis

Modal analysis showed that the first 20 modes had a time period greater than 1 second after including soil-structure interaction which evident in Table 4.1. The first six mode shapes are shown in Fig. 4.1 to Fig. 4.3.

4.2. Time History Analysis

Soil-Structure Interaction (SSI) increased the fundamental period of vibration to a large extent by eliminating the fixity at the foundation level. The time period of the fundamental mode of vibration was 2.3 seconds when SSI was not considered while it increased to 2.72 seconds when SSI was taken into account. A series of nonlinear time history analyses were carried out on this bridge using the ground motions presented in section 3.1.2. The deck displacement, deck accelerations, pounding force, and bent top displacement time histories were monitored.

4.2.1. Neglecting Soil-Structure Interaction

First the bridge was analyzed under a set of ground motions without taking soil-structure interaction in consideration. This analysis was necessary to show the impact of SSI on the behavior of the structure. The results obtained in this section will be compared with those of section 4.2.2. The gap between the girders and abutment wall is 75 mm and

Table 4-1 Periods and mass participation ratios of first 30 modes of the bridge

Mode Number	Period (s)	Horizontal-X	Horizontal-Y	Vertical
1	2.724	0.07614	8.0800E-03	6.968E-08
2	2.223	0.00293	1.1400E-03	5.667E-06
3	2.029	0.03452	7.7000E-04	2.901E-07
4	1.837	0.05688	5.6670E-02	1.112E-05
5	1.736	0.00171	4.7800E-03	8.484E-07
6	1.647	0.13812	6.9900E-03	7.165E-08
7	1.538	0.19357	5.2500E-03	1.059E-07
8	1.458	0.03472	1.5000E-04	6.398E-06
9	1.453	0.01660	1.7970E-02	3.067E-08
10	1.277	0.00104	9.5360E-05	4.185E-07
11	1.140	0.01586	1.7900E-03	3.370E-07
12	1.121	0.00519	9.4330E-10	9.716E-06
13	1.101	0.00955	3.4500E-03	1.886E-05
14	1.006	0.01744	3.8040E-05	1.600E-04
15	0.982	0.00359	1.5000E-04	3.614E-05
16	0.925	0.00411	4.9089E-01	8.838E-05
17	0.912	0.00700	2.5100E-02	7.155E-05
18	0.882	0.00037	1.5780E-02	2.500E-04
19	0.825	0.01375	6.5000E-04	1.570E-03
20	0.798	0.00392	1.8300E-03	1.720E-03

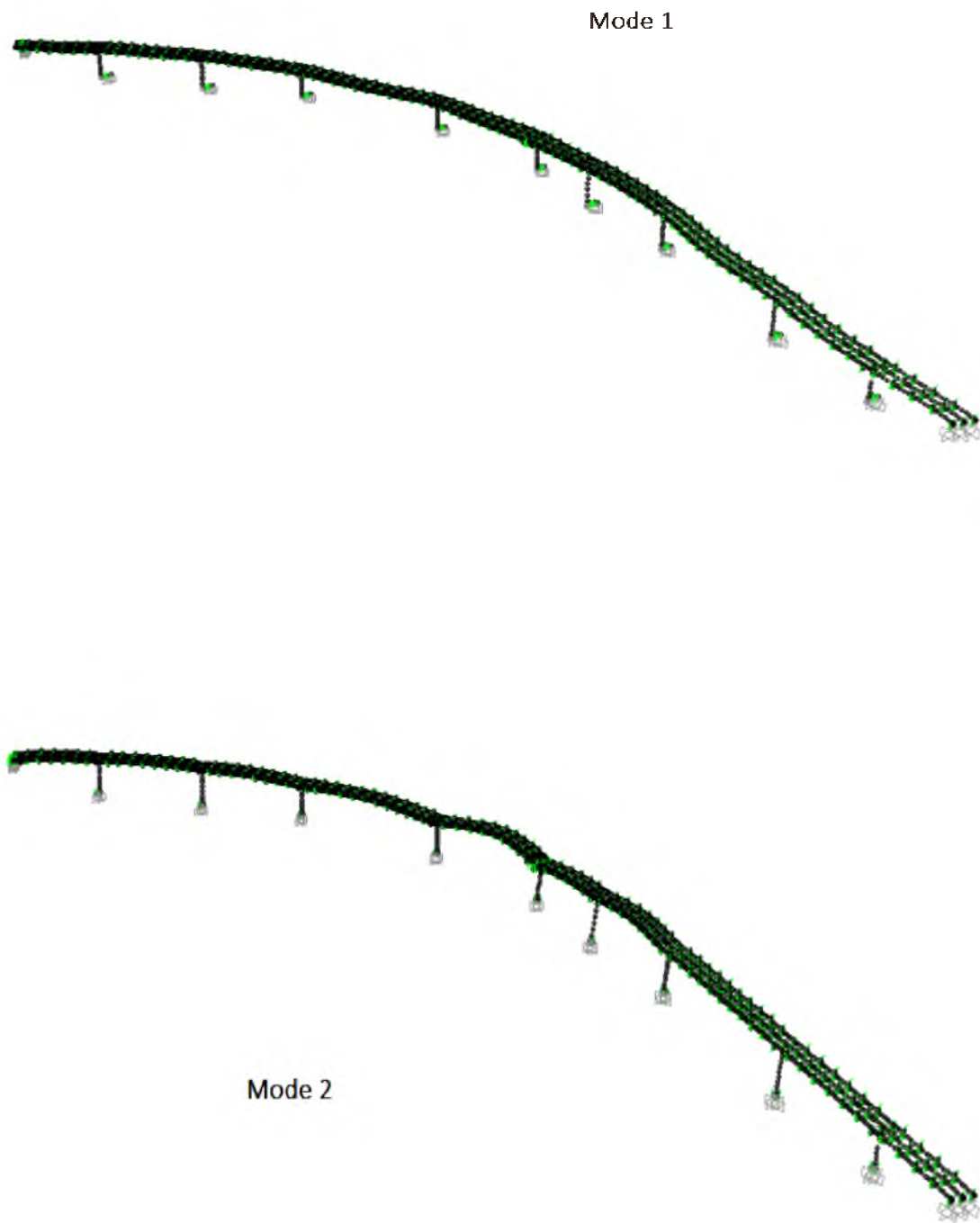


Figure 4.1 Mode 1st and 2nd with SSI

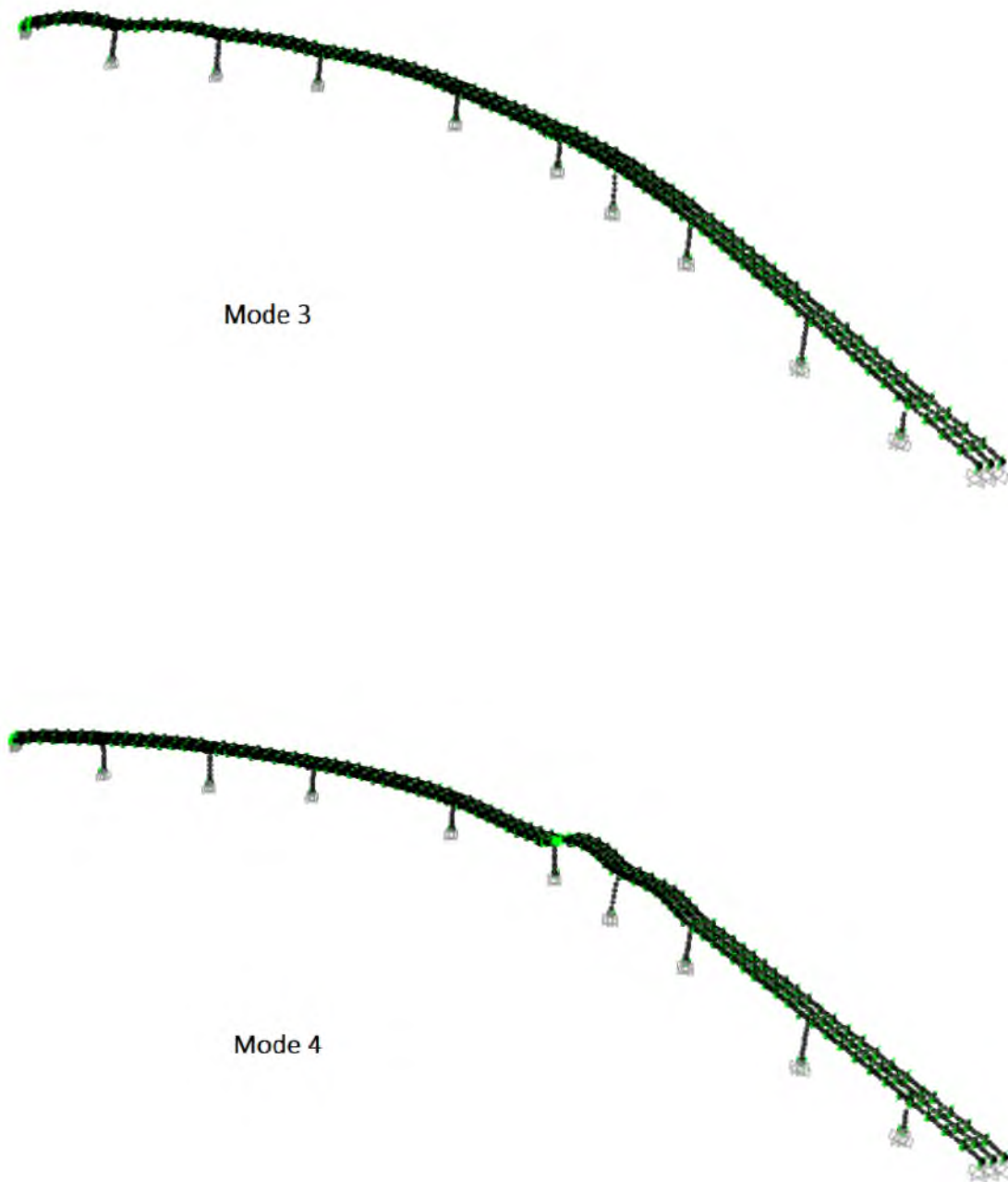


Figure 4.2 Mode 3rd and 4th with SSI

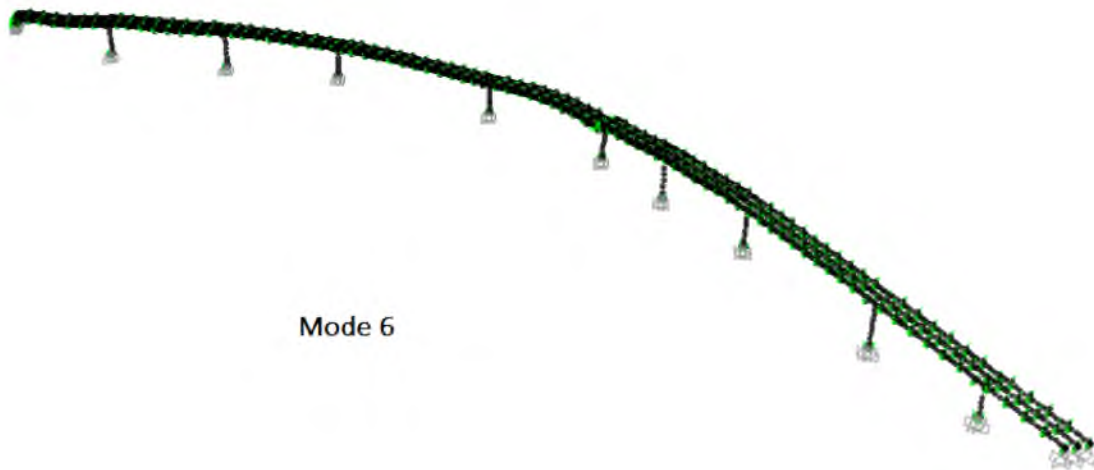
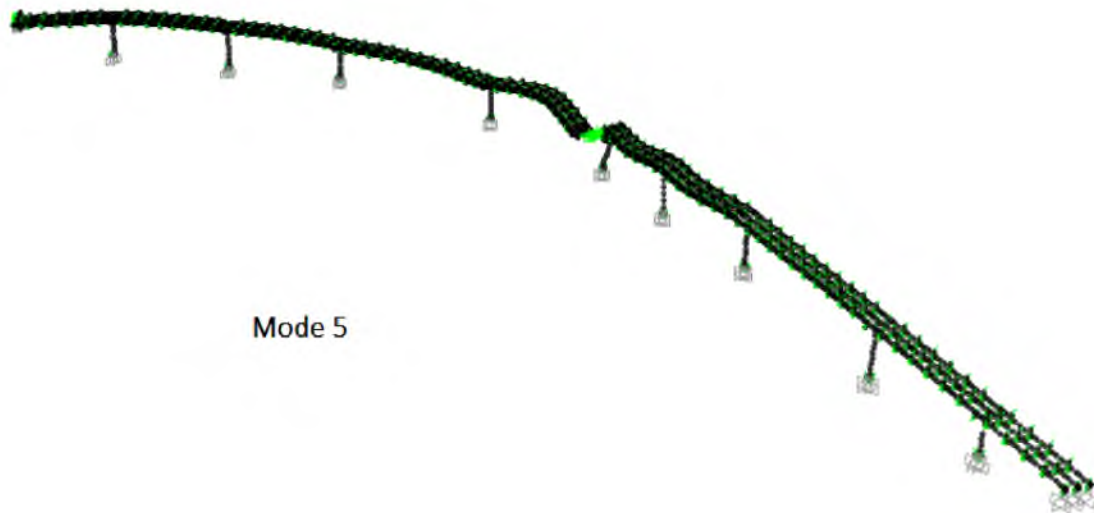


Figure 4.3 Mode 5th and 6th with SSI

girder displacement should be at least 75 mm towards the abutment to generate any pounding. From Fig. 4.4, it can be observed that the maximum girder displacement is less than 75 mm and hence no pounding was observed when soil-structure interaction was neglected in the analysis. Response acceleration of the girders at the abutments for Irpenia (1980) ground motion is presented in Fig. 4.5 which shows that SSI increases the number of peaks in response acceleration of the structures.

An incremental dynamic analysis (IDA) was performed on the bridge model using Chalfant Valley (1986) and Kobe (1995) ground motion data without considering soil-structure interaction. The peak axial force in the restrainer rods increased with the peak ground acceleration. However, the axial force in the restrainer rod remained less than the yield force value, 519 kN, when soil structure interaction (SSI) was neglected in the time history analysis using all 15 earthquake ground motions. The structure was further analyzed by modeling soil springs in the computer model to understand the effect of SSI.

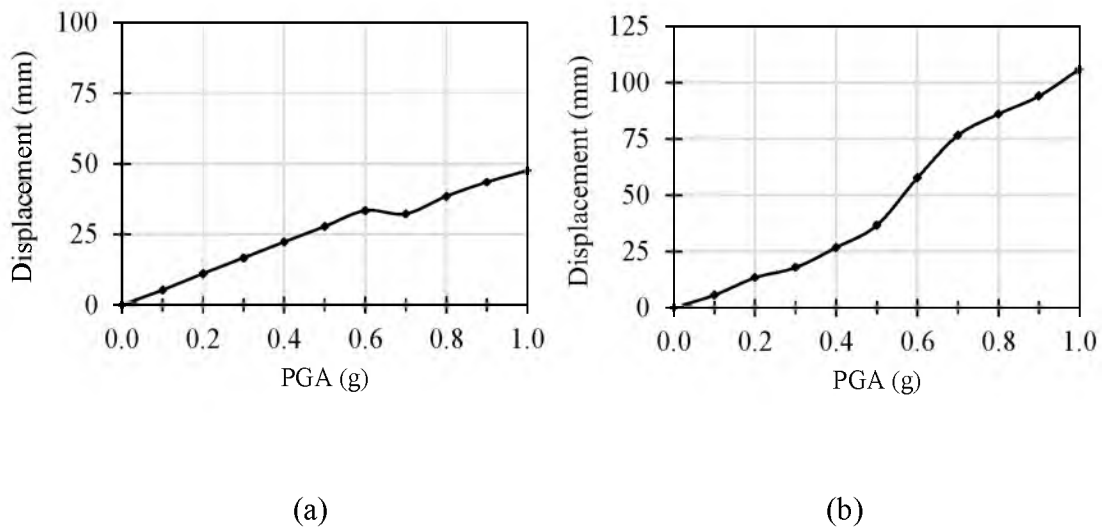


Figure 4.4 Maximum displacement of girder G1 towards the abutment for (a) Chalfant Valley, 1986 and (b) Kobe ground motion data, 1995, without considering SSI

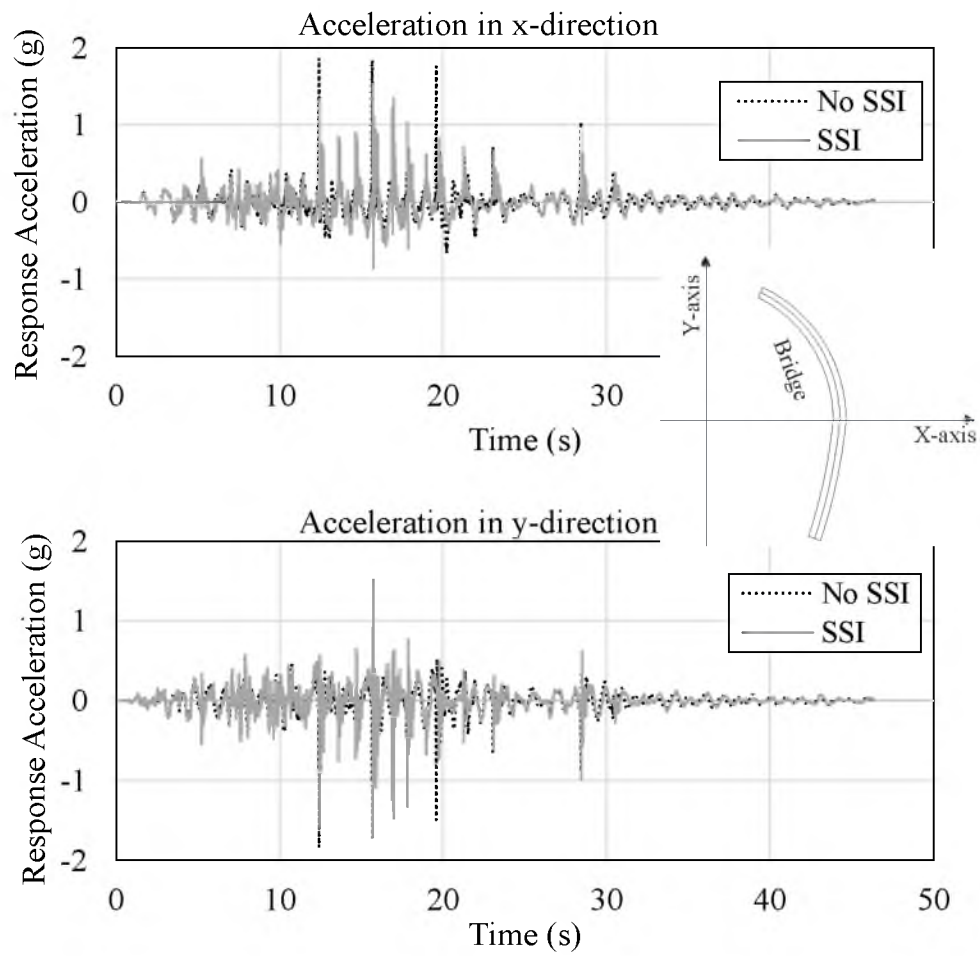


Figure 4.5 Response acceleration of girder G1 at abutment for Irpenia, Italy ground motion (1980)

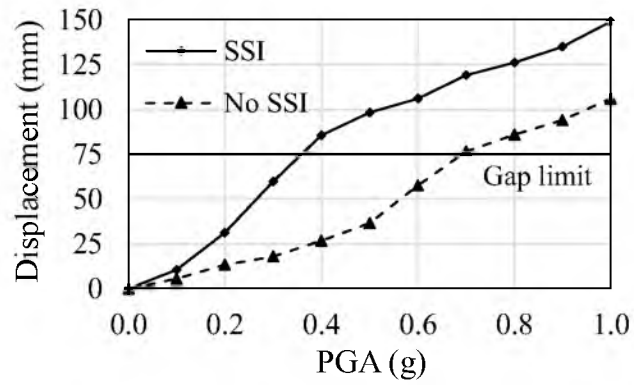
4.2.2. Effect of Soil Structure Interaction

The soil borehole data show that the bridge was constructed on soft soil and it is important to understand the effects of SSI on the structure's performance. SSI increased the fundamental period from 2.3 seconds to 2.7 seconds, hence shifting it to the displacement based region of the design spectrum. Table 4.2 shows the effect of SSI on the first three modes of vibration. The peak girder displacement, which was 21 mm before inclusion of SSI, was observed to be more than 75 mm for all the ground motions listed in section 2.2. As the construction gap between the girder and abutment was 75 mm, pounding between them was expected. An incremental dynamic analysis (IDA) using Kobe ground acceleration data was performed for the bridge and the results with and without SSI are shown in Fig. 4.6. It is evident that soil-structure interaction played an important role and increased the likelihood of pounding.

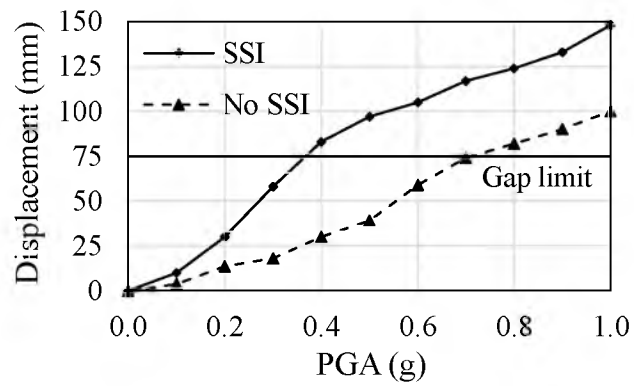
To calculate the pounding forces on girders and abutment, gap type compression only elements were modeled between girder nodes and abutment nodes as described in Chapter 2. Fig. 4.7 shows the time-history of normalized girder displacement and normalized pounding force. Both quantities were normalized using their peak values. It is evident that after pounding, the girder was displaced away from the abutment as a reaction which in turn led to further pounding. Displacement of the girder away from the abutment is shown

Table 4-2 Effect of soil-structure interaction on first three modes of vibration

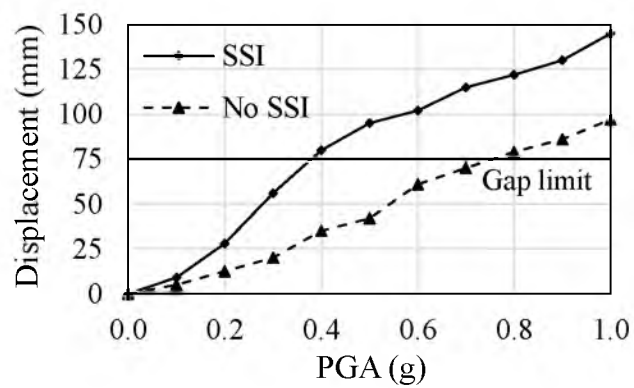
	1 st Mode Period (s)	2 nd Mode Period (s)	3 rd mode Period (s)
Without SSI	2.31	2.16	2.08
With SSI	2.72	2.65	2.61



(a) Girder 1



(b) Girder 2



(c) Girder 3

Figure 4.6 Effect of SSI on relative displacement between girders and abutment.

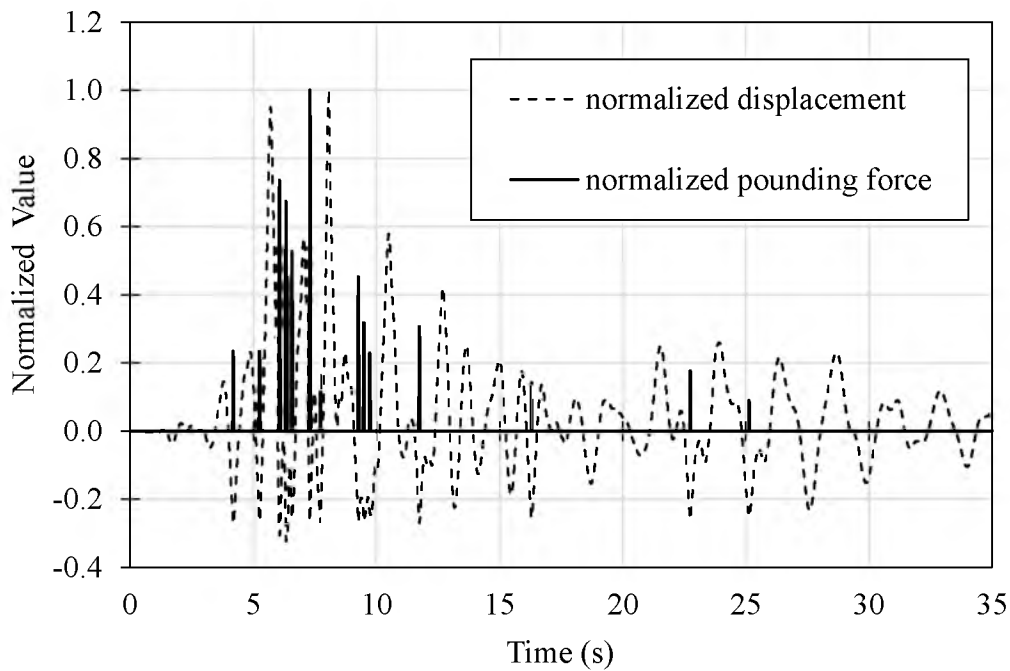


Figure 4.7 Normalized girder displacement and pounding between girder G1 and abutment including SSI

in the positive direction, which follows the pounding force spike in the time-history. Two conclusions can be reached from Fig. 4.7: (i) to prevent pounding, it is required to limit the peak girder displacements towards the abutment below 75 mm, and (ii) in order to reduce the number of pounding events, it is necessary to damp the oscillations of the girders. Using Buckling Restrained Braces between the three girders and the abutment could be a solution to this problem. The pounding force time-histories for Kobe (1995) groundmotion for girders G1, G2 and G3 of the curved bridge are compared in Fig. 4.8, which shows that the force was highest for the exterior girder and lowest for the interior girder. Fig. 4.9 to 4.14 show the pounding force time-histories of girder G1 for various earthquakes. All the earthquake ground motions caused significant pounding force at the abutment.

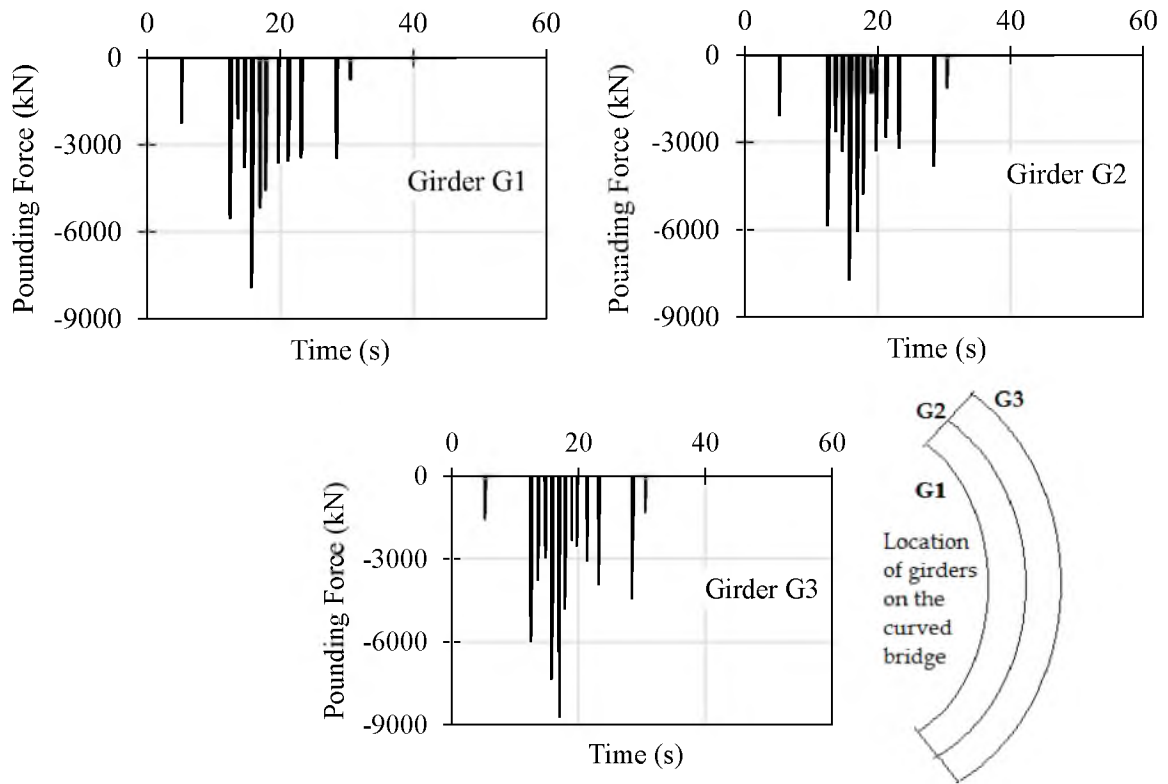


Figure 4.8 Pounding between abutment and girders for Kobe ground motion

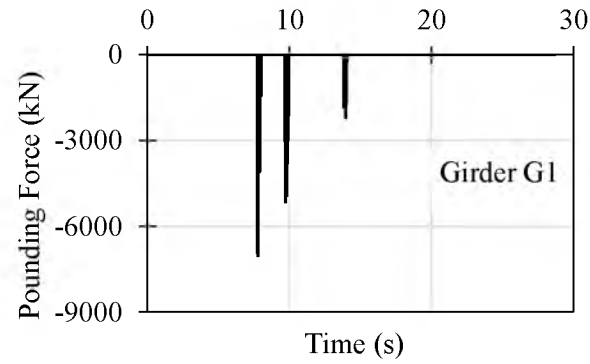


Figure 4.9 Pounding between abutment and girder for Cape-Mandosino ground motion, 1992

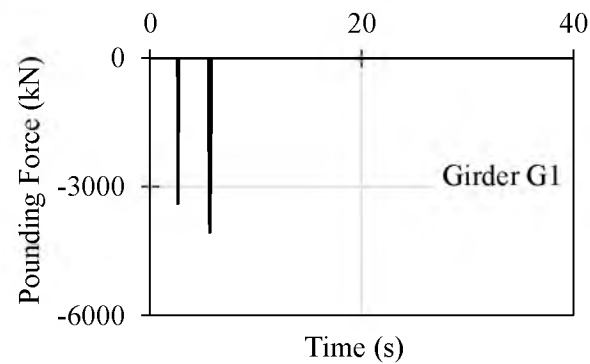


Figure 4.10 Pounding between abutment and girder for Chalfant Valley ground motion, 1986

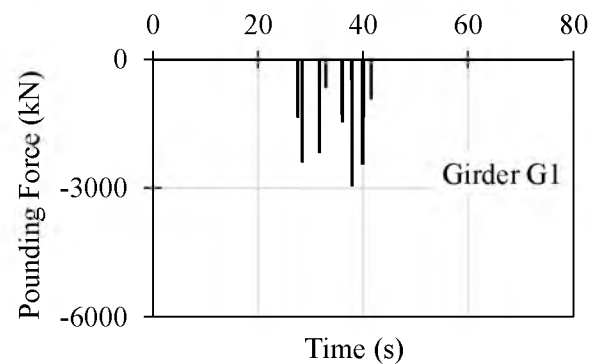


Figure 4.11 Pounding between abutment and girder for ChiChi, Tiwan ground motion, 1999

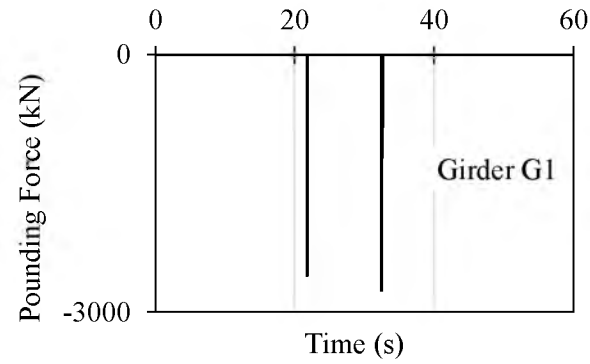


Figure 4.12 Pounding between abutment and girder for Chuetsu-oki Japan ground motion, 2007

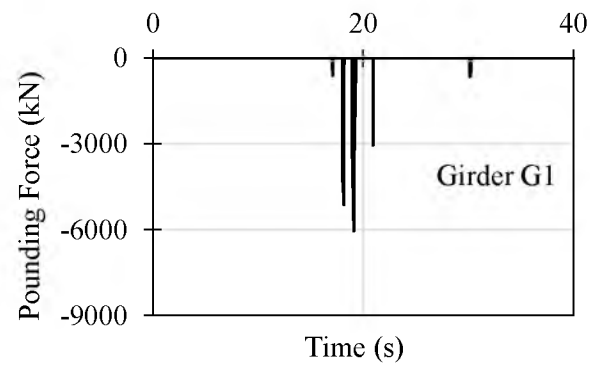


Figure 4.13 Pounding between abutment and girder for Duzce, Turkey ground motion, 1999

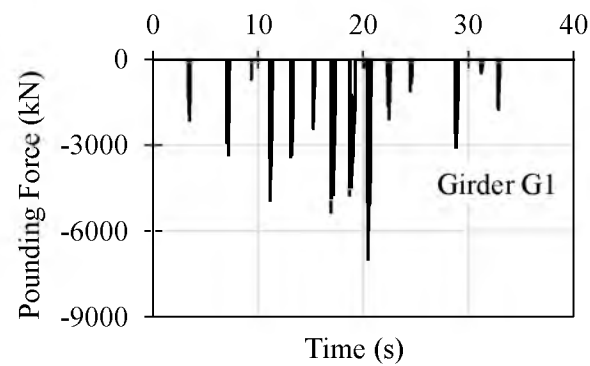


Figure 4.14 Pounding between abutment and girder for Parkfield ground motion, 1966

Earthquake restrainer rods were used at the expansion joints of the curved bridge to prevent excessive relative displacement of the girders and potential unseating and fallout. These rods were 40 mm in diameter and had a nominal yielding force of 519 kN each. However, it is well known that the ultimate stress of the steel rods can be as much as 1.8 times the yield stress; therefore, the rods can be assumed to be working up to an axial force of 934 kN. Analyses showed that the peak axial forces generated in the rods were greater than 1000 kN and these axial forces crossed the yield capacity many times during an earthquake event as shown in Fig. 4.15. Based on this information, it was assumed that the restrainer rods suffered complete tensile failure and pounding between the girders at the expansion joint was expected. A further analysis was done by removing the steel restrainer rods from the bridge model.

Yield force calculation for restrainer rods:

Rod diameter = 40 mm

Cross-sectional area = 1256 mm²

Yield stress of steel = 412 MPa

Yield force = Yield stress x Cross-sectional area
= 519 kN

Ultimate force = 1.8 x 519 kN
= 935 kN

Analysis of the bridge after removing the restrainer rods showed pounding between the girders at the expansion joints. However, the pounding was not repetitive and there were only a few spikes in the time history analysis, as shown in Fig. 4.16, but the pounding force was up to 2000 kN. This high pounding force can cause severe damage to the deck. Along

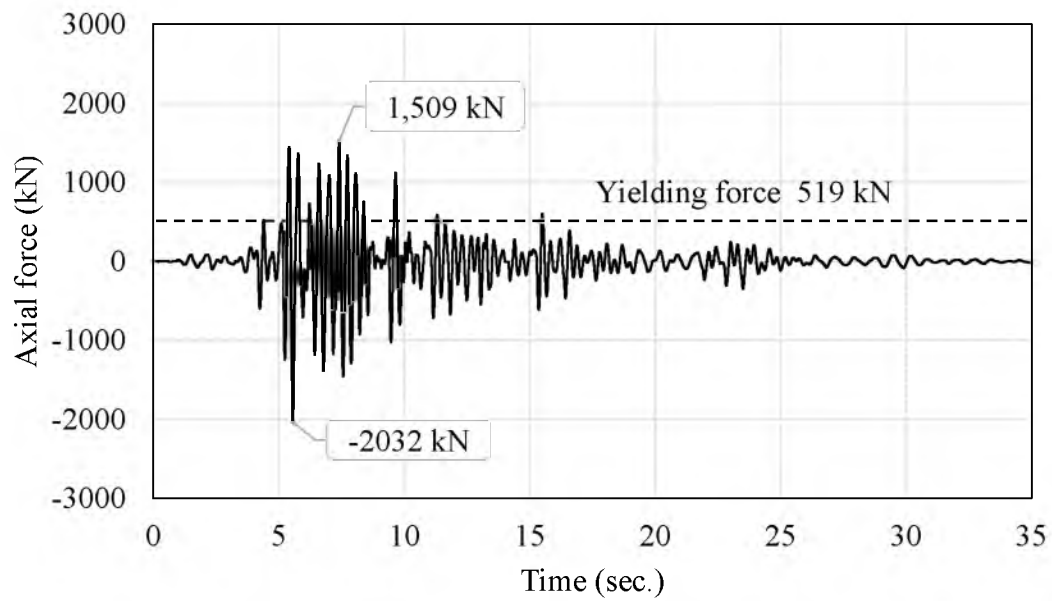
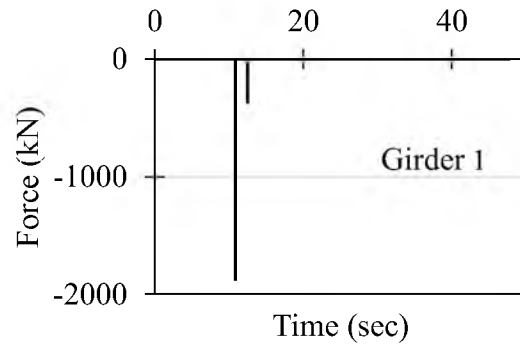
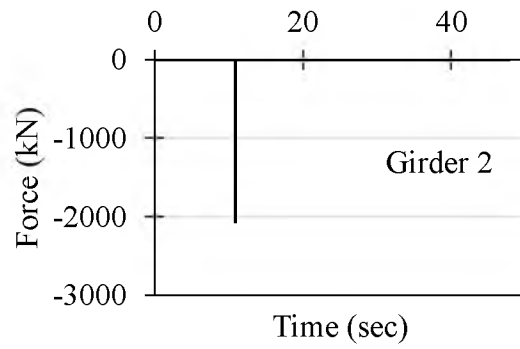


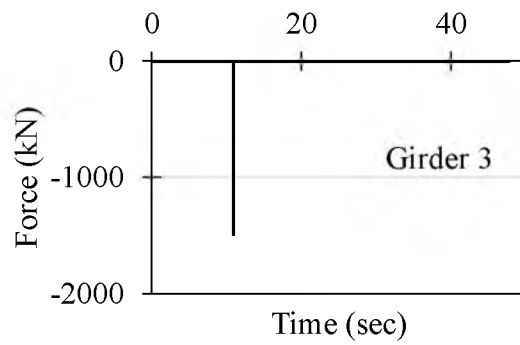
Figure 4.15 Axial force time-history in one of the restrainer rods at expansion joint for scaled Kobe ground motion, 1995



(a)



(b)



(c)

Figure 4.16 Pounding between girders at expansion joint for scaled Kobe ground motion, 1995

with the longitudinal movement of the girders, lateral (to the axis of the bridge), movement of the girders was also observed and pounding between concrete shear key and the steel girders was expected.

To calculate this pounding force, compression only gap type link elements were included in the model, between concrete shear key and steel girder. Fig. 4.17 and Fig. 4.18 show the location of concrete shear keys and gap type link elements in the numerical model, respectively. Once the lateral seismic force on the girder exceeded the yield capacity of the bearings supporting the girders on the bent cap beam, it caused the girders to move laterally. This lateral movement caused the gap closure leading to pounding. The pounding occurred for several ground motions and the time-history of pounding force, at girder G1, for Kobe ground motion (1995) is shown in Fig. 4.19. The pounding force at all three girders was high, which can be considered as risk for the damage to the concrete shear keys, hence the girders are susceptible to unseating in lateral direction.

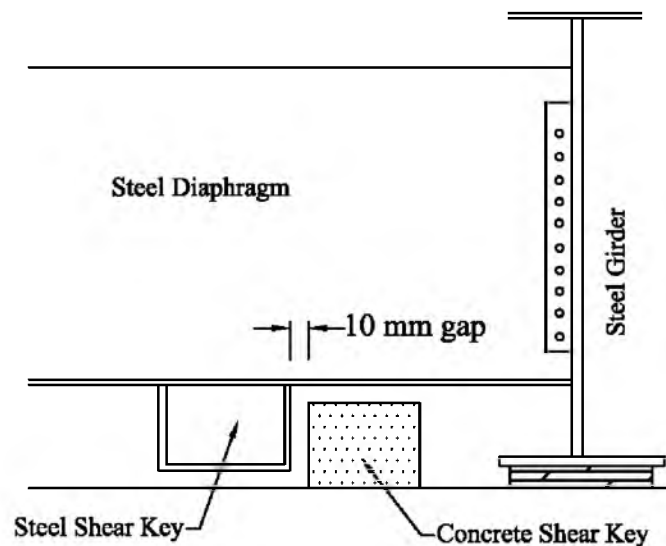


Figure 4.17 Location of concrete shear key and gap between steel girder and shear key



Figure 4.18 Shear keys on the bridge bent

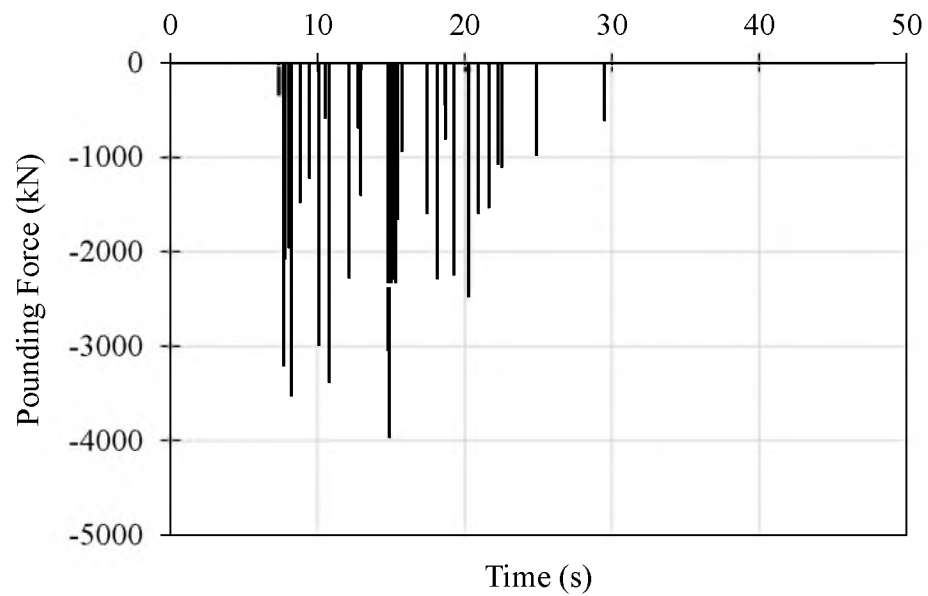


Figure 4.19 Pounding force time-history between concrete shear keys and steel girder G1 for Kobe ground motion, 1995

The peak pounding force was less than the ultimate capacity of the connection between steel shear key and the diaphragm; however, the force exceeded the concrete shear key capacity. Usually the concrete shear keys in a bridge are sacrificial and their function is to dissipate energy by getting damaged, thus preventing damage from occurring to the superstructure. Although the damage mechanism is good for energy dissipation, there might be a probability of unseating of the girders. Repairing the girders after an earthquake is time consuming, and the strength of the repaired shear keys is less than the original.

4.2.3. Application of Buckling Restrained Braces

The bridge model was retrofitted by installing one BRB on each girder in the longitudinal direction, as shown in Figs. 4.20 and 4.21. The BRBs were designed following the procedure given by ASCE-07 (2014) for lateral stiffness of multicolumn bridge bents. It is recommended that 70% of the seismic weight should be resisted by the BRBs and 30% should be resisted by the columns. But for this retrofit, it is assumed that 100% of the seismic weight is resisted by the BRBs. This assumption was made on the basis that the pounding at the abutment was due to abutment excitation which is a result of soil-structure interaction. Hence, the movement of the abutment and foundations played a major role in the displacement of the girders relative to the abutment and hence BRBs were supposed to provide sufficient stiffness to reduce that. The backbone curve for longitudinal BRBs, adopted from the analysis in Chapter 3, is shown in Fig. 4.22. An Incremental Dynamic Analysis was performed on the retrofitted bridge model. Fig. 4.23 and Fig. 4.24 show the relative displacement of girder G1 for various earthquakes. It is evident that BRBs were successful in preventing the pounding completely.

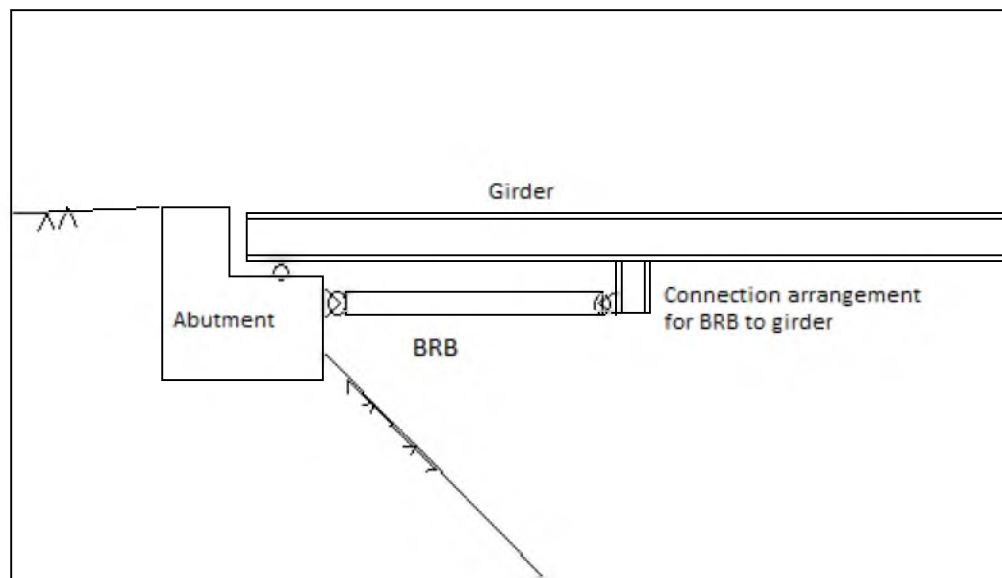


Figure 4.20 Application of longitudinal BRB at the abutment

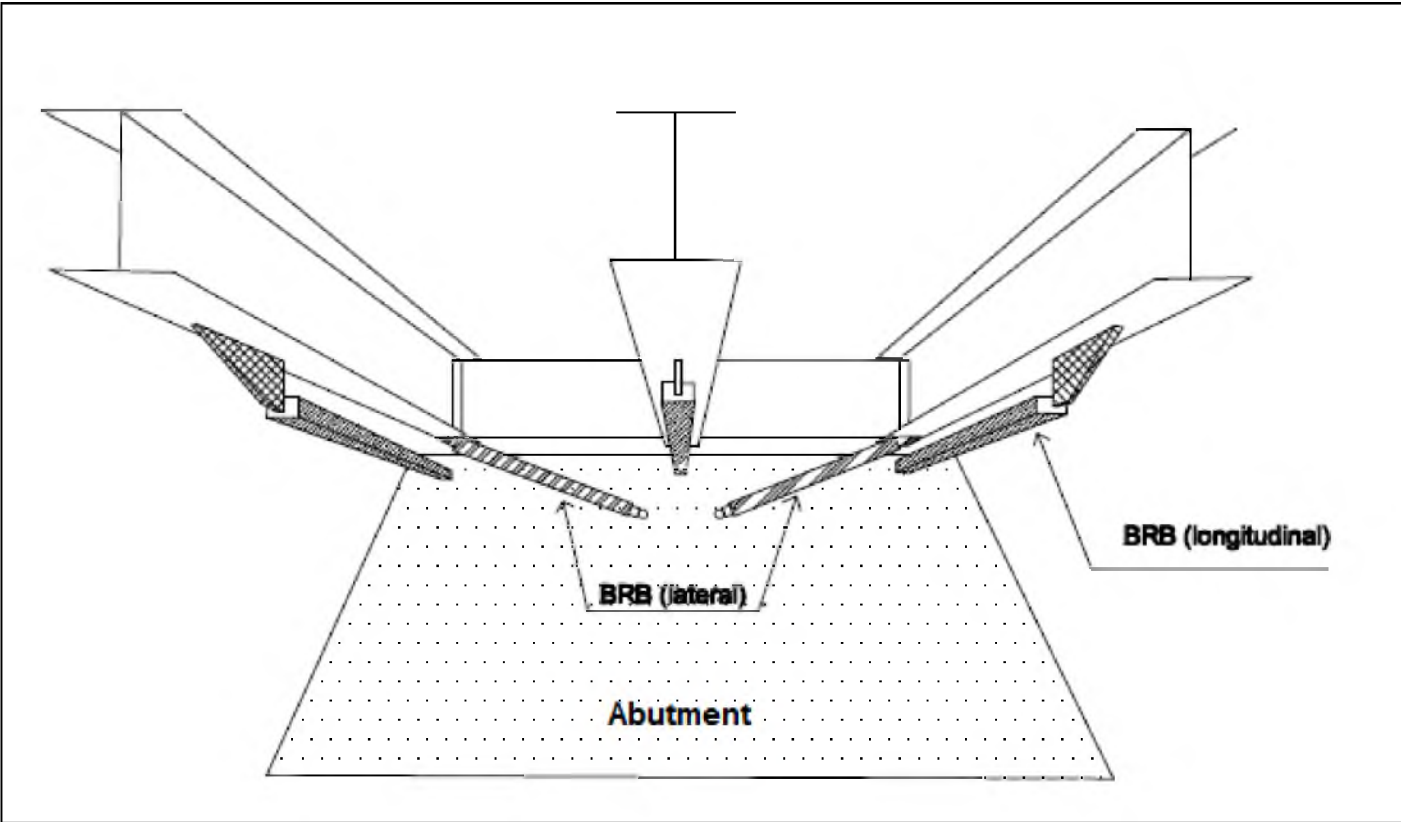


Figure 4.21 Retrofit scheme using BRBs at abutment

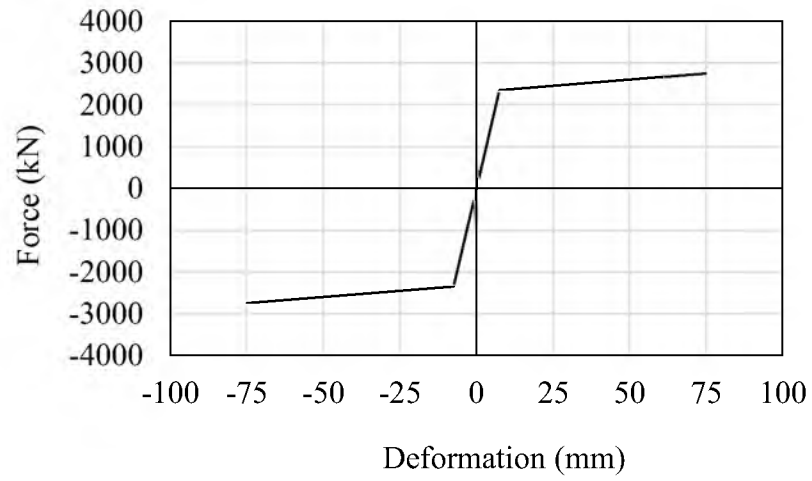


Figure 4.22 Bilinear backbone curve used for longitudinal BRB

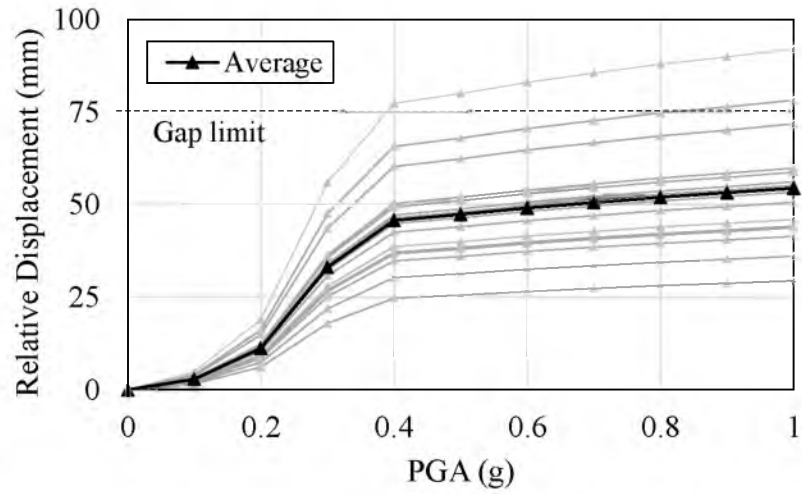


Figure 4.23 IDA results of retrofitted bridge abutment

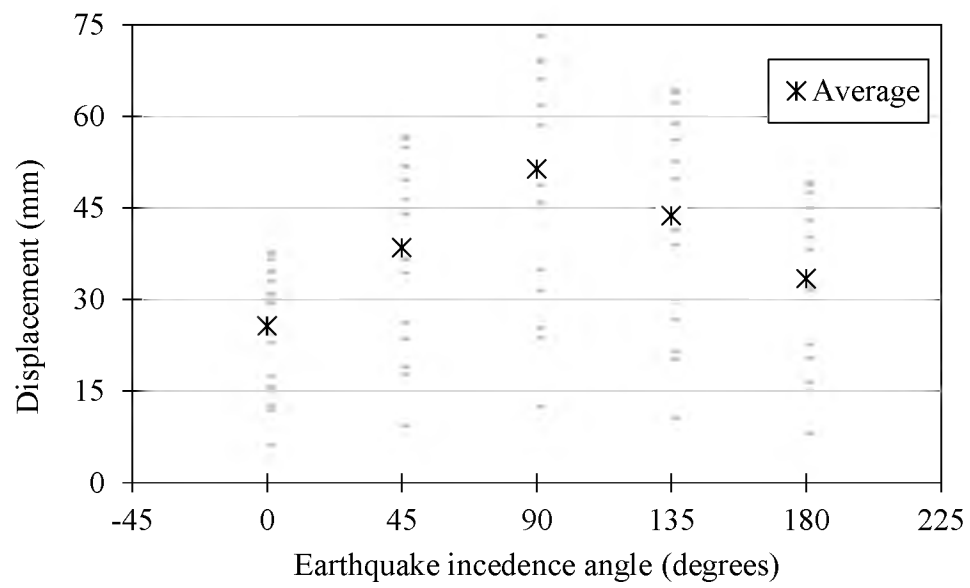


Figure 4.24 Peak relative displacements of girder (G1) for ground motion at various angles of incidence

Response acceleration time history of girder G1 at the abutment is shown in Fig. 4.25 and it is clear that BRBs provided extra stiffness between girders and the abutments which resulted in reduced response acceleration. The hysteresis of the BRBs for various earthquakes, Fig. 4.26, shows that BRBs performed well and dissipated earthquake energy to prevent the structure. Although BRBs prevented the pounding between abutment and girders, permanent deformation in the BRBs was observed at the end of seismic event. The permanent deformation of BRBs is shown in Fig. 4.27.

To prevent pounding between concrete shear keys and steel shear keys attached to the diaphragm, additional BRBs were used in the lateral direction. As shown in Fig. 4.22, lateral BRBs were connected to the bottom of the outer girders at one end and to the abutment wall at the other end. As it is not feasible to put lateral BRBs in a horizontal plane because of the girder in the middle (G2), it was decided to put these BRBs at some angle. To utilize most of the capacity of the BRBs, the angle should be low and hence an angle of 30° was selected. The adopted BRB backbone curve is shown in Fig. 4.28 based on the analysis presented in Chapter 3. Analysis showed that low strength BRBs of a load capacity of 1350 kN and ultimate deformation capacity of 55 mm successfully prevented pounding between the shear keys. An incremental dynamic analysis (IDA) was performed with Kobe ground acceleration data (1980) to analyze the performance of lateral BRBs with increasing peak ground acceleration (Fig. 4.29). The negative deformation of lateral BRBs in the hysteresis curves is a measure of the relative displacement of the girder towards the concrete shear key. The hysteresis curves of one lateral BRB for the scaled Kobe ground motion (Fig. 4.30) shows that the peak deformation was 7.5 mm in compression and 7.7 mm in tension, which is less than the gap between concrete and steel shear keys (10 mm).

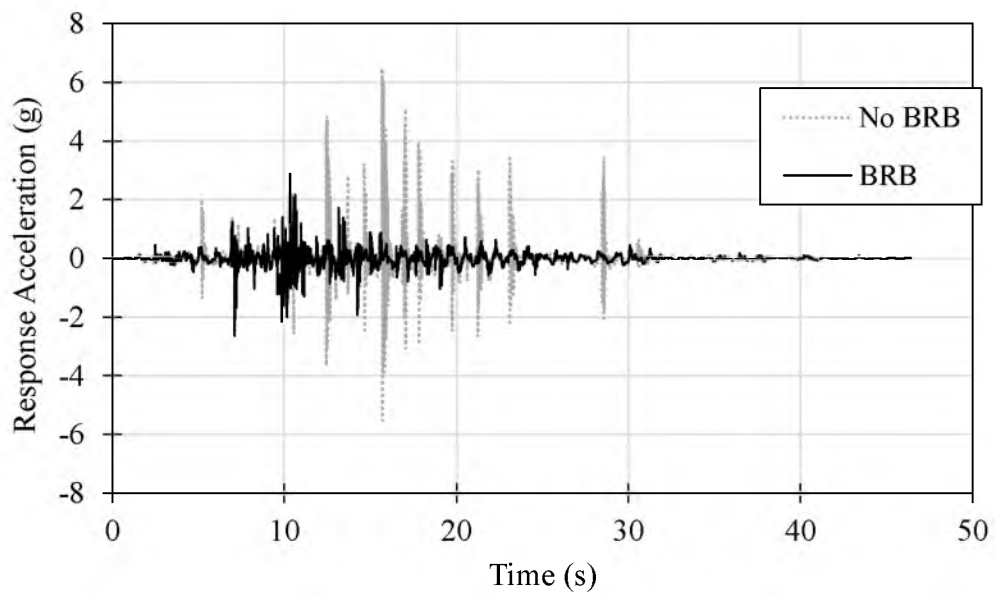


Figure 4.25 Response acceleration time history of end of girder G1 for Irpenia, Italy ground-motion

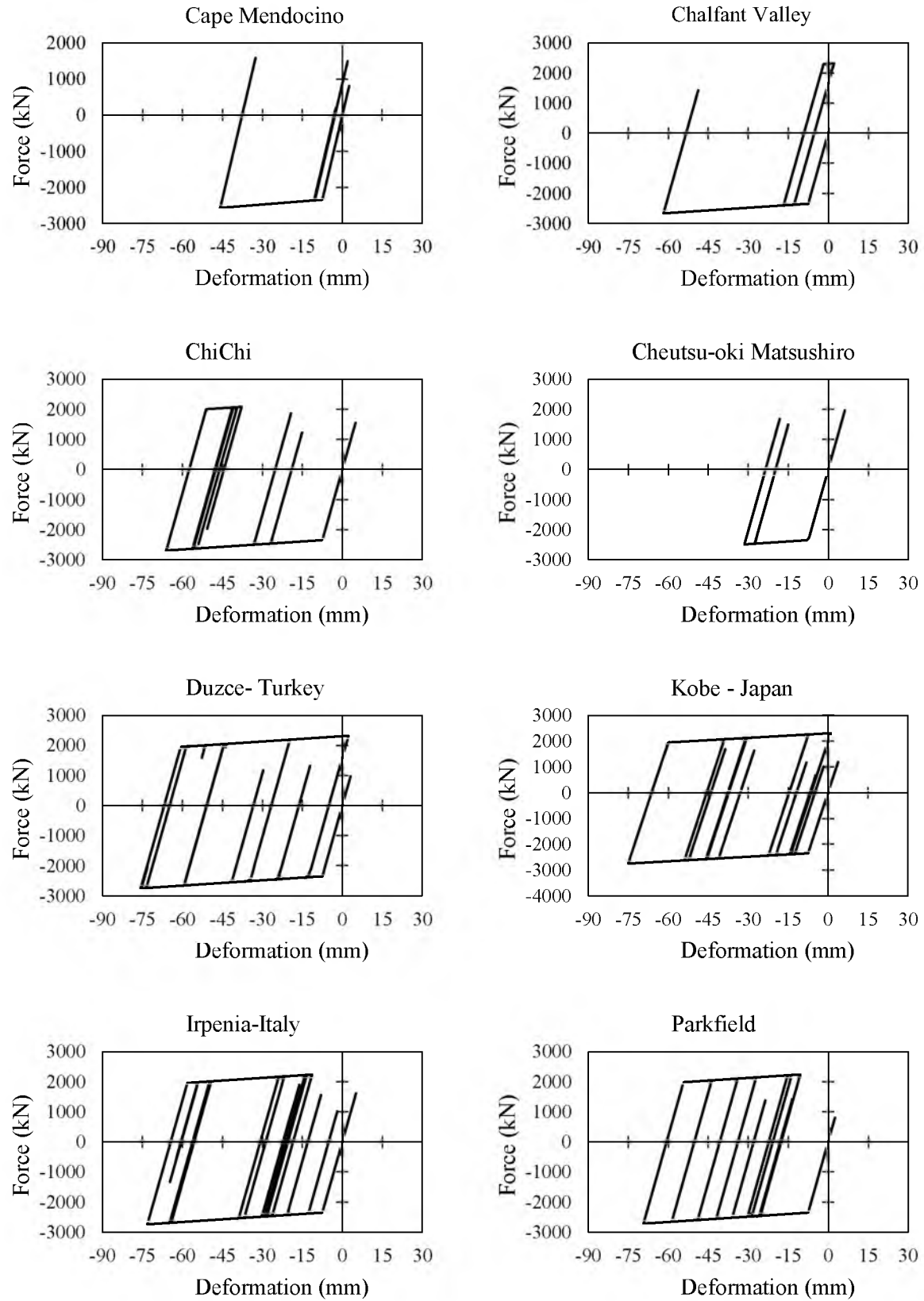


Figure 4.26 Hysteresis of one longitudinal BRB for scaled ground motions

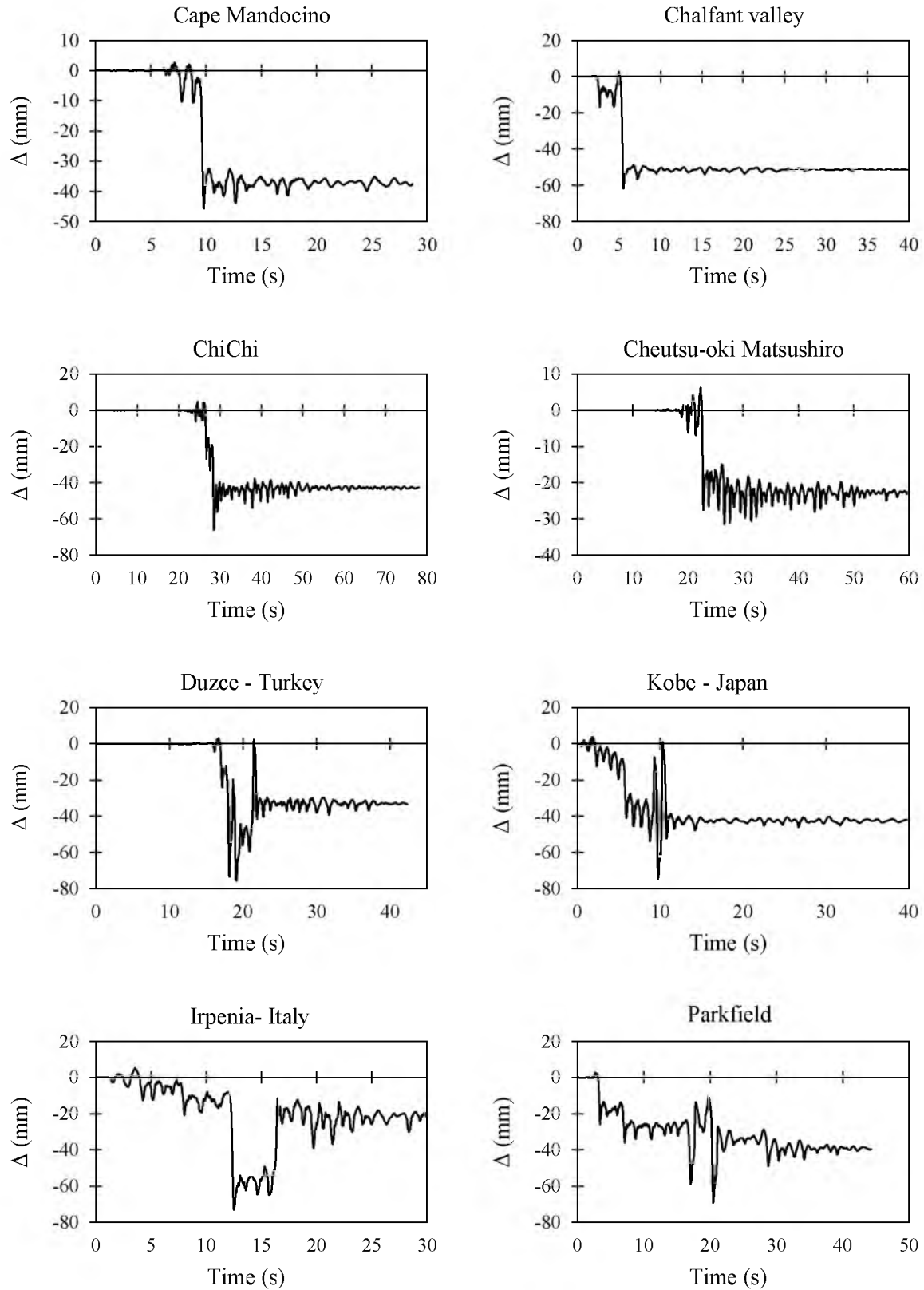


Figure 4.27 Displacement time-history of one longitudinal BRB for scaled ground motions

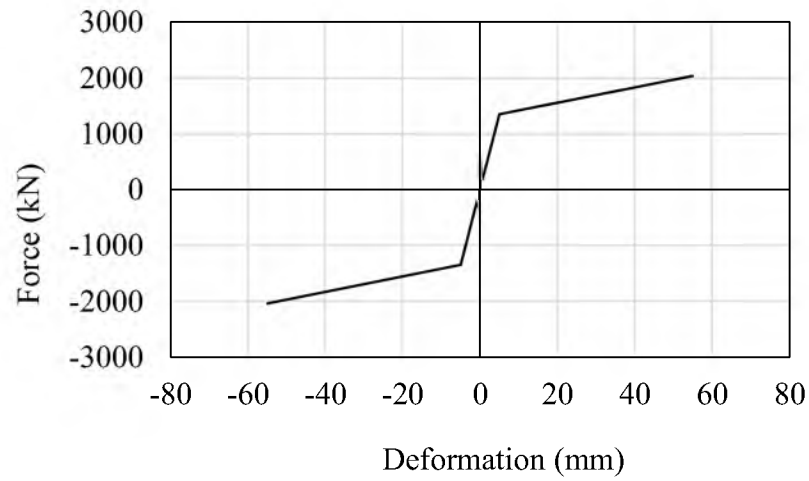


Figure 4.28 Backbone curve for lateral BRBs

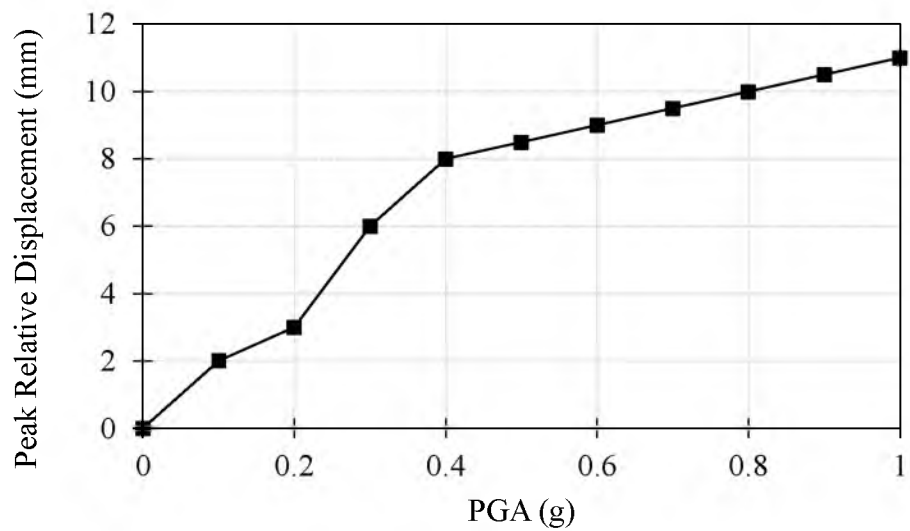


Figure 4.29 Peak displacement of girder relative to concrete shear key during IDA using Kobe (1995) ground motion

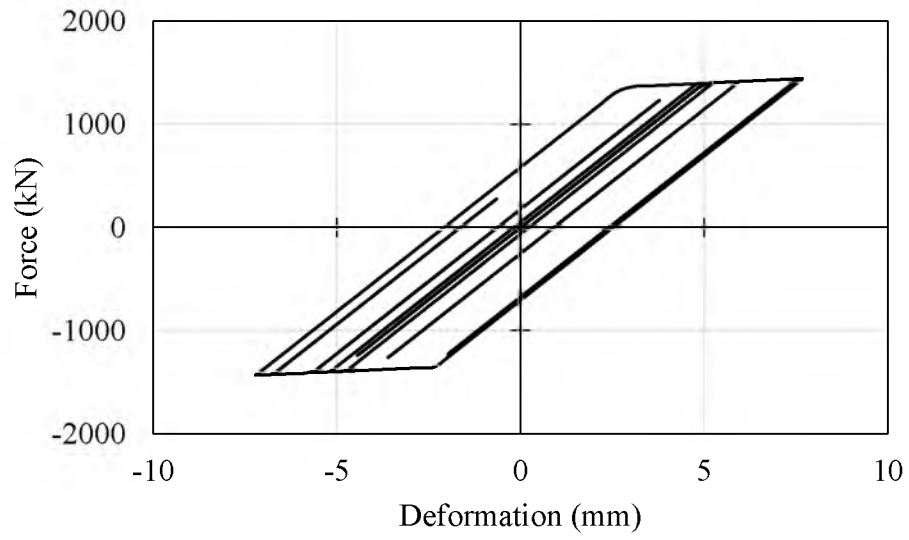


Figure 4.30 Hysteresis of one lateral BRB for scaled Kobe ground motion, 1995

5. CONCLUSIONS

The effects of pounding on curved bridges were studied considering soil-structure interaction. Time history analyses showed that Buckling Restrained Braces can be successfully implemented to prevent structural pounding at the bridge abutments. A nonlinear finite element model of the bridge was built and tested for pounding using several strong earthquake data scaled to site requirement; in addition, Incremental Dynamic Analysis (IDA) was used to examine bridge performance under various earthquake scenarios.

- The bridge model was first analyzed without soil-structure interaction and it was found that the girder displacement was less than the gap provided between the abutment and the girders. No pounding was observed in this case and the columns had sufficient strength to resist the seismic force demand in the pushover analysis.
- The bridge model was then re-analyzed by including soil-structure interaction and it was observed that SSI increased the fundamental period of vibration significantly. The relative movement between girders and abutment was more than 75 mm (the gap provided for girder movement) which led to pounding between the girders and the abutment. The pounding force varied with the PGA (as shown by Incremental Dynamic Analysis) and the characteristic of the earthquake (as shown by the analysis with scaled ground motion data).
- A bilinear BRB backbone curve was selected based on a sensitivity analysis

by comparing the energy dissipation in quasi-static cyclic full-scale load tests carried out at the University of Utah. The selected backbone curve predicted the experimental energy dissipation with a 4% error. The strength of BRB was calculated using ASCE 7-10 and the AISC seismic design manual.

- Nonlinear time-history analyses showed that BRBs successfully prevented seismic pounding between girder and abutment from occurring for the fifteen earthquakes used in the study. IDA and the analysis with scaled ground motions show that the relative displacement between girders and abutment was reduced up to 50% after the retrofit. BRBs placed in the lateral direction were able to prevent concrete shear key damage.

- A BRB of yield strength equal to 2350 kN, for each girder, was required to prevent pounding between abutment and girders. Using BRBs with a yield strength less than 2350 kN reduces the pounding forces. In the lateral direction, two BRBs having strength of 1350 kN placed at an angle 30° (in vertical plane) from the horizontal were able to prevent pounding between girder and concrete shear key.

- Analysis showed that pounding between the girders at the expansion joint was prevented with the help of one BRB on each girder with yield strength of 1500 kN.

- To compare the performance of the BRB element in SAP 2000 and OpenSees, a three column bridge bent was analyzed in the transverse direction using a 2D analysis. The Menegotto-Pinto material model in OpenSees and a bilinear model in SAP 2000 were used to model BRBs. There was a significant difference in nonlinear analysis results between the two structural analysis software. OpenSees

predicted a residual drift in the time-history analysis but the results from SAP 2000 were symmetric without a residual drift. It can be concluded that the bilinear model in SAP 2000 underestimated the displacement demands significantly.

The following recommendations for future research work can be made based on the conclusions mentioned above,

- The curved bridge should be analyzed in OpenSees to document the difference between BRB strength demands predicted by the two platforms.
- As this study observed permanent deformations in BRBs, feasibility of retrofitting the bridge using Self-Centering device can be studied in future research.

APPENDIX A

**CURVED BRIDGE DRAWINGS AND
SITE PHOTOGRAPHS**

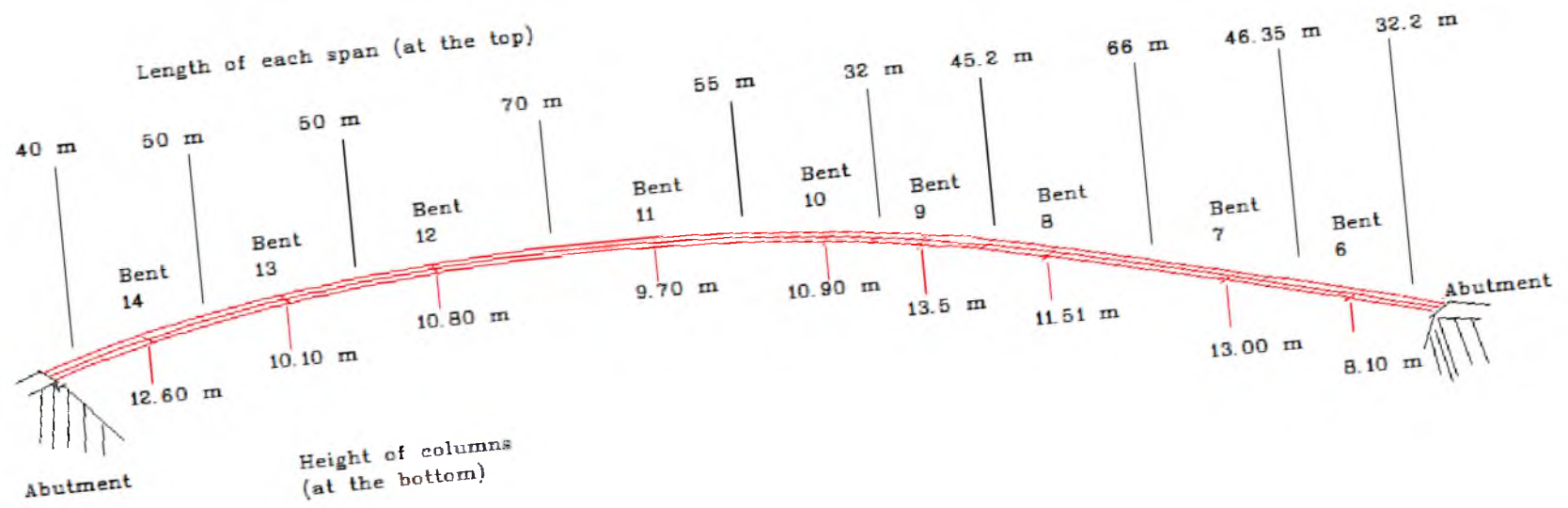


Figure A.1 Plan and elevation of bridge spans

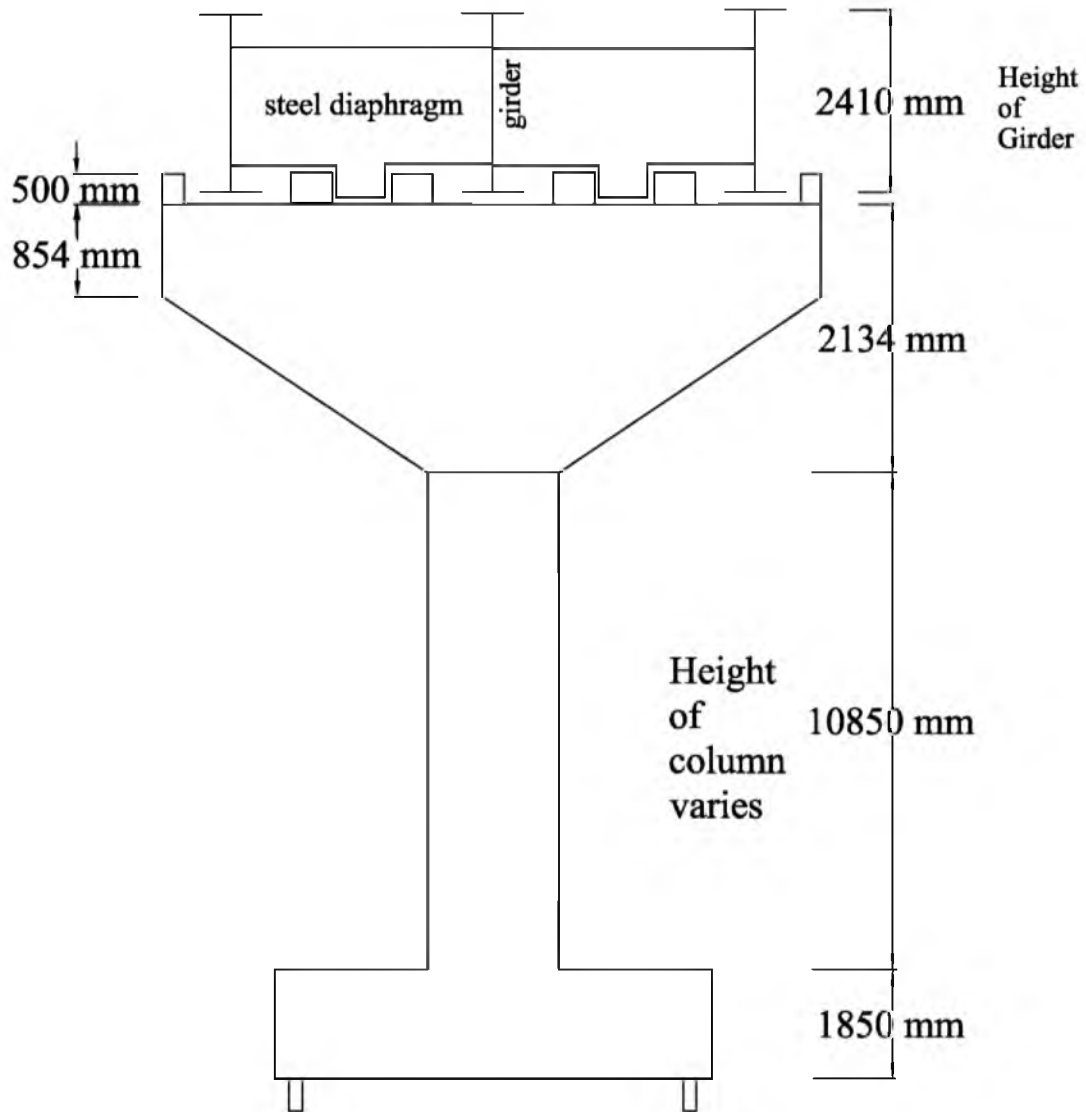


Figure A.2 Elevation of bent 10

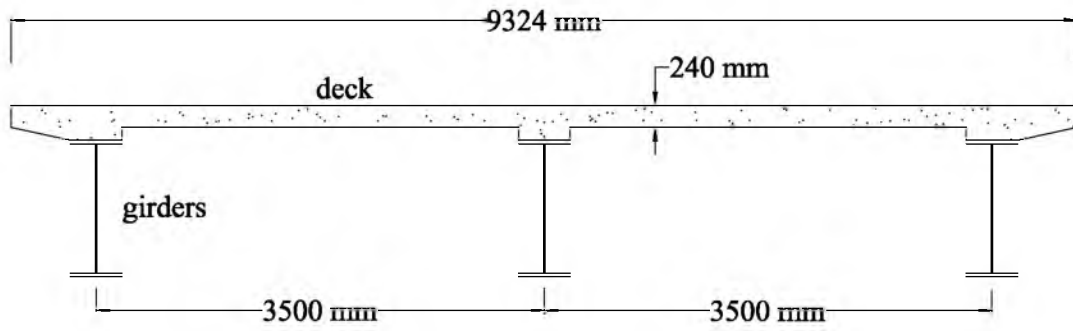


Figure A.3 Dimensions of the concrete deck.

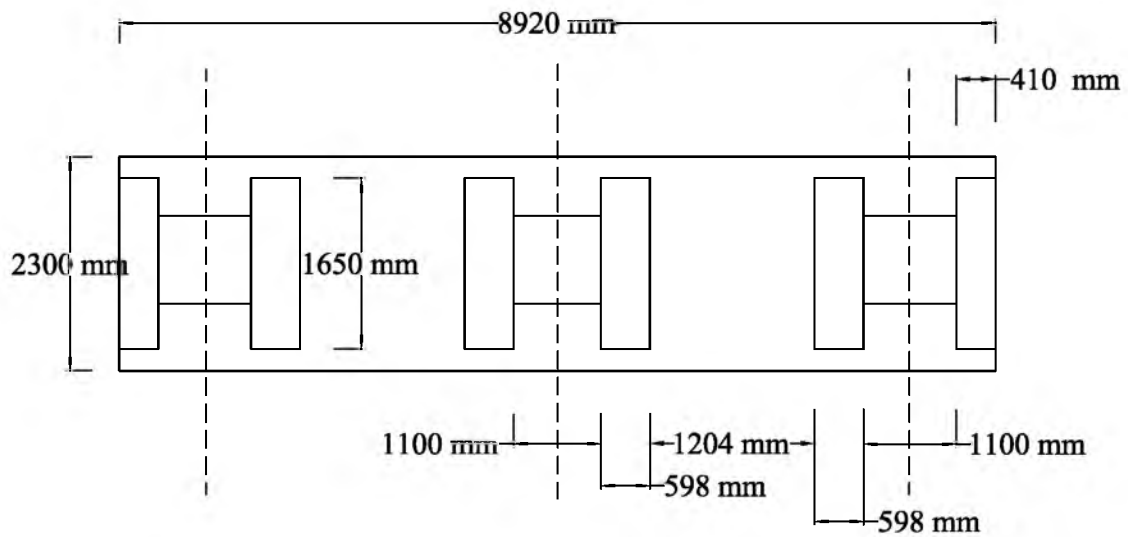


Figure A.4 Top view of the bent beam

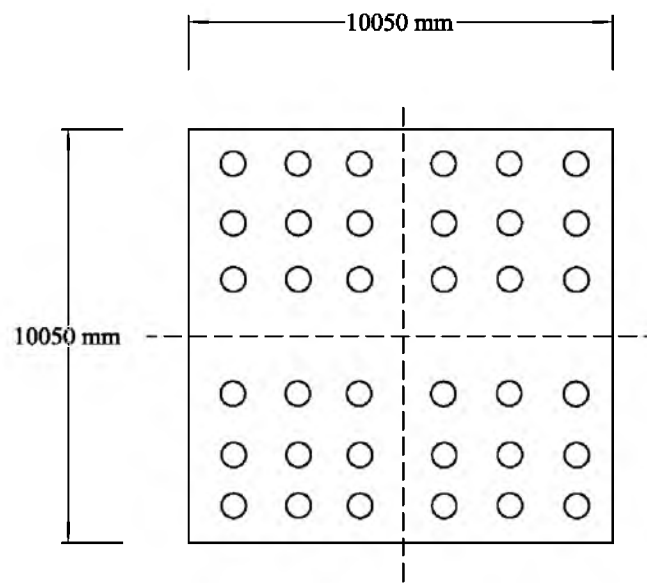


Figure A.5 Pile group and pile cap at bent 11 (see Table A.1 for more details)

Table A-1 Details of pile groups and pile caps at various bents.

Bent No.	Length	Width	Thickness	No. of Piles	Pile Dia.
	mm	mm	mm		mm
2	7920	7920	1850	24	324
3	7920	7920	1850	24	324
4	7920	7920	1850	24	324
5	7920	7920	1850	24	324
6	7920	7920	1850	24	324
7	7920	7920	1850	24	324
8	7920	7920	1850	24	324
9	10050	10050	1850	36	324
10	7920	7920	1850	26	324
11	7920	7920	1850	32	324
12	10050	10050	1850	24	324
13	10050	10050	1850	32	324
14	10050	10050	1850	42	324

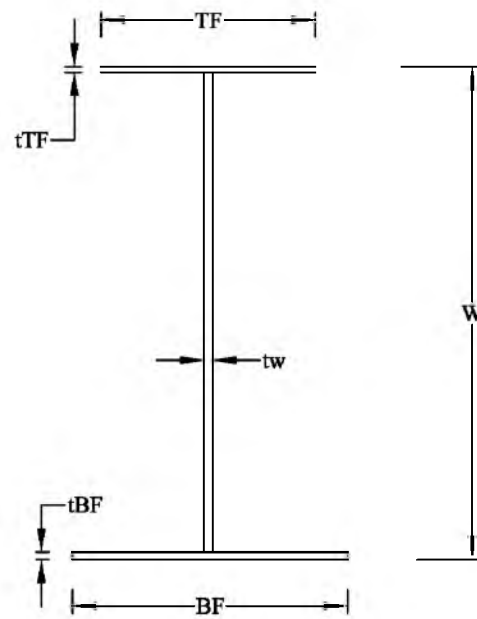


Figure A.6 Section of steel girder used in the curved bridge (see Table A.2 for details)

Table A-2 Steel girder sections used in the curved bridge

S. No.	W	TF	tTF	tw	BF	tBF
	m	m	m	m	m	m
1	2.336	0.350	0.020	0.020	0.684	0.030
2	2.356	0.350	0.035	0.020	0.684	0.035
3	2.426	0.684	0.070	0.020	0.684	0.070
4	2.396	0.610	0.055	0.018	0.684	0.055
5	2.396	0.684	0.055	0.018	0.684	0.550
6	2.344	0.458	0.028	0.016	0.684	0.030
7	2.366	0.458	0.030	0.016	0.684	0.050
8	2.341	0.458	0.020	0.016	0.684	0.035
9	2.356	0.350	0.020	0.016	0.684	0.050
10	2.341	0.458	0.020	0.016	0.684	0.035
11	2.366	0.508	0.030	0.018	0.684	0.050
12	2.336	0.350	0.020	0.016	0.684	0.030
13	2.356	0.458	0.035	0.020	0.684	0.035
14	2.346	0.350	0.025	0.022	0.684	0.035
15	2.374	0.458	0.038	0.022	0.684	0.050
16	2.461	0.684	0.080	0.022	0.684	0.095
17	2.411	0.690	0.060	0.020	0.684	0.065
18	2.411	0.690	0.060	0.020	0.684	0.065
19	2.341	0.350	0.020	0.018	0.684	0.035



Figure A.7 Site photograph of the curved bridge (Bents 11,12,13, and 14)

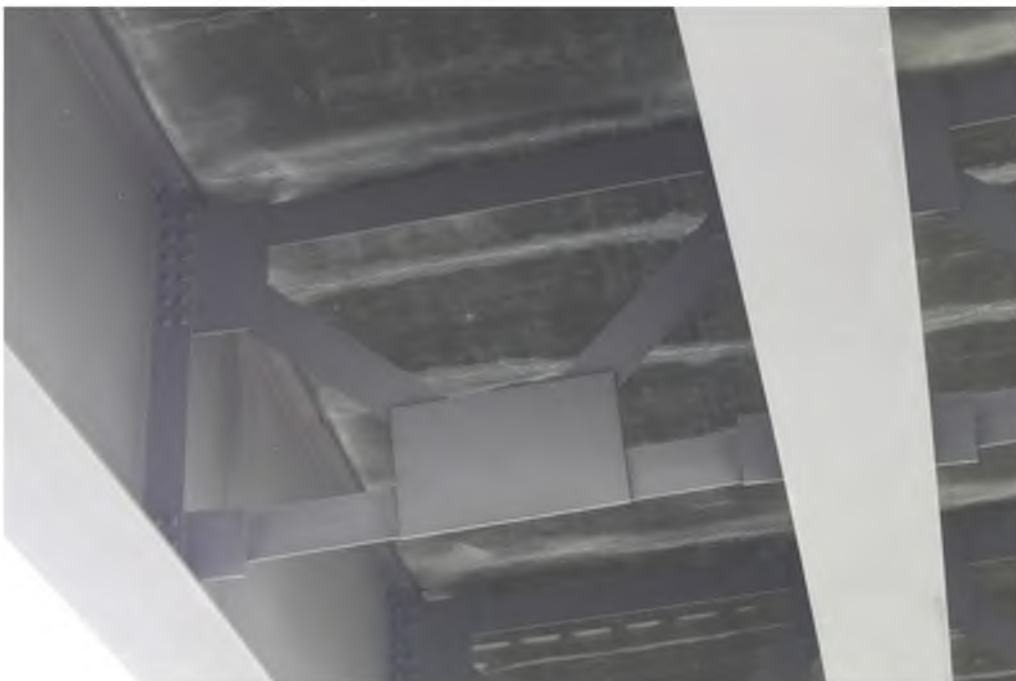


Figure A.8 Site photograph of cross-frames connecting the girders

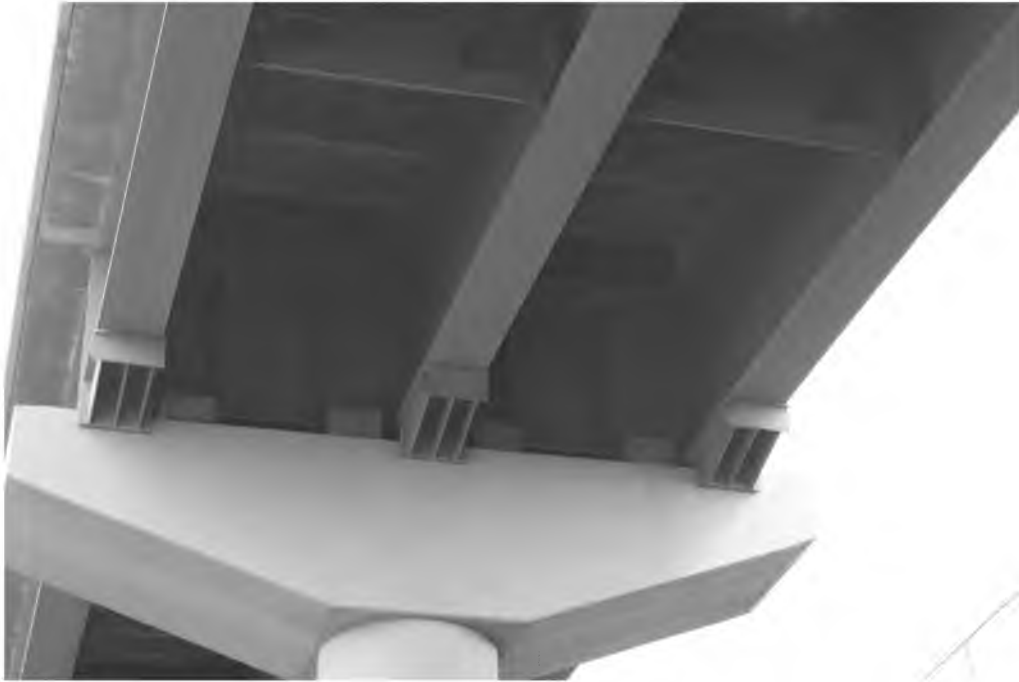


Figure A.9 Site photograph of fixed bearing condition

APPENDIX B

SOIL SPRING CONSTANTS

B.1 Pile Cap-Soil Spring Constant

Soil spring constants for pile caps were calculated based on the directions given in FEMA 356 document in Chapter 4 (Foundations and Geologic Site Hazards). These spring constants are based on the values of soil shear modulus, Poisson's ratio, dimension of the pile-cap and depth of the foundation from the soil surface. From the soil bore-log data (Fig. B.1 and B.2), it is safe to assume the modulus of elasticity of the soil to be 200 MPa and Poisson's ratio 0.2. Effective shear modulus can be calculated using Table 4-7 of the FEMA document. However, shear modulus is a function of peak ground acceleration (PGA) and the value of shear modulus decreases with the increasing value of PGA. This is because the shear waves traveling through a soil stratum change the physical properties of that particular soil stratum resulting in reduction in shear modulus. For simplification, the shear modulus was considered to be constant in this study. Fig. B.3 shows the equations recommended by FEMA 356 document to calculate the soil spring constants for shallow foundations. This value of spring constant should be added to the pile-soil spring constants in parallel combination to get true value. If pile-soil spring constant is comparatively lower than the pile cap-soil spring constant, pile-soil spring constant can be neglected.

B.2 Pile Group

Lateral stiffness of pile group was calculated using procedure (Fig. B.4) to develop P-y curves for piles in clay with no free water given by Welch and Reese (1972). Table B.1 shows the calculation for Y_s , Y_c , and P for soil springs at various depth from the surface. P-y curves for each spring were then calculated (Table B.2) and a trilinear curve was calculated based on equal area method for Sap 2000 input (Table B.3 and Fig. B.5).

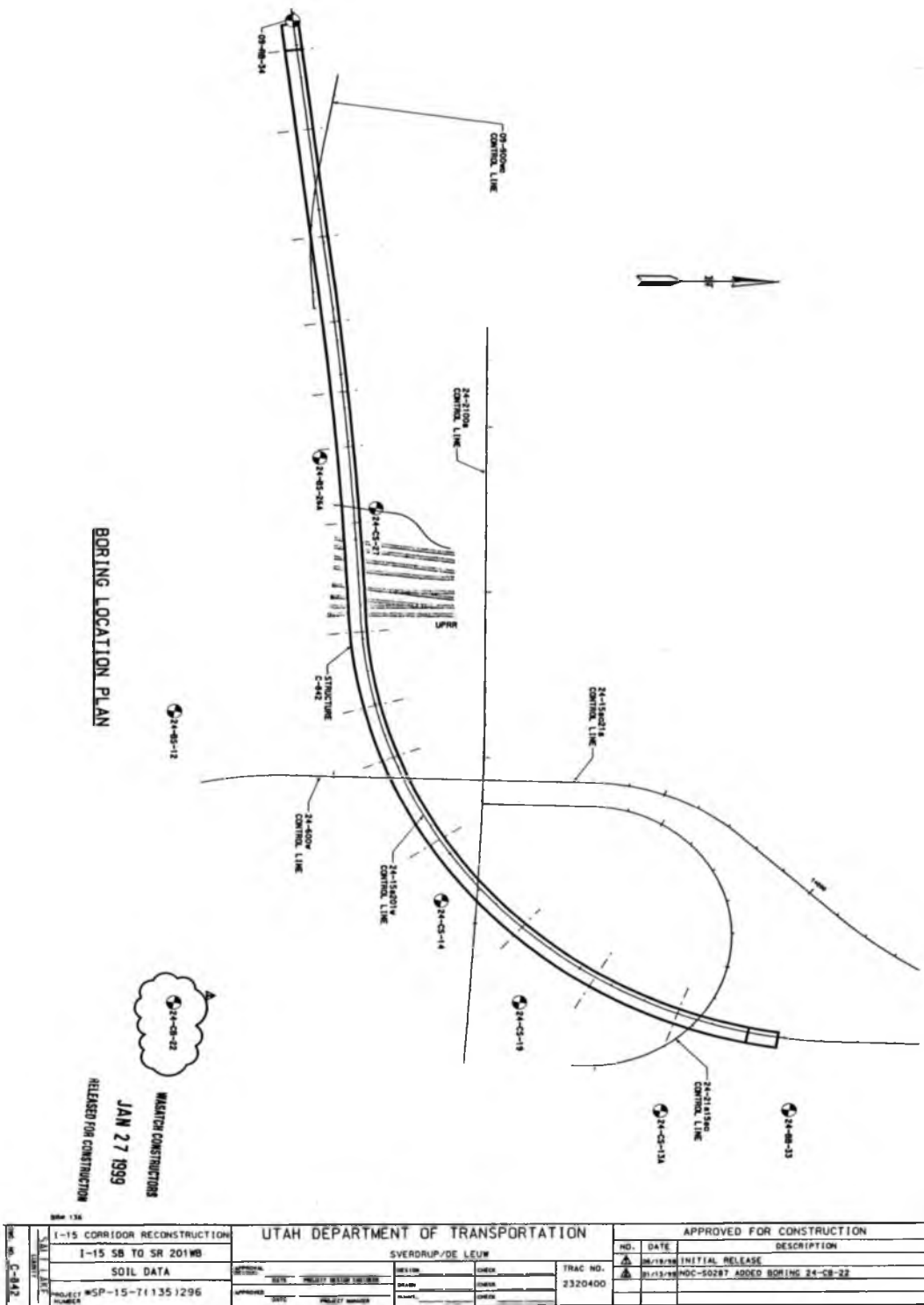
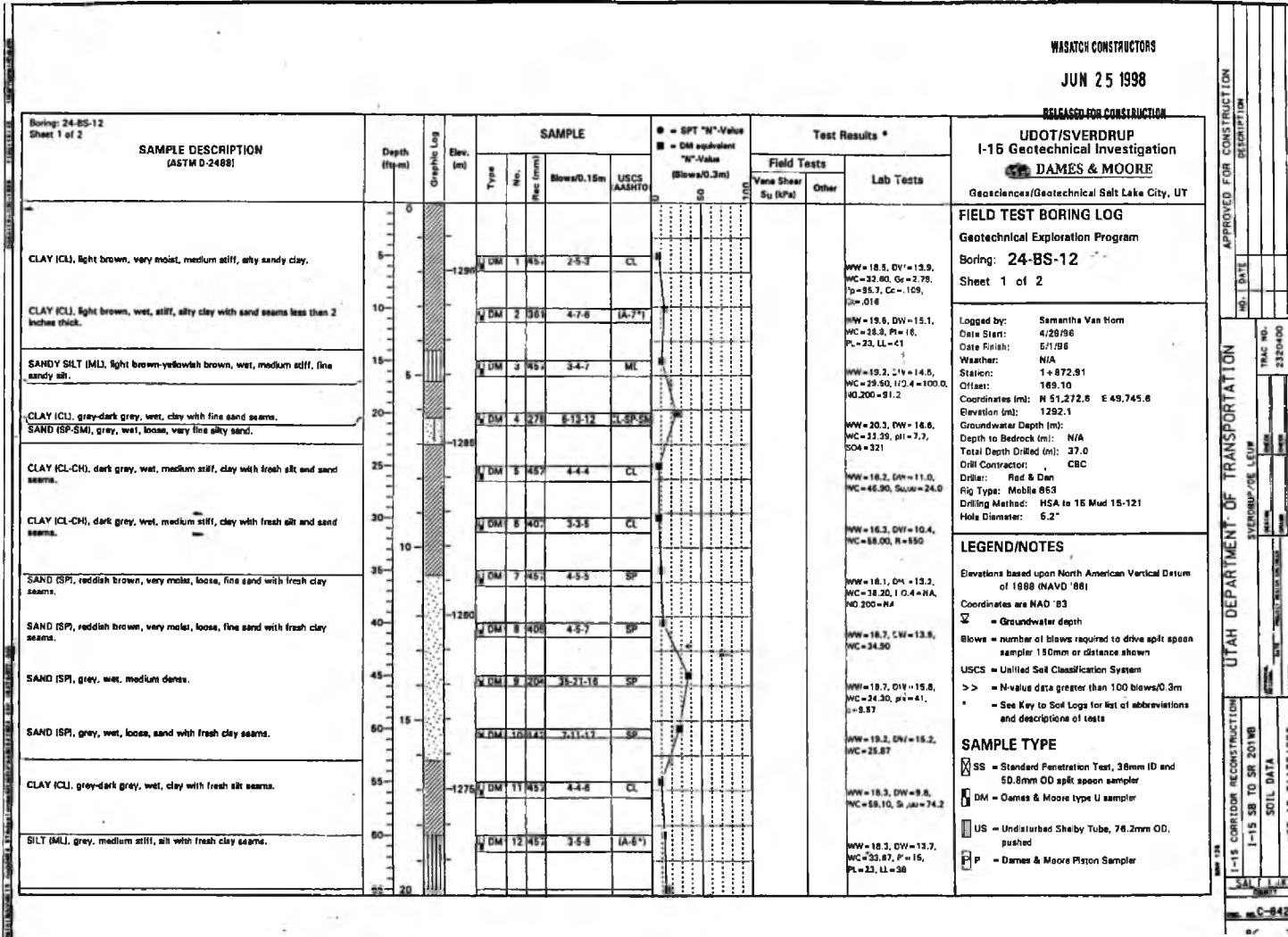


Figure B.1 Location of boreholes

Figure B 2 Soil borehole data



APPROVED FOR CONSTRUCTION
 NO. DATE
 UTAH DEPARTMENT OF TRANSPORTATION
 SVERDRUP/DE LEUM
 TRAC NO. 2320400
 I-15 CORRIDOR RECONSTRUCTION
 I-15 SB TO SR 201WB
 SOIL DATA
 SHEET MSP-13-7(135)296
 SAL L LK
 C-842

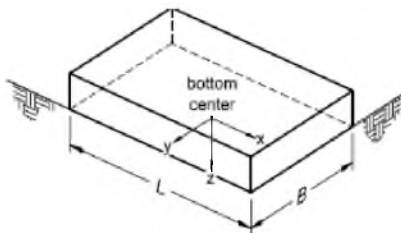
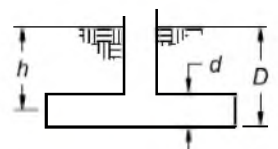
Degree of Freedom	Stiffness of Foundation at Surface	Note
Translation along x-axis	$K_{x, sur} = \frac{GB}{2-\nu} \left[3.4 \left(\frac{L}{B} \right)^{0.65} + 1.2 \right]$	 <p>Orient axes such that $L \geq B$</p>
Translation along y-axis	$K_{y, sur} = \frac{GB}{2-\nu} \left[3.4 \left(\frac{L}{B} \right)^{0.65} + 0.4 \frac{L}{B} + 0.8 \right]$	
Translation along z-axis	$K_{z, sur} = \frac{GB}{1-\nu} \left[1.55 \left(\frac{L}{B} \right)^{0.75} + 0.8 \right]$	
Rocking about x-axis	$K_{xx, sur} = \frac{GB^3}{1-\nu} \left[0.4 \left(\frac{L}{B} \right) + 0.1 \right]$	
Rocking about y-axis	$K_{yy, sur} = \frac{GB^3}{1-\nu} \left[0.47 \left(\frac{L}{B} \right)^{2.4} + 0.034 \right]$	
Torsion about z-axis	$K_{zz, sur} = GB^3 \left[0.53 \left(\frac{L}{B} \right)^{2.45} + 0.51 \right]$	
Degree of Freedom	Correction Factor for Embedment	Note
Translation along x-axis	$\beta_x = \left(1 + 0.21 \frac{\bar{D}}{\sqrt{B}} \right) \cdot \left[1 + 1.6 \left(\frac{hd(B+L)}{BL^2} \right)^{0.4} \right]$	 <p>d = height of effective sidewall contact (may be less than total foundation height) h = depth to centroid of effective sidewall contact</p> <p>For each degree of freedom, calculate $K_{emb} = \beta K_{sur}$</p>
Translation along y-axis	$\beta_y = \beta_x$	
Translation along z-axis	$\beta_z = \left[1 + \frac{1}{21} \frac{D}{B} \left(2 + 2.6 \frac{B}{L} \right) \right] \cdot \left[1 + 0.32 \left(\frac{d(B+L)}{BL} \right)^{2/3} \right]$	
Rocking about x-axis	$\beta_{xx} = 1 + 2.5 \frac{d}{B} \left[1 + \frac{2d}{B} \left(\frac{d}{D} \right)^{-0.2} \sqrt{\frac{B}{L}} \right]$	
Rocking about y-axis	$\beta_{yy} = 1 + 1.4 \left(\frac{d}{L} \right)^{0.6} \left[1.5 + 3.7 \left(\frac{d}{L} \right)^{1.9} \left(\frac{d}{D} \right)^{-0.6} \right]$	
Torsion about z-axis	$\beta_{zz} = 1 + 2.6 \left(1 + \frac{B}{L} \right) \left(\frac{d}{B} \right)^{0.9}$	

Figure B.3 Equations to calculate foundation-soil spring constants (FEMA 356)

Static Loading

1. Compute ultimate soil resistance, P_u (using the smaller values)	$P_u = \left[3 + \frac{\gamma^*}{C_u} z + \frac{J}{D} z \right] C_u D$ $P_u = 9C_u D$
2. Compute deflection at one-half the ultimate soil resistance, y_{50}	$y_{50} = 2.5 \varepsilon_{50} D$
3. Develop p - y curves using the following expression	$\frac{P}{P_u} = 0.5 \left(\frac{y}{y_{50}} \right)^{1/4} \quad \text{for } y \leq 16 y_{50}$ $P = P_u \quad \text{for } y > 16 y_{50}$

Cyclic Loading

1. Develop p - y curves for static loading	Follow step 1 to 3
2. Determine parameter describing effect of repeated loading, C	$C = 9.6 \left(\frac{P}{P_u} \right)^4$
3. Determine y for cyclic loading, y_c	$y_c = y_s + y_{50} C \log N$

Where: C_u	=	Undrained shear strength
D	=	Pile diameter
J	=	Constant =0.5
N	=	Number of cycles
P_{ult}	=	Ultimate soil resistance
y_{50}	=	Deflection at One-half the ultimate soil resistance
y_c	=	Deflection under N-cycles of load
y_s	=	Deflection under short-term static
Z	=	Depth
ε_{50}	=	Strain at one-half ultimate soil resistance 0.020 for soft clay, 0.010 for medium clay, and 0.005 for stiff clay
γ^*	=	Effective soil unit weight

Figure B.4 P-y curve calculation procedure

Table B-1 Calculation of Y_s , Y_c , and P at various depth

Depth Z	Unit weight	$S_{U,u}$	Pile Dia. D	J	$P_{U,1}$	$P_{U,2}$	ϵ_{50}	Y_{50}	P_u
m	kN/m ³	kN/m ²	m		kN	kN		m	
2	19.00	25.00	0.324	0.5	61.60	72.90	0.005	0.00405	72.90
3	19.00	25.00	0.324	0.5	80.20	72.90	0.005	0.00405	80.26
4	19.00	25.00	0.324	0.5	98.90	72.90	0.005	0.00405	98.92
5	19.00	24.00	0.324	0.5	114.10	69.90	0.005	0.00405	114.10
6	19.00	24.00	0.324	0.5	132.20	69.90	0.005	0.00405	132.26
7	19.00	25.00	0.324	0.5	154.80	72.90	0.005	0.00405	154.89
8	19.00	25.00	0.324	0.5	173.50	72.90	0.005	0.00405	173.54
9	19.00	30.46	0.324	0.5	222.10	88.80	0.005	0.00405	222.11
10	19.00	35.93	0.324	0.5	276.10	104.70	0.005	0.00405	276.15
11	19.00	41.39	0.324	0.5	335.60	120.70	0.005	0.00405	335.65
12	19.00	46.86	0.324	0.5	400.60	136.60	0.005	0.00405	400.62
13	19.00	52.30	0.324	0.5	471.00	152.60	0.005	0.00405	471.06
14	19.00	57.79	0.324	0.5	546.90	168.50	0.005	0.00405	546.96
15	19.00	63.26	0.324	0.5	628.30	184.40	0.005	0.00405	628.33
16	19.00	68.73	0.324	0.5	715.20	200.40	0.005	0.00405	715.17
17	19.00	74.20	0.324	0.5	807.40	216.30	0.005	0.00405	807.47

Table B-2 Calculation of P-y curve at depth $Z = 2$ m.

Y_s	Y_{50}	P_U	P	N	C	Y_c	Area under curve
m	m	kN/m	kN/m			m	
0	0.00405	61.61	0	20	0	0	
0.001	0.00405	61.61	21.71	20	0.148	0.001	0.0193
0.002	0.00405	61.61	25.82	20	0.296	0.003	0.0423
0.003	0.00405	61.61	28.57	20	0.444	0.005	0.0484
0.004	0.00405	61.61	30.71	20	0.592	0.007	0.0527
0.008	0.00405	61.61	36.52	20	1.185	0.014	0.2394
0.012	0.00405	61.61	40.41	20	1.777	0.021	0.2739
0.016	0.00405	61.61	43.43	20	2.370	0.028	0.2986
0.02	0.00405	61.61	45.92	20	2.962	0.035	0.3182
0.024	0.00405	61.61	48.06	20	3.555	0.042	0.3347
0.028	0.00405	61.61	49.95	20	4.148	0.049	0.3490
0.032	0.00405	61.61	51.64	20	4.740	0.056	0.3618
0.036	0.00405	61.61	53.19	20	5.333	0.064	0.3733
0.04	0.00405	61.61	54.61	20	5.925	0.071	0.3839
0.044	0.00405	61.61	55.92	20	6.518	0.078	0.3936
0.048	0.00405	61.61	57.15	20	7.111	0.085	0.4027
0.052	0.00405	61.61	58.31	20	7.703	0.092	0.4112
0.056	0.00405	61.61	59.40	20	8.296	0.099	0.4192
0.06	0.00405	61.612	60.4379	20	8.88	0.106837	0.4267867
0.064	0.00405	61.612	61.612	20	9.60	0.114584	0.4727582
0.068	0.00405	61.612	61.612	20	9.60	0.118584	0.246448
0.072	0.00405	61.612	61.612	20	9.60	0.122584	0.246448
0.076	0.00405	61.612	61.612	20	9.60	0.126584	0.246448
0.08	0.00405	61.612	61.612	20	9.60	0.130584	0.246448
0.084	0.00405	61.612	61.612	20	9.60	0.134584	0.246448
0.088	0.00405	61.612	61.612	20	9.60	0.138584	0.246448
0.092	0.00405	61.612	61.612	20	9.60	0.142584	0.246448
0.096	0.00405	61.612	61.612	20	9.60	0.146584	0.246448
0.1	0.00405	61.612	61.612	20	9.60	0.150584	0.246448

Total area under the curve = 7.8404 (to generate a tri-linear curve)

Table B-3 Tri-linear curve points for P-y curve at Z=2 m

Point	Y (kN/m)	P (m)	Area
1	0	0	
2	0.007122	30.806	0.1097
3	0.079412	61.612	3.340446
4	0.15058	61.612	4.384806

Total area under the tri-linear curve = 7.8349

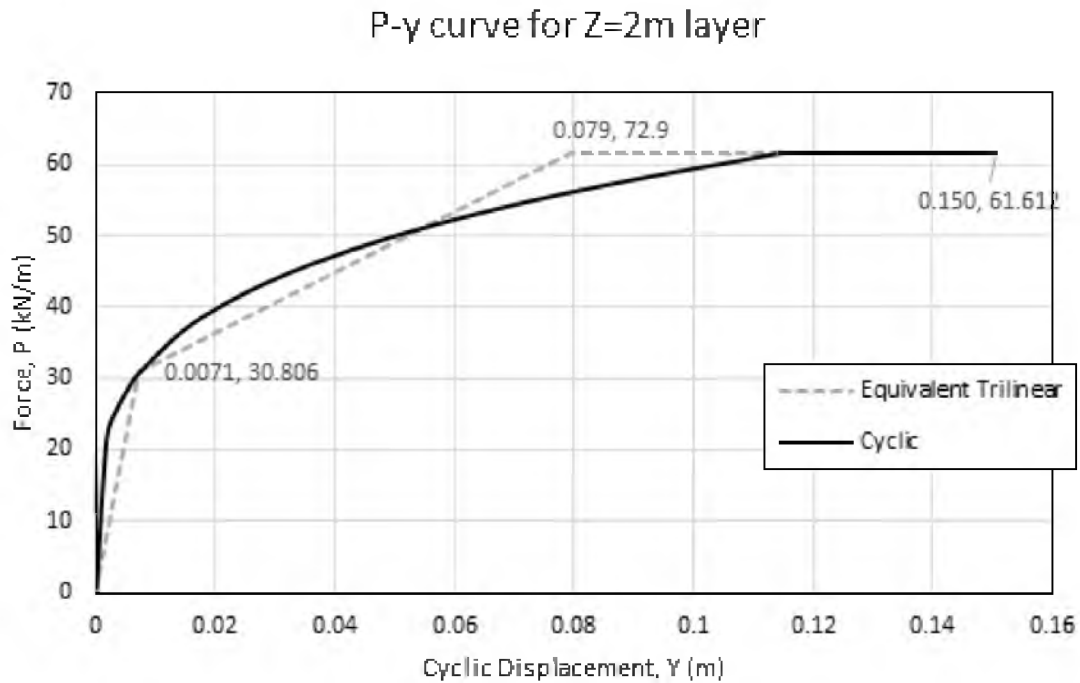


Figure B.5 P-y curve for pile at Z=2m

APPENDIX C

**COMPARISON OF BRB PERFORMANCE IN
SAP 2000, PERFORM 3D, AND OPENSEES**

As SAP 2000 does not provide any material model with Isotropic hardening, it was decided to compare the SAP 2000 bilinear model for BRB with Isotropic hysteresis models available in Opensees (Open System for Earthquake Engineering Simulation, 2014). This comparative study was done on a three column bridge bent to estimate the difference between results using the SAP 2000 bilinear model, and the Steel-02 Menegotto-Pinto material model in the OpenSees library. Hysteretic material constructs a uniaxial bilinear hysteretic material object with pinching of force and deformation, damage due to ductility and energy, and degraded unloading stiffness based on ductility. A comparison of Menegotto-Pinto model and SAP 2000 bilinear model is shown in Fig. C.1.

C.1 Bridge Bent Details

The bridge located on South Temple, Salt Lake City, was designed in the early 1960s. As a part of Interstate-15 reconstruction project, this bridge was studied by Pantelides et al. (2000) for carbon fiber retrofit before demolition. Fig. C.2 and Fig. C.3 show the bridge bent used in this study and sections detail, respectively.

In the analysis model, the cap beam was considered as a rigid elastic element and it was assumed that beam-column and column-pile cap joints were strong enough to withstand shear forces, i.e., no material degradation was considered in this study. The total deck load was 1920 kN and was assigned to the middle node of the bent cap in the numerical model. The weight of the columns (144 kN) each was included as concentrated loads at the top and bottom of the columns. The specified concrete strength was 21MPa, and the yield strength of the longitudinal and the transverse reinforcement was given as 276MPa. The supports were modeled as fixed.

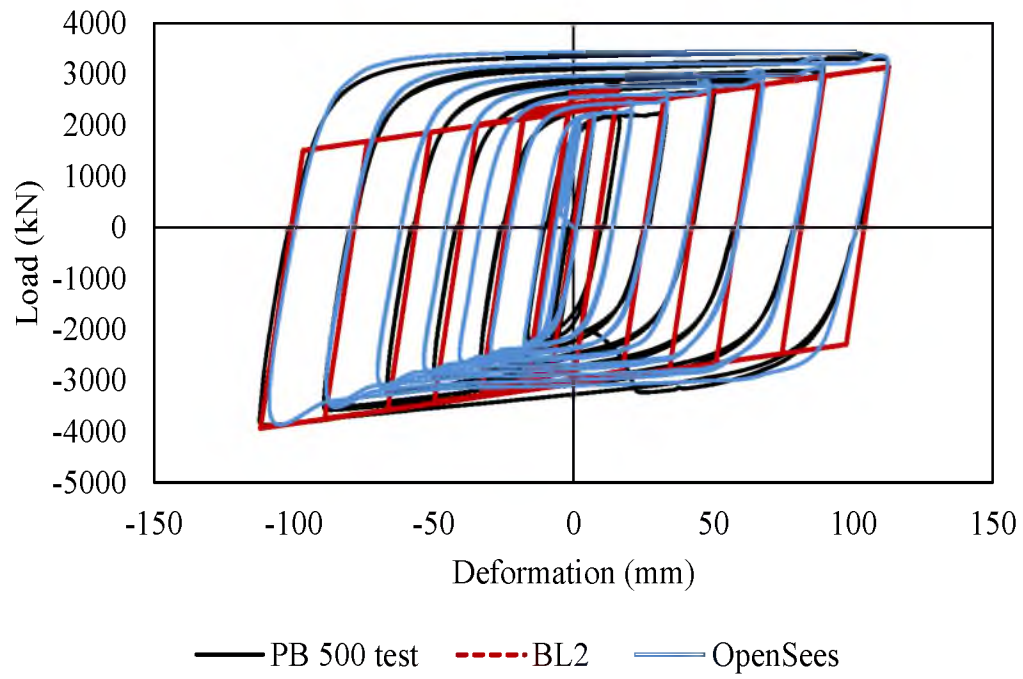


Figure C.1 Comparison of OpenSees and SAP 2000 BRB model with lab tests by Xu (2016)

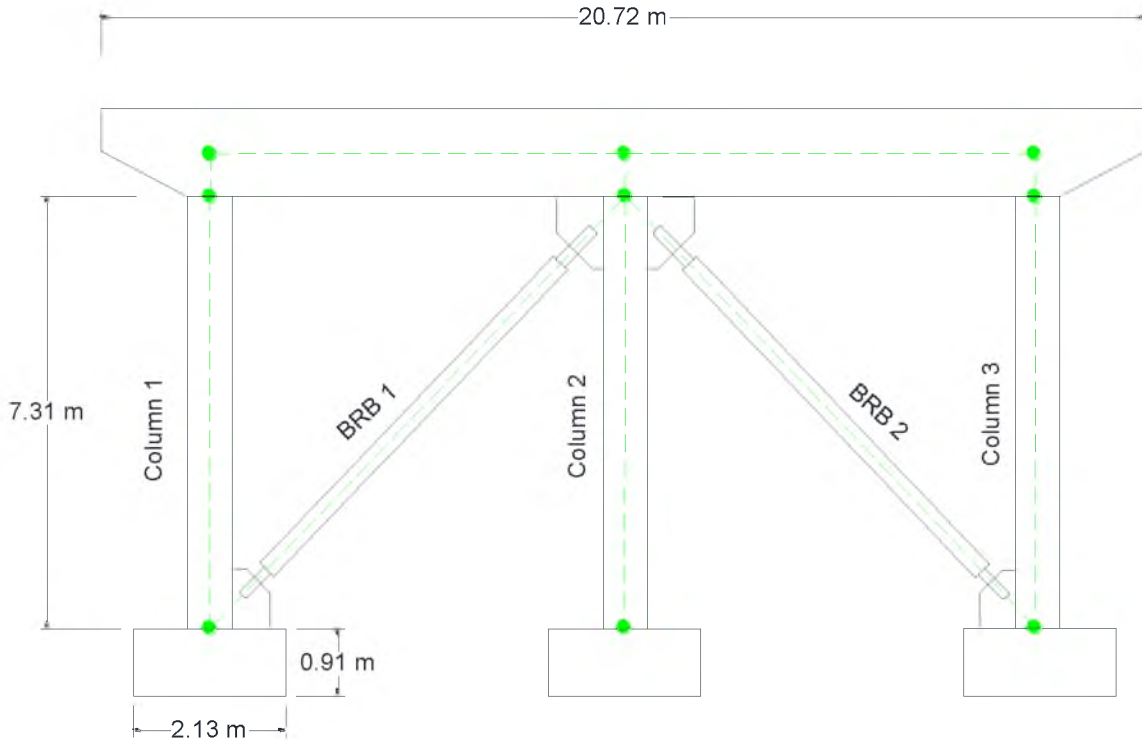


Figure C.2 I-15 Bridge bent dimensions

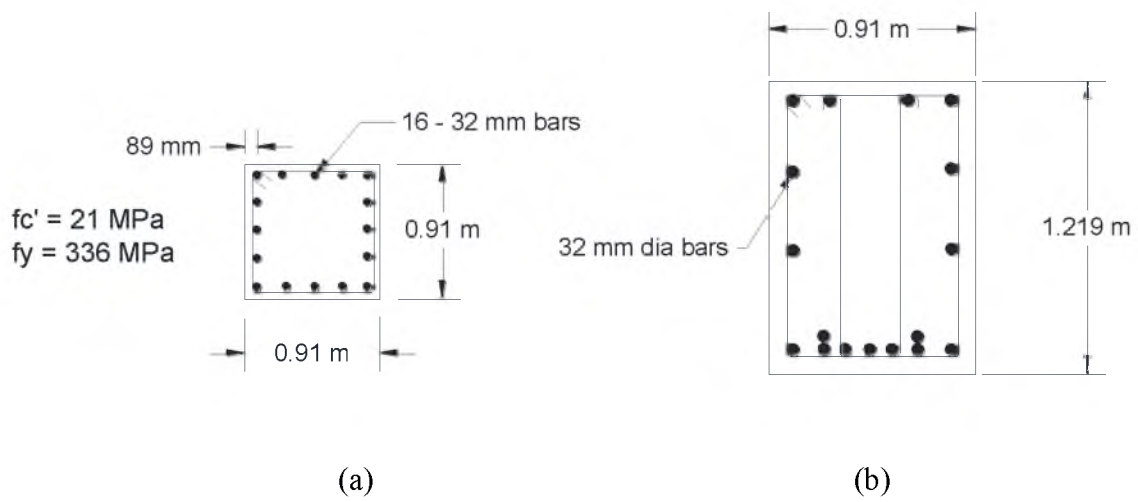


Figure C.3 Sectional details of (a) Column and (b) Bent beam

C.2 Design of BRB

The Buckling Restrained Brace was designed following the iterative procedure given by ASCE -07 and AISC (American Institute of Steel Construction) seismic manual. The work-point length of the brace was considered from node to node, as $L_{BRB} = 10.30$ m. A length ratio of 70% was considered which is commonly used in most BRB designs. The Length ratio is defined as the ratio of length of core to length of connection plates. Area of connection plates was considered very large to keep the stiffness higher than the core part. Following is the calculation for design of BRB for the bent,

Gravity load and seismic force were calculated as follows,

Dead Load (Deck + Bent Beam) = 1919.97 kN

Live Load = 19438.63 kN (based on AASHTO recommendation)

Concrete compressive strength = 21 MPa

Steel strength = 276 MPa

Using ASCE 7-10 procedure

From Fig. 2.9 we get,

$S_{ds} = 0.901g$

$S_{d1} = 0.434g$

Importance Factor, $I_e = 1$

Response Modification Factor, $R = 8$

$C_s = 0.113$

Base Shear, $V = 216.23$ kN

Overstrength, $\Omega_0 = 2.5$

Therefore,

Design Base Shear, $V_{\text{Design}} = 540.59 \text{ kN}$

BRB design earthquake load, $P_{\text{EQ}} = 405.44 \text{ kN}$

Axial force in BRB, $F_{\text{BRB}} = 287.71 \text{ kN}$

Therefore required compressive and tensile strength of the brace are:

$$\rho = 1.3$$

$$P_u = T_u = \rho P_{\text{QE}} = 1.3(405.44) = 374 \text{ kN}$$

BRB can be designed as follows,

Yield stress of core steel = 281.96 MPa (Given by manufacturer)

Modulus of elasticity, $E = 200,000 \text{ MPa}$

Yield Strain = 0.00141 m/m

Angle of BRB = 45.22° (Fig. C.2)

(Iterative procedure, the values given here are from last iteration)

Core area (A_{core}) = 2580 mm^2

Length of BRB (L_{BRB}) = 10.30 m

Length ratio = 0.7 (ratio of length of core to length of BRB)

Area of connection plates (A_{bound}) = 12900 mm^2

Stiffness calculation:

$$K_{\text{core}} = \frac{A_{\text{core}}E}{(\text{ratio})L_{\text{BRB}}} = 2580 \times 10^{-6} \times 200 \text{ GPa}/(0.7 \times 10.30)$$

$$= 71500 \text{ kN/m}$$

$$K_{bound} = \frac{A_{bound}E}{(1-ratio)L_{BRB}} = 12900 \times 10^{-6} \times 200 \text{ GPa}/(0.3 \times 10.30)$$

$$= 834177 \text{ kN/m}$$

$$\frac{1}{K_{BRB}} = \frac{1}{K_{core}} + \frac{1}{K_{bound}}$$

Hence,

$$\mathbf{K_{BRB} = 61036.66 \text{ kN/m}}$$

Column stiffness (section 0.91 m x 0.91 m.)

$$K_{Column} = 16502.16 \text{ kN/m}$$

Hence, frame stiffness

$$K_{Frame} = K_{Column} + 2 K_{BRB}$$

$$= 220052.43 \text{ kN/m}$$

Lateral drift,

$$\Delta = 2.46 \text{ mm}$$

Following AISC procedure,

$$P_{Story} = (1.2 + 0.2 S_{DS}) \text{ Dead Load} + 1.2 \text{ Design Base Shear} + 0.5 \text{ Live Load}$$

$$= 13018 \text{ kN}$$

$$P_{e,story} = 1 \times \text{Design Base shear} \times L_{Beam} \times \Delta$$

$$= 1598549 \text{ kN}$$

$$\delta = 1$$

$$B_2 = \frac{1}{1 - \frac{\delta P_{Story}}{P_{e,story}}} = 1.008$$

$$P_{u2} = B_2 P_u = 377.073 \text{ kN}$$

Required core area, $A_{Core} = P_{u2}/0.9 \cdot F_y$

$$= 1483.87 \text{ mm}^2$$

Use a core with area = 4 in²

$$\begin{aligned}\phi P_n &= 0.9 A_{\text{core}} F_y \\ &= 654.952 \text{ kN}\end{aligned}$$

Design story drift

$$\Delta_{\text{design}} = 5 * \Delta = 12.2 \text{ mm}$$

$$2 \Delta_{\text{design}} = 24.6 \text{ mm}$$

$$2\% \text{ story drift } \Delta_{2\%} = 0.02 \times H_{\text{Column}} = 146.3 \text{ mm (Governs)}$$

Hence,

Brace deformation

$$\begin{aligned}\Delta_{\text{brace}} &= (H_{\text{col}}^2 + (\Delta_{2\%} L_{\text{beam}})^2)^{0.5} - L_{\text{BRB}} \\ &= 103.63 \text{ mm}\end{aligned}$$

Strain in core,

$$\begin{aligned}\epsilon &= \Delta_{\text{brace}} / L_{\text{core}} \\ &= 1.44 \%\end{aligned}$$

Input for OpenSees model:

$$A_{\text{core}} = 2580 \text{ mm}^2$$

Yield deformation = Yield strain x core length

$$\begin{aligned}&= 0.00141 \text{ m/m} \times (0.7 \times 10.30 \text{ m}) \\ &= 10.92 \text{ mm.}\end{aligned}$$

Yield force can be calculated as

$$P_y = K_{BRB} \times \Delta_{yield} = 61036.66 \times 0.0109$$

$$= 620.968 \text{ kN}$$

Hence, the input for the BRB model is as follows,

Yield force = 620.97 kN

Yield displacement = 10.93 mm

Initial stiffness = 61036.66 kN/m

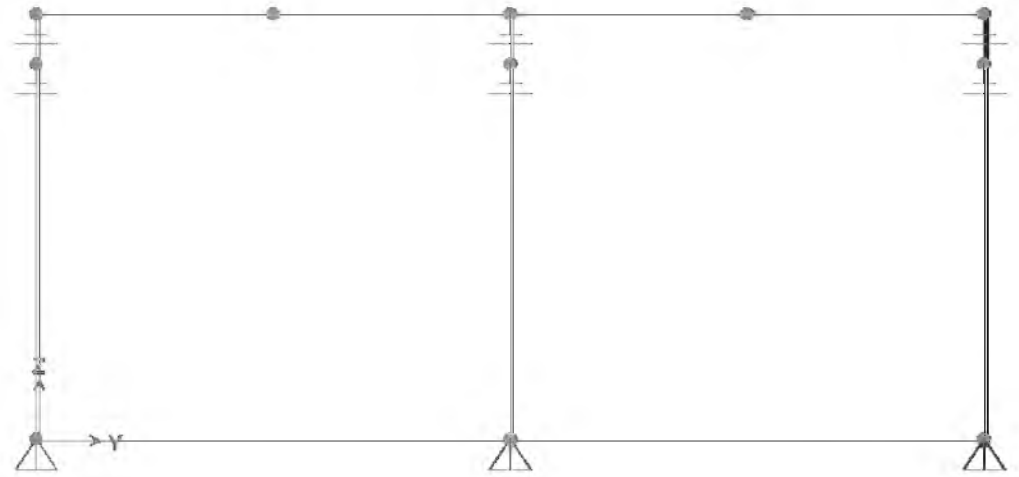
Based on literature following values were adopted,

$$\beta = 1.03$$

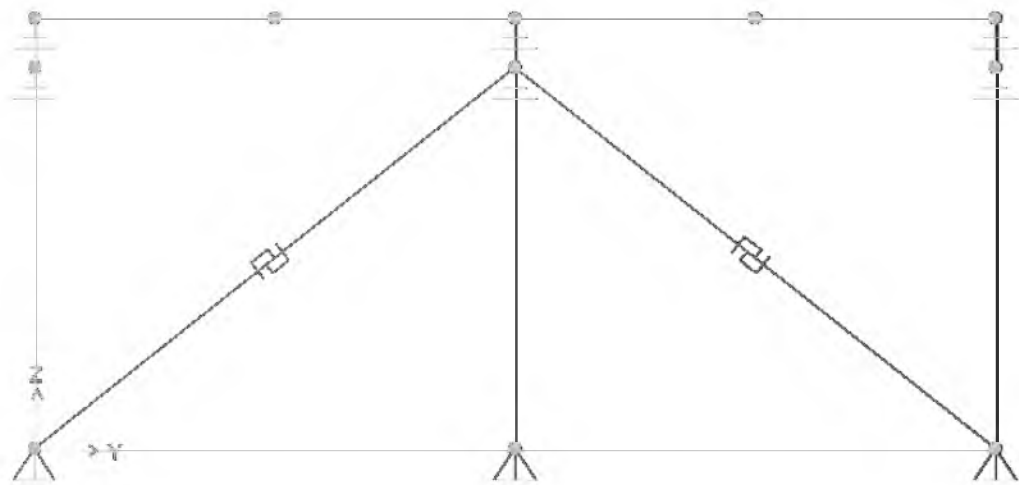
$$\omega = 1.22$$

C.3 Comparison of results from SAP 2000, OpenSees and, Perform 3D

BRBs were installed in the bridge bent in a configuration shown in Fig. C.4. Modal analysis results from both platforms are presented in Table C.1 which shows that the 1st mode of vibration was predicted closely by both SAP 2000, Perform 3D and OpenSees. After using BRB link element, the periods were 0.27 sec. by SAP 2000 and 0.25 sec. by OpenSees which shows that BRBs increased the stiffness of the system. The structure was subjected to Kobe ground motion shown in Fig. C.5. Fig. C.6 shows drift time histories for bent top. The values predicted by the SAP 2000 and OpenSees models were close to each other for as-built conditions. The peak bent top displacement was observed as 38 mm for both OpenSees and SAP 2000 models while for Perform 3D model the peak displacement was 41 mm. These data support the similarity between the fundamental periods of vibration calculated by all the software platforms.

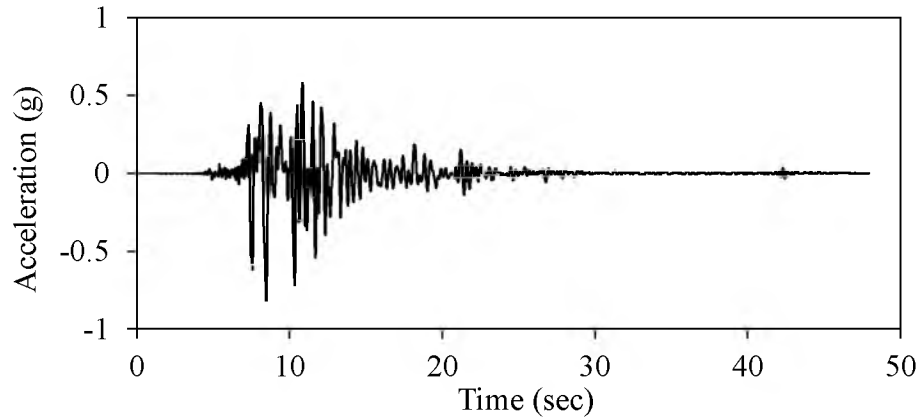


(a)

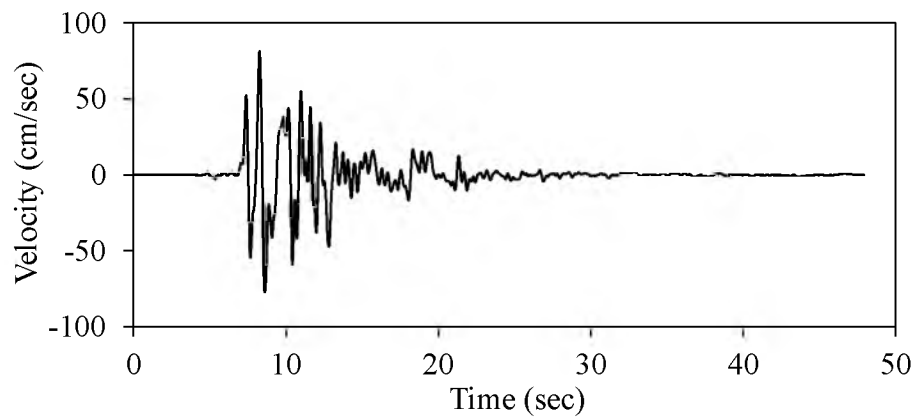


(b)

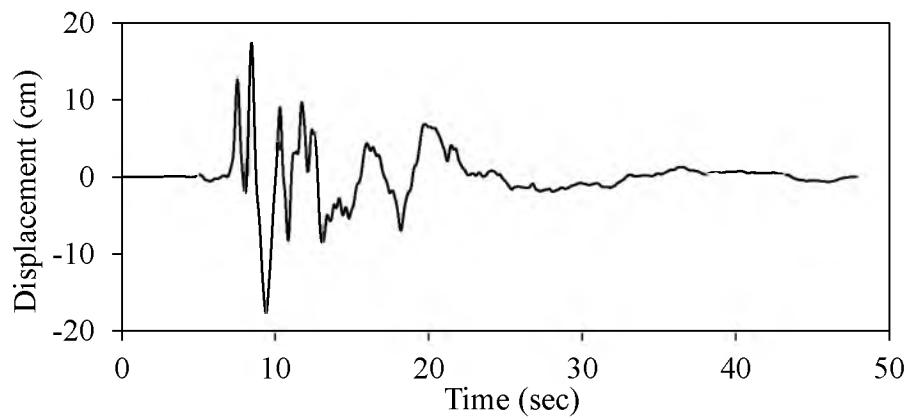
Figure C.4 Bent model in SAP 2000 (a) without BRB and (b) with BRB



(a)



(b)



(c)

Figure C.5 Kobe (1995) ground motion (a) acceleration, (b) velocity and, (c) displacement

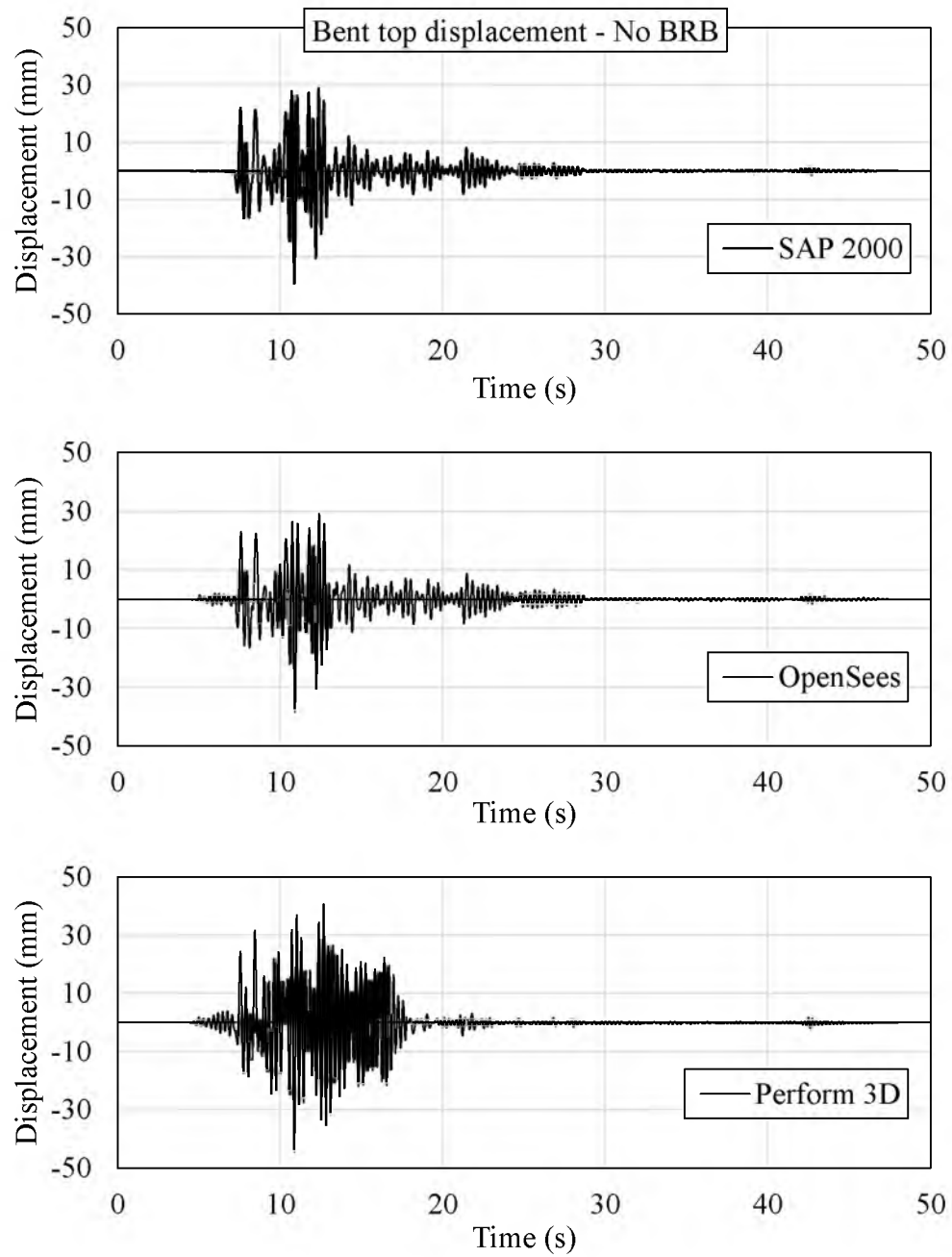


Figure C.6 As-built bent top displacement time histories for Kobe (0.8g) ground motion

Fig. C.7 shows the bent top displacement time histories after retrofitting with BRBs. It can be observed that BRBs successfully reduced the bent top displacement significantly. The bent top displacement values with BRB element by SAP 2000 were symmetric about zero and the peak displacement was 16 mm but the values predicted by OpenSees were not symmetric and the peak value was 24 mm. The residual displacement calculated by SAP 2000 was zero but by OpenSees it was 4 mm, which shows that SAP 2000 model underestimated the displacement values.

Incremental Dynamic Analysis (IDA) was performed on the bent with BRB using the Kobe ground motion. IDA shows that for small peak ground accelerations SAP 2000 and Perform 3D predicted results close to each other. As the peak ground acceleration increases, the displacement values calculated by SAP 2000 and Perform 3D remained symmetric with residual displacement close to zero while values calculated by OpenSees were shifted on one side with a large residual displacement. These observations are evident in Fig. C.8. Energy dissipated by BRB in SAP 2000, Perform 3D and OpenSees for IDA (Fig. C.9) which shows the effectiveness of BRBs in the frame with increasing peak ground acceleration. Fig. C.10 shows the hysteresis of BRBs by SAP 2000, Perform 3D and OpenSees (Menegotto-Pinto) for Kobe (0.8g). It is clear that OpenSees predicted very high energy dissipation and deformation was unsymmetrical.

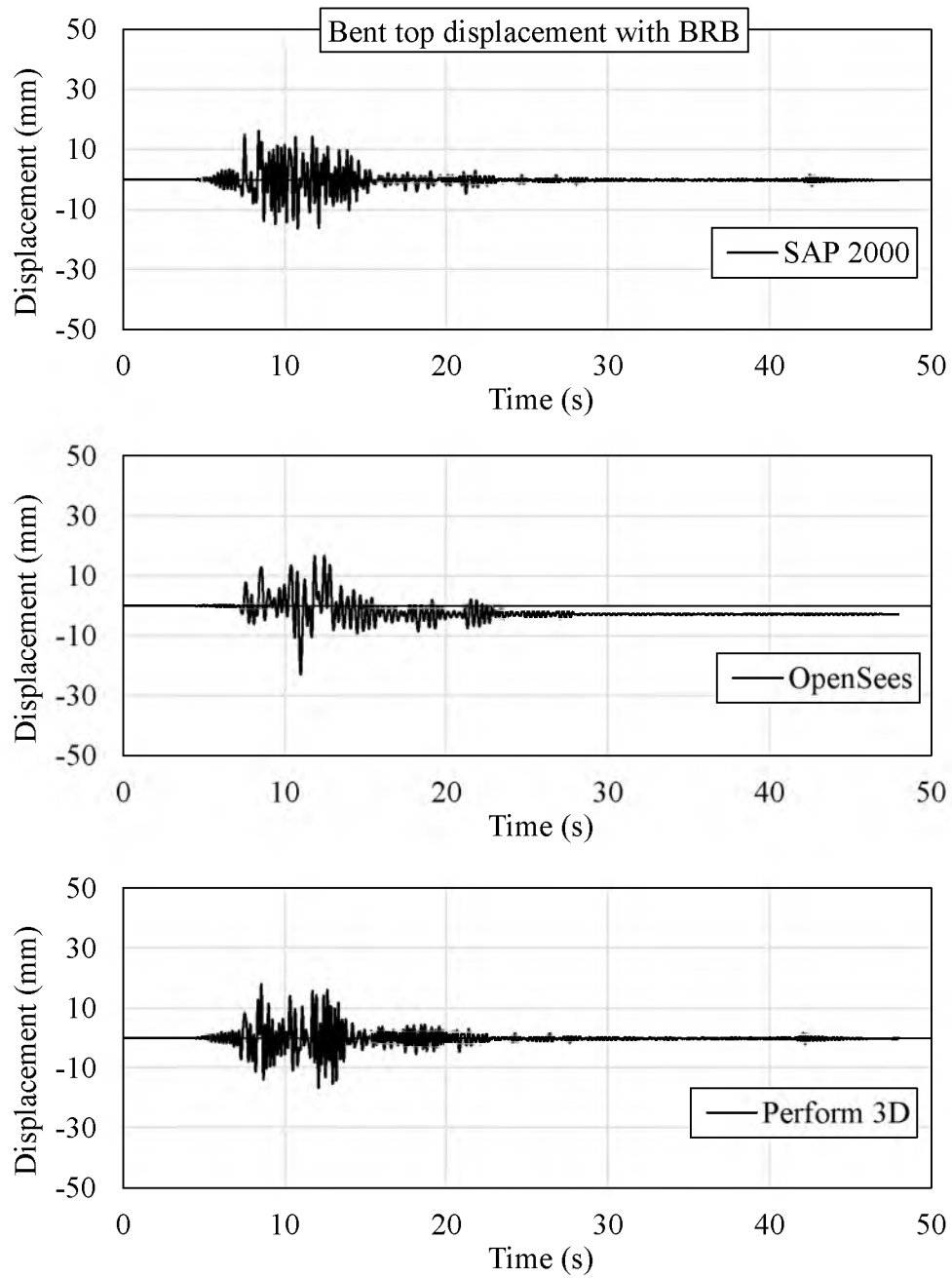


Figure C.7 Retrofitted bent top displacement time histories for Kobe (0.8g) ground motion

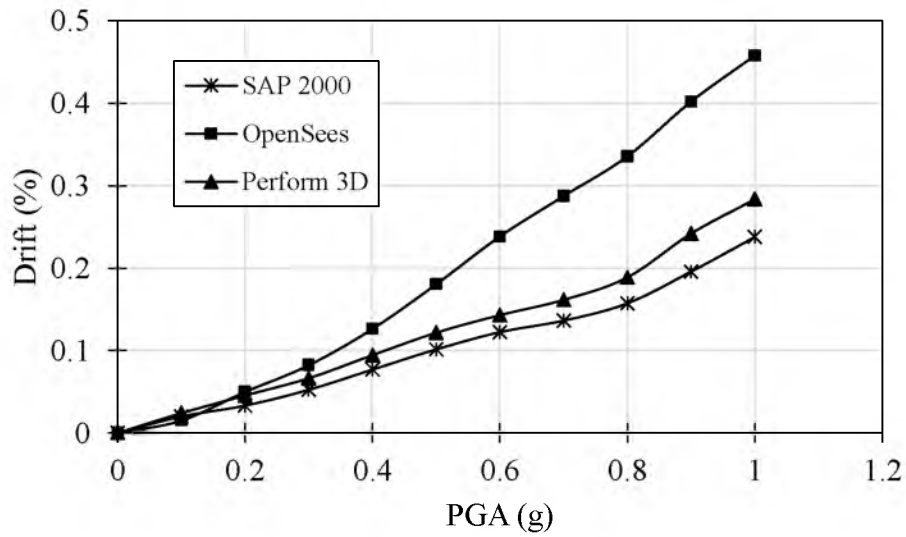


Figure C.8 Bent top drift values for IDA using Kobe (1995) ground motion

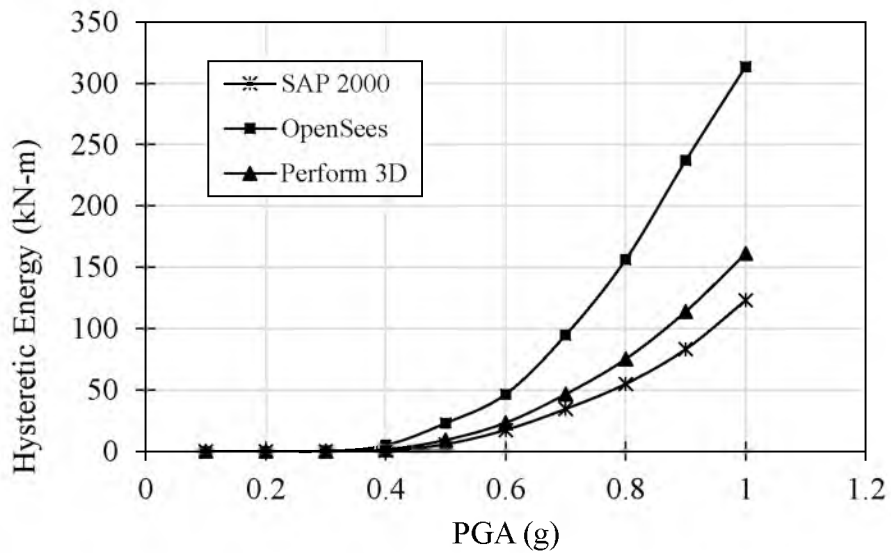


Figure C.9 Energy dissipated by BRB for IDA using Kobe (1995) ground motion

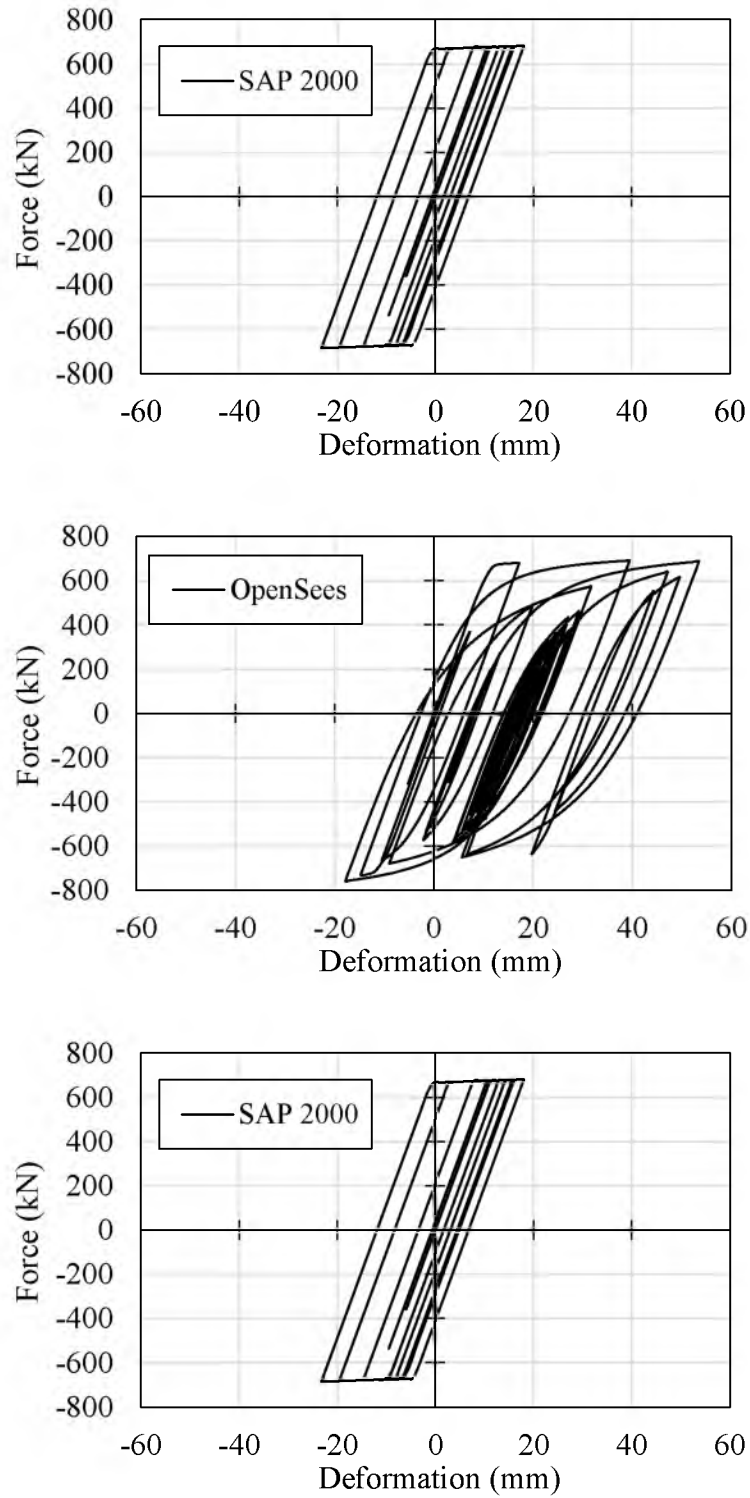


Figure C.10 BRB hysteresis for Kobe ground motion (PGA 0.8 g)

REFERENCES

AASHTO. (2012). AASHTO LRFD bridge design specifications, 6th Ed., American Association of State Highway and Transportation Officials, Washington, DC.

Anagnostopoulos, S. A., and Karamaneas, C. E. (2008). "Use of collision shear walls to minimize seismic separation and to protect adjacent buildings from collapse due to earthquake-induced pounding." *Earthquake Eng. Struct. Dyn.*, 37, 1371–1388.

Andrawes, B. and DesRoches, R. (2007). "Comparison between Shape Memory Alloy Seismic Restrainers and Other Bridge Retrofit Devices," *J. Bridge Eng.*, 12(6), 700-709,

ASCE. (2013). "Minimum Design Loads For Buildings and Other Structures." Standards ASCE/SEI 7-10.

Bi, K., and Hao, H. (2013). "Numerical simulation of pounding damage to bridge structures under spatially varying ground motions." *Engineering Structures*, 46(5), pp. 62–76.

Bi, K., Hao, H., and Chouw, N. (2013). "3D FEM Analysis of Pounding Response of Bridge Structures at a Canyon Site to Spatially Varying Ground Motions. *Advances in Structural Engineering*, 16(4), 619–640.

Black, C., Makris, N., and Aiken, I. (2004). "Component Testing, Seismic Evaluation and Characterization of Buckling-Restrained Braces." *J. Struct. Eng.*, 130(6), 880–894.

Bruneau, M., Wilson, J. C., and Tremblay, R. (1996). "Performance of steel bridges during the 1995 Hyogo-ken Nanbu (Kobe, Japan) earthquake." *Can. J. Civ. Eng.*, 23, 678-713.

Buckle, Ian G.; Yen, Wen-huei (Phillip); Marsh, M. Lee; Monzon, Eric V. (2012). "Implications of bridge performance during Great East Japan earthquake for U.S. seismic design practice." *Proceedings of the International Symposium on Engineering Lessons Learned from the 2011 Great East Japan Earthquake*, March 1-4, 2012, Tokyo, Japan. Page 1323-1332.

Capron, M. R., (1999). "Seismic Retrofit of the Poplar Street Bridge." *Conference Proceedings, Structural Engineering in the 21st Century, Structures Congress*, April 1-19, 1999, Pages 37-40.

Caltrans, S. D. C. (California Department of Transportation). (2010). "Caltrans Seismic Design Criteria version 1.6.", Sacramento, California.

Celik, O. C., and Bruneau, M. (2009). "Seismic behavior of bidirectional-resistant ductile end diaphragms with buckling restrained braces in straight steel bridges." *Engineering Structures*, 31(2), 380–393.

Celik, O. C., and Bruneau, M. (2011). "Skewed Slab-on-Girder Steel Bridge Superstructures with Bidirectional-Ductile End Diaphragms. *Journal of Bridge Engineering*." 16(2), 207–218.

Computers and Structures Inc. (2013). "SAP 2000 v.16", Analysis software. <https://www.csiamerica.com/products/sap2000>.

DesRoches, R., and Muthukumar, S. (2002). "Effect of Pounding and Restraints on Seismic Response of Multiple-Frame Bridges." *J. of Struct. Eng.*, 128(7), 860–869.

Dicleli, M., and Bruneau, M. (1995). "Seismic Performance of Multispan Simply Supported Slab-on-girder Steel highway Bridges". *Engineering Structures*, 17(1), 4–14.

El-Bahey, S., Bruneau, M., (2011). "Buckling restrained braces as structural fuses for the seismic retrofit of reinforced concrete bridge bents." *Engineering Structures*, 33(3), 1052-1061.

El-Bahey, S., and Bruneau, M. (2012). "Bridge Piers with Structural Fuses and Bi-Steel Columns. I: Analytical Investigation." *Journal of Bridge Engineering*, 17(1), 36–46.

FEMA. (2000). "Seismic Rehabilitation Prestandards." FEMA 356, Federal Emergency Management Agency, Washington D.C.

FEMA. (2009). "NEHRP Recommended Seismic Provisions." FEMA P-750, Federal Emergency Management Agency, Washington D.C.

G. L. Zhou, Q. L. Meng, (2011). "Using Cable Restraints to Mitigate the Seismic Pounding between Adjacent Structure Members." *Applied Mechanics and Materials*, Vol 71-78, pp. 598-602.

Hao, H., and Chouw, N. (2008). "Seismic Design of Bridges for Prevention of Girder Pounding." *e-JSE Special Issue*, 133–141.

Huo, Y. and Zhang, J. (2013). "Effects of Pounding and Skewness on Seismic Responses of Typical Multispan Highway Bridges Using the Fragility Function Method." *J. Bridge Eng.*, 18(6), 499–515.

Itani, A. M., Bruneau, M., Carden, L., Buckle, I. G. (2004). "Seismic Behavior of Steel Girder Bridge Superstructures", *Journal of Bridge Engineering*, P243-P249.

Jankowski, R. (2005), "Nonlinear viscoelastic modelling of earthquake-induced structural pounding." *Earthquake Eng. Struct. Dyn.*, 34: 595–611.

Kanaji, H., Kitazawa, M., and Suzuki, N. (2005). "Seismic Retrofit Strategy using Damage Control Design Concept and the Response Reduction Effect for a Long-span Truss Bridge." *Proc., of US-Japan Bridge Workshop*, Tsukuba, Japan.

Konagai, K., Yin, Y., and Muroto, Y. (2003). "Single beam analogy for describing soil-pile group interaction." *Soil Dynamics and Earthquake Engineering*, 23(3), 213–221.

Li, B., Bi, K., Chouw, N., Butterworth, J. W., and Hao, H. (2013). "Effect of abutment excitation on bridge pounding." *Engineering Structures*, 54, pp.57-68.

Mander, J. B., Priestley, M. J. N., and Park, R. (1988). "Theoretical Stress-Strain Model for Confined Concrete." *J. Struct. Engg., ASCE*, 114(8), 1804-1826.

Makris, N. and Zhang, J. (2002). "Structural Characterization and Seismic Response Analysis of a Highway Overcrossing Equipped with Elastomeric Bearings and Fluid Dampers: A Case Study." Report No. PEER – 2002/17, University of California, Berkeley, CA.

McKenna F., Fenves G.L., Scott M.H. (2000). *Open System for Earthquake Engineering Simulation (OpenSees) version 2.4.5* [Software]. Available from <http://opensees.berkeley.edu/>.

NEHRP. (2012). "Selecting and Scaling Earthquake Ground Motions for Performing Response-History Analyses." NEHRP Synthesis 428. TRB, Washington D.C.

Nielson, B. G., DesRoches, R. (2006). "Influence of modeling assumptions on the seismic response of multi-span simply supported steel girder bridges in moderate seismic zones." *Engineering Structures*, 28(8), 1083-1092.

Pantelides, C. P., and Ma, X. (1998). "Linear and nonlinear pounding of structural systems." *Computers and Structures*, 66(1), 79–92.

Pantelides, C. and Gergely, J., Reaveley, L. D. (2001). "In-situ verification of rehabilitation and repair of reinforced concrete bridge bents under simulated seismic loads." *Earthquake Spectra*, 17(3), 507-530.

Padgett, J. E., and DesRoches R. (2008). "Three-dimensional nonlinear seismic performance evaluation of retrofit measures for typical steel girder bridges", *Engineering Structures*, 30(7), 1869-1878.

Pan, Y., Agrawal, A., and Ghosn, M. (2007). "Seismic Fragility of Continuous Steel Highway Bridges in New York State." *J. Bridge Eng.*, 12(6), 689–699.

Pan, Y., Agrawal, A., Ghosn, M., and Alampalli, S. (2010). "Seismic Fragility of Multispan Simply Supported Steel Highway Bridges in New York State. I: Bridge Modeling, Parametric Analysis, and Retrofit Design." *J. Bridge Eng.*, 15(5), 448–461.

Pan, Y., Agrawal, A., Ghosn, M., and Alampalli, S. (2010). "Seismic Fragility of Multispan Simply Supported Steel Highway Bridges in New York State. II: Fragility Analysis, Fragility Curves, and Fragility Surfaces." *J. Bridge Eng.*, 15(5), 462–472.

PEER (2013). NGA-West2 database flatfile, Pacific Earthquake Engineering Research Center, available: <http://peer.berkeley.edu/ngawest2/databases/>. Last accessed 14 October 2014.

Raheem, A. S. E. (2009). Pounding mitigation and unseating prevention at expansion joints of isolated multi-span bridges. *Engineering Structures*, 31(10), 2345–2356.

Reno, M. L., and Pohll, M. N. (2013). "Application of Buckling Restrained Braces (BRB) on Foresthill Bridge Seismic Retrofit." *Seventh National Seismic Conference on Bridges and Highways* (pp. 1–12). Pakland, CA.

SeismoSoft (2013) - "SeismoMatch v.2.1.2". www.seismosoft.com.

Soneji, B. B., and Jangid, R. S. (2008). "Influence of soil-structure interaction on the response of seismically isolated cable-stayed bridge." *Soil Dynamics and Earthquake Engineering*, 28(4), 245–257.

Sun, L., Wei, J., and Xie, W. (2012). "Experimental Investigation on Energy Dissipation Subsidiary Piers for Long Span Cable-Stayed Bridges." *15th WCEE World Conference on Earthquake Engineering*.

Takabatake, H., Yasui, M., Nakagawa, Y. and Kishida, A. (2014). "Relaxation method for pounding action between adjacent buildings at expansion joint." *Earthquake Eng. Struct. Dyn.*, 43: 1381–1400.

UDOT (Utah Department of Transportation). (1998). "Dwg. No. C-842." I-15 Corridor Construction Project, Salt Lake City.

USGS. (2014). "Seismic Design Map Tools." US Geological Survey. <http://earthquake.usgs.gov/designmaps/us/application.php>

Van Mier, J., Pruijssers, A., Reinhardt, H., and Monnier, T. (1991). "Load-Time Response of Colliding Concrete Bodies." *J. Struct. Eng.*, 117(2), 354–374.

Xu, W. (2016). "Experiments, Analysis and Design Improvements for New Generation BRBs." (Unpublished PhD Dissertation), Salt Lake City, University of Utah.